

การหาค่าตัวประกอบสำหรับการออกแบบด้านทานแผ่นดินไหวของโครงสร้างแนวทแยงโดยใช้ท่อ
เหล็กกลมกรอกคอนกรีต



จุฬาลงกรณ์มหาวิทยาลัย

บทคัดย่อและแฟ้มข้อมูลฉบับเต็มของวิทยานิพนธ์ตั้งแต่ปีการศึกษา 2554 ที่ให้บริการในคลังปัญญาจุฬาฯ (CUIR)
เป็นแฟ้มข้อมูลของนิสิตเจ้าของวิทยานิพนธ์ ที่ส่งผ่านทางบัณฑิตวิทยาลัย

The abstract and full text of theses from the academic year 2011 in Chulalongkorn University Intellectual Repository (CUIR)
are the thesis authors' files submitted through the University Graduate School.

วิทยานิพนธ์นี้เป็นส่วนหนึ่งของการศึกษาตามหลักสูตรปริญญาวิศวกรรมศาสตรมหาบัณฑิต

สาขาวิชาวิศวกรรมโยธา ภาควิชาวิศวกรรมโยธา

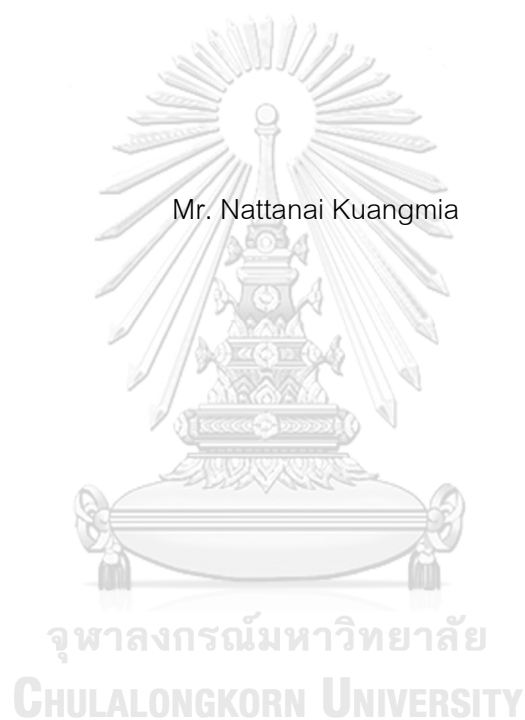
คณะวิศวกรรมศาสตร์ จุฬาลงกรณ์มหาวิทยาลัย

ปีการศึกษา 2560

ลิขสิทธิ์ของจุฬาลงกรณ์มหาวิทยาลัย

QUANTIFICATION OF SEISMIC PERFORMANCE FACTORS FOR CIRCULAR
CONCRETE-FILLED STEEL TUBE DIAGRID STRUCTURES

Mr. Nattanaï Kuangmia



A Thesis Submitted in Partial Fulfillment of the Requirements
for the Degree of Master of Engineering Program in Civil Engineering

Department of Civil Engineering

Faculty of Engineering

Chulalongkorn University

Academic Year 2017

Copyright of Chulalongkorn University

ณัฐน้อย กวงเมี้ย : การหาค่าตัวประกอบสำหรับการออกแบบต้านทานแผ่นดินไหวของ
 โครงตารางแนวทแยงโดยใช้ท่อเหล็กกลมกรอกคอนกรีต (QUANTIFICATION OF
 SEISMIC PERFORMANCE FACTORS FOR CIRCULAR CONCRETE-FILLED
 STEEL TUBE DIAGRID STRUCTURES) อ.ที่ปรึกษาวิทยานิพนธ์หลัก: ผศ. ดร. จัตุร
 พันธุ์ จินตนาภักดี, 146 หน้า.

ในศตวรรษที่ ๒๑ ระบบโครงตารางแนวทแยงได้รับความนิยมเพิ่มขึ้นในการใช้เป็นระบบ
 ด้านแรงด้านข้างสำหรับอาคารสูงอย่างกว้างขวางทั่วโลก ระบบนี้ประกอบด้วยองค์อาคารที่รวมตัว
 กันเป็นตารางจำนวนมากในแนวทแยงที่รอบตัวอาคาร ระบบนี้ทำหน้าที่เป็นทั้งโครงแกนด้าน
 แรงด้านข้างและองค์อาคารรับน้ำหนักบรรทุกทุกแนวตั้งในเวลาเดียวกัน เนื่องจากระบบนี้เป็นระบบ
 ด้านแรงด้านข้างแบบใหม่ มาตรฐานการออกแบบอาคารในปัจจุบันยังไม่ได้ให้ค่าตัวประกอบ
 สำหรับการออกแบบต้านทานแผ่นดินไหวอย่างชัดเจน อันได้แก่ ค่าตัวประกอบปรับผลตอบแทน
 ตัวประกอบขยายค่าการโก่งตัว และ ตัวประกอบกำลังส่วนเกิน ที่เอาไปใช้สำหรับการออกแบบ
 วิทยานิพนธ์นี้มีจุดมุ่งหมายที่จะกำหนดค่าตัวประกอบเหล่านี้ที่เหมาะสมสำหรับระบบโครงตาราง
 แนวทแยงโดยใช้ท่อเหล็กกลมกรอกคอนกรีต เพื่อให้วิศวกรโครงสร้างสามารถออกแบบระบบนี้
 ตามมาตรฐานการออกแบบ การวิจัยนี้ใช้วิธีการของ FEMA P695 เพื่อหาค่าตัวประกอบเหล่านี้
 โดยตรวจสอบสมรรถนะการพังทลายของอาคารโดยวิธีวิเคราะห์การตอบสนองของโครงสร้างไม่
 เชิงเส้นแบบประวัติเวลาประกอบกับความไม่แน่นอนในหลายตัวแปร ค่าตัวประกอบที่เหมาะสม
 เป็นค่าที่ทำให้มั่นใจว่าความเป็นไปได้ที่โครงสร้างจะพังทลายภายใต้แผ่นดินไหวรุนแรงสูงสุดที่
 พิจารณาในการออกแบบมีค่าที่น้อยมากในเกณฑ์ที่รับได้ อาคารตัวอย่างเป็นอาคารสูง ๑๘, ๒๔
 และ ๓๖ ชั้น ที่ใช้ระบบโครงตารางแนวทแยงโดยใช้ท่อเหล็กกลมกรอกคอนกรีตเป็นระบบด้านแรง
 ด้านข้าง อาคารตัวอย่างกำหนดให้ตั้งอยู่ในกรุงเทพมหานคร แต่ละตัวอย่างถูกวิเคราะห์โดยใช้คลื่น
 แผ่นดินไหวจำนวน ๑๒ คลื่น แล้วแต่คาบการสั่นของอาคาร อาคารตัวอย่างที่ออกแบบโดยใช้
 ค่าตัวประกอบปรับผลตอบแทน เท่ากับ ๕ ผ่านเกณฑ์ที่รับได้ของ FEMA P695 ตัวประกอบขยาย
 ค่าการโก่งตัวสามารถใช้ค่าเท่ากับ ๕ และ ตัวประกอบกำลังส่วนเกินสามารถใช้ค่าเท่ากับ ๓

ภาควิชา วิศวกรรมโยธา ลายมือชื่อนิสิต

สาขาวิชา วิศวกรรมโยธา ลายมือชื่อ อ.ที่ปรึกษาหลัก

ปีการศึกษา 2560

5970158221 : MAJOR CIVIL ENGINEERING

KEYWORDS: DIAGRID / CONCRETE-FILLED STEEL TUBE / SEISMIC PERFORMANCE FACTORS / INCREMENTAL DYNAMIC ANALYSIS / FEMA P695

NATTANAI KUANGMIA: QUANTIFICATION OF SEISMIC PERFORMANCE FACTORS FOR CIRCULAR CONCRETE-FILLED STEEL TUBE DIAGRID STRUCTURES. ADVISOR: ASST. PROF. CHATPAN CHINTANAPAKDEE, Ph.D., 146 pp.

In 21st century, diagrid structures become more popular lateral force-resisting systems for high-rise buildings world-wide. It consists of several grids of diagonal members on building perimeter serving as both lateral bracing and vertical-load carrying members. Since the diagrid structure is a relatively new type of lateral force-resisting system, current building codes do not explicitly provide the seismic performance factors (SPFs) for this system to use in design process. This thesis aims to determine appropriate SPFs for the diagrid structure incorporating circular concrete-filled steel tube to enable structural engineers to design this system according to seismic performance expected in building codes. This research follows FEMA P695 procedure to evaluate SPFs by examining collapse performance of buildings based on nonlinear response history analysis considering various sources of uncertainties. The verified SPFs ensure an acceptably low likelihood of structural collapse under extremely rare earthquake ground motions or maximum considered earthquake. Sample buildings in this thesis are 18, 24 and 36-story buildings using circular concrete-filled steel tube diagrid as lateral force-resisting system. The buildings were assumed to locate in downtown Bangkok. Each sample building was subjected to 12 ground motion records based on its periods of vibration. The sample buildings designed with response modification coefficient equal to 5 meet the acceptance criteria of FEMA P695. A deflection amplification factor can be used as 5, and a system overstrength factor can be used as 3.

Department: Civil Engineering Student's Signature

Field of Study: Civil Engineering Advisor's Signature

Academic Year: 2017

ACKNOWLEDGEMENTS

Over two years at Chulalongkorn University, I have encountered many energetic and motivated individuals who have inspired me to become a great engineer. I would like to express my very great appreciation to my advisor, Dr. Chatpan Chintanapakdee. My advisor was such a great researcher who enjoyed complexity and state of the art of structural engineering and earthquake engineering. During my apprenticeship with him, he trained me to think outside of the box, understand every step and every process and be more like a professional engineer. He crafted my engineering skills to the level comparable to practicing engineers. In this thesis, I am thankful to him for letting me pursue my interests in the topic of my research with his invaluable advice and careful guidance. Beside my advisor, I am particularly grateful for assists given by the rest of my thesis committee: Dr. Anat Ruangrassamee and Dr. Nuttawut Thanasisathit. Dr. Anat trained me to understand the art of structural engineering. He trained me to focus the behavior of structure and how engineers look at structure. Dr. Nuttawut guided me through the difficult topics and provided me invaluable support throughout the degree. Furthermore, I am grateful for all the knowledge I learned during my master courses from all teachers at Chulalongkorn University. I wish to acknowledge the support from all individuals at Center of Excellence in Earthquake Engineering and Vibration, Chulalongkorn University. To Tek Nath Kararia, thank you for your inspirations and adulthood which turns this boy into a man; further my knowledge in a field of Earthquake Engineering. To Khonesavanh Pormeuangpieng, thank you for drawing all CAD figures in this thesis. This thesis would not complete without these figures. Also, I am thankful to my colleagues at the center: Teerit Wutthisirisart, Pakawats Minchainant and everyone. Lastly, I am grateful to my family, friends and my girlfriend who provided me love and moral support throughout my long journal in this thesis. Thank you everybody for the support you gave, I appreciate them.

CONTENTS

	Page
THAI ABSTRACT	iv
ENGLISH ABSTRACT	v
ACKNOWLEDGEMENTS.....	vi
CONTENTS.....	vii
LIST OF TABLES.....	x
LIST OF FIGURES	xi
CHAPTER 1 INTRODUCTION	1
1.1 Development of diagrid structure.....	1
1.2 Motivations.....	4
1.3 Goals of the research	4
1.4 Scopes of the research	5
1.5 Research methodology	5
1.6 Outline of thesis	5
CHAPTER 2 METHODOLOGY	7
2.1 FEMA P695	7
2.1.1 Objective	7
2.1.2 Seismic performance factors	8
2.1.3 Collapse margin ratio	10
2.2 Procedure in FEMA P695	11
2.2.1 Conceptual development of structural system	12
2.2.2 Development of performance groups.....	13
2.2.3 Development of models	14

	Page
2.2.3.1 Fundamental period.....	14
2.2.3.2 Seismic base shear	15
2.2.3.3 Design load combinations	15
2.2.4 Nonlinear static pushover analysis	16
2.2.5 Incremental dynamic analysis	17
2.2.6 Collapse fragility curve	18
2.2.7 Adjusted collapse margin ratio	19
2.2.8 Total system collapse uncertainty	19
2.2.9 Acceptable values of ACMR.....	20
2.2.10 Evaluation of response modification coefficient	20
2.2.11 Evaluation of system overstrength factor and evaluation of deflection amplification factor.....	21
CHAPTER 3 DIAGRID STRUCTURES	22
3.1 Static analysis of diagrid structures	22
3.2 SPFs for steel diagrid	24
3.2.1 Proposed methodology for steel diagrid framed system	24
3.2.2 Results of steel diagrid framed system	26
CHAPTER 4 BUILDINGS AND GROUND MOTIONS.....	29
4.1 Performance group.....	29
4.2 Earthquake ground motions	32
4.3 Description of buildings.....	34
4.4 Fiber section of CCFT braces	38
4.4.1 Steel material.....	38

	Page
4.4.2 Concrete material.....	39
4.4.3 Diagrid module.....	40
CHAPTER 5 RESULTS.....	41
5.1 Pushover analysis.....	41
5.2 Nonlinear response history analysis	45
5.3 Incremental dynamic analysis.....	48
5.4 Collapse uncertainty.....	53
5.5 Collapse fragility curve.....	54
5.6 Seismic performance factors	58
CHAPTER 6 CONCLUSIONS.....	60
6.1 Summary.....	60
6.2 Recommendations for future research.....	61
REFERENCES.....	62
APPENDICES.....	65
APPENDIX A FEMA P695.....	66
APPENDIX B DIAGRID	79
APPENDIX C BUILDINGS AND GROUND MOTIONS	87
APPENDIX D RESULTS.....	129
ACRONYMS.....	143
SYMBOLS	144
VITA	146

LIST OF TABLES

	Page
Table 2.1	Generic performance group (FEMA, 2009)..... 14
Table 4.1	Index archetype configurations. 30
Table 4.2	Selected index archetype configurations. 31
Table 4.3	Bangkok response spectrums. 34
Table 4.4	Summary of archetype descriptions. 35
Table 5.1	Pushover static results. 43
Table 5.2	Collapse uncertainties of archetypes 54
Table 5.3	Summary of collapse margins and comparison to acceptance criteria 59
Table A.1	SPFs of composite braced frames in ASCE 7-05 (ASCE, 2005)..... 67
Table A.2	Coefficient C_u (ASCE, 2005)..... 67
Table A.3	Coefficient C_t and x (ASCE, 2005). 68
Table A.4	Spectral shape factor (SSF) for archetype designed for SDC B, C, or Dmin (FEMA, 2009)..... 70
Table A.5	Spectral shape factor (SSF) for archetype designed for SDC Dmax (FEMA, 2009). 70
Table A.6	Quality rating of design requirements (FEMA, 2009). 74
Table A.7	Quality rating of test data (FEMA, 2009)..... 74
Table A.8	Quality rating of index archetype models (FEMA, 2009). 75
Table A.9	Acceptable values of adjusted collapse margin ratio (FEMA, 2009)..... 76
Table A.10	Damping coefficient (ASCE, 2005)..... 78
Table B.1	Compactness of steel section (AISC, 2010b). 80
Table B.2	Ductility of steel section (AISC, 2010a). 82
Table B.3	Expected strength of steel material (AISC, 2010a). 83

LIST OF FIGURES

	Page
Figure 1.1 John Hancock Center.	2
Figure 1.2 Swiss Re Building.....	2
Figure 1.3 The Hearst Tower.....	3
Figure 1.4 Development from braced tube to diagrid structure (Moon et al., 2007).	3
Figure 2.1 Key components of FEMA P695 methodology (FEMA, 2009).....	8
Figure 2.2 Illustration of SPFs as defined in the commentary of the NEHRP recommended provisions (FEMA, 2009).	8
Figure 2.3 Illustration of SPFs as defined by FEMA P695 (FEMA, 2009).	9
Figure 2.4 Procedure of FEMA P695.....	12
Figure 2.5 Idealized nonlinear static pushover curve (FEMA, 2009).	16
Figure 2.6 Incremental dynamic analysis response plot of spectral acceleration versus maximum story drift ratio (FEMA, 2009).	17
Figure 2.7 Collapse fragility curve in form of cumulative distribution function (FEMA, 2009).	18
Figure 3.1 Diagrid module: (a) effect of gravity load, (b) effect of overturning moment and (c) effect of shear force (Mele et al., 2014).	23
Figure 3.2 Diagrid module: effect of gravity load along the diagonal length (Mele et al., 2014).	23
Figure 3.3 Parameters of interest for diagrid (W. Baker et al., 2010).	25
Figure 3.4 Development of archetype models (W. Baker et al., 2010).	25
Figure 3.5 Element behavior in analysis model (W. Baker et al., 2010).	25
Figure 3.6 Estimation of collapse margin ratio criteria (W. Baker et al., 2010).	26
Figure 3.7 Sample nonlinear static pushover curve (W. Baker et al., 2010).	28
Figure 3.8 Iterative estimation of R-factor (W. Baker et al., 2010).	28
Figure 4.1 Response spectra at MCE level for Bangkok with damping ratio of 5%.	33
Figure 4.2 Response spectra at MCE level for Bangkok with damping ratio of 2.5%. .	33

Figure 4.3	Equivalent viscous damping versus building height based on Eq. 4-1 (PEER, 2017).	35
Figure 4.4	Plan view of all buildings in FEM models (CSI, 2015).	36
Figure 4.5	3D view of 18R5 in FEM model (CSI, 2015).	36
Figure 4.6	3D view of 24R5 in FEM model (CSI, 2015).	37
Figure 4.7	3D view of 36R5 in FEM model (CSI, 2015).	37
Figure 4.8	Fiber discretization of CCFT cross section.....	38
Figure 4.9	Elastic-perfectly-plastic steel material with expected strength equal to 1.6 times nominal yield strength of 241 MPa.	39
Figure 4.10	Stress-strain relation of confined concrete in CCFT based on D/t ratio.....	39
Figure 4.11	Sample 6-story diagrid module.....	40
Figure 5.1	Nonlinear gravity loads applied (CSI, 2015).	42
Figure 5.2	Performing pushover by pushing in first mode direction (CSI, 2015).....	42
Figure 5.3	Pushover curve of 18R5.....	43
Figure 5.4	Pushover curve of 24R5.....	44
Figure 5.5	Pushover curve of 36R5.....	44
Figure 5.6	Modal analysis with Ritz vectors based on gravity loads and horizontal accelerations (CSI, 2015).	45
Figure 5.7	RAMPQS function for static load pattern (CSI, 2015).....	46
Figure 5.8	Initial nonlinear gravity loads for response history analysis (CSI, 2015).....	46
Figure 5.9	Sample time history function (CSI, 2015).	47
Figure 5.10	Sample NLRHA (CSI, 2015).....	47
Figure 5.11	IDA results of 18R5.	50
Figure 5.12	IDA results of 24R5.	51
Figure 5.13	IDA results of 36R5.	52
Figure 5.14	Collapse fragility curve of 18R5.	55
Figure 5.15	Collapse fragility curve of 24R5.	56
Figure 5.16	Collapse fragility curve of 36R5.....	57
Figure A.1	Idealized nonlinear static pushover curve (FEMA, 2009).	69

Figure A.2	Fragility curve constructing from spectral acceleration and maximum inter-story drift ratio (Chompoothawach, 2009).	71
Figure B.1	Monotonic steel stress-strain relationship including local buckling (Denavit & Hajjar, 2014).	84
Figure C.1	Story plan for all buildings at ground level.	105
Figure C.2	Story plan for all buildings in-between module.	105
Figure C.3	Story plan for all buildings at mid and end module level.	106
Figure C.4	Sample diagrid module expands to six stories for all buildings.	106
Figure C.5	Elevation view of 18R5 with plastic hinges (CSI, 2015).	107
Figure C.6	Elevation view of 24R5 with plastic hinges.	108
Figure C.7	Elevation view of 36R5 with plastic hinges (CSI, 2015).	109
Figure C.8	3D view of 18R5 (CSI, 2015).	110
Figure C.9	3D view of 24R5 (CSI, 2015).	111
Figure C.10	3D view of 36R5 (CSI, 2015).	112

CHAPTER 1

INTRODUCTION

1.1 Development of diagrid structure

Structural systems for tall buildings can be divided into two categories: interior structures and exterior structures. When the main part of lateral load resisting systems locates inside of the building, the system is interior structures. On the other hand, when the main part of lateral load resisting systems locates at the building perimeter, the system is exterior structures. Examples of interior structures are moment-resisting frame, shear truss, and shear wall. The most typical exterior structure is the tube, which uses the entire building perimeter to resist lateral loads. The tube structure can be further classified to framed tube, braced tube, and more.

In the late 20th century, exterior structures were initially applied to tall buildings. The first one was the 100-story John Hancock (1969) in Chicago (Figure 1.1). The John Hancock applied the idea of braced tube to configure exterior structure such that the diagonal brace locates along the exterior perimeter of the building.

Since the early 21st century, some high-rises have been designed with triangulated exterior structures, named diagrid systems. Diagrid systems become more popular lateral force-resisting systems for high-rise buildings world-wide. It consists of several grids of diagonal members on building perimeter serving as both lateral bracing and vertical-load carrying members. The diagonal perimeter members are tied together to provide significant overall bending resistance and rigidity. The most famous diagrid high-rises are designed by Sir Norman Foster: the Swiss Re Building (2004) (Figure 1.2) in London and the Hearst Tower (2006) (Figure 1.3) in New York City. After completion of these two buildings, the diagrid structure became popular and replaced the old braced tube structure due to its architectural appeal. The major development from braced tube structure to current diagrid structure is that, for diagrid structure, external columns are

eliminated as shown in Figure 1.4 (Moon, Cornor, & Fernandez, 2007). The advantage of this new system is explained in chapter 3.



Figure 1.1 John Hancock Center.

(<http://www.skyscrapercenter.com/building/875-north-michigan-avenue/345>)



Figure 1.2 Swiss Re Building.

(http://history.swissre.com/item_detail.php?id=54)

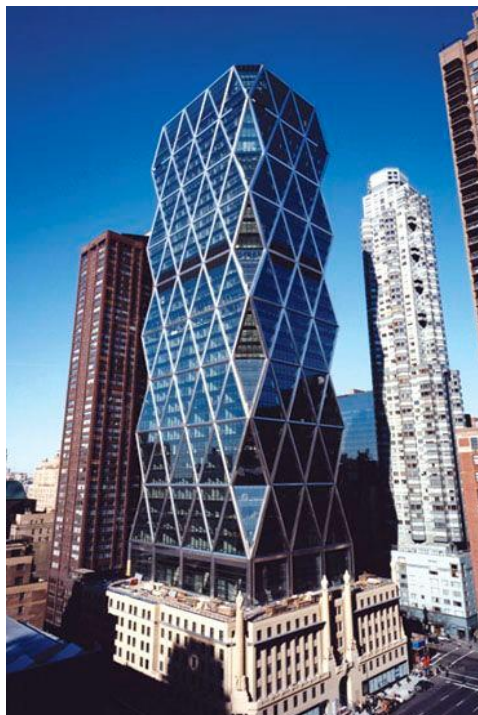
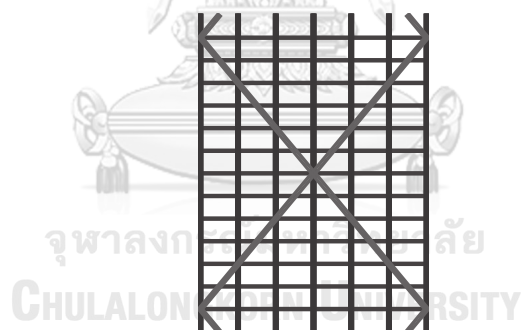
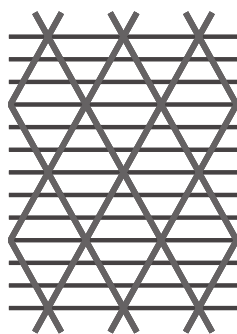


Figure 1.3 The Hearst Tower.

(<https://www.popularmechanics.com/technology/gadgets/a904/4198919/>)



Braced Tube



Diagrid

Figure 1.4 Development from braced tube to diagrid structure (Moon et al., 2007).

1.2 Motivations

For well-established structural systems, the current building code, ASCE 7-16 (ASCE, 2016), addresses the seismic performance factors (SPFs): response modification coefficient (R), system overstrength factor (Ω_0), and deflection amplification factor (C_d). These factors greatly influence performance of seismic-resisting system which is explained in chapter 2. Since this diagrid system is a relatively new seismic structural system, not much research has yet been conducted to understand its performance thoroughly. In particular, ASCE 7-16 does not provide SPFs for designing a diagrid system. In practice, the diagrid system is designed as a dual system, and the response modification coefficient (R) is estimated about 5.5 to 8.0. This assumption is acceptable since the typical tall buildings combine an exterior diagrid frame with an interior core structure. The problem arises when one wants to design the entire building's lateral system with standalone diagrid structure. In this case, reliable SPFs need to be quantified with appropriate procedure to better understand the behavior of diagrid system and use in the design of tall buildings. Since many researchers have conducted the similar study for steel diagrid structure, the author focuses the study to a CCFT diagrid structure which have not yet been exposed in previous studies.

1.3 Goals of the research

This thesis aims to investigate the seismic performance of diagrid structure incorporating circular concrete-filled steel tube (CCFT) and determine appropriate SPFs to enable structural engineers to design this system according to seismic performance expected in building codes. The author analyzes the seismic performance of standalone diagrid structure. Upon completion of this study, engineers would better understand the performance of diagrid exterior frame and further use the outcomes to design a standalone seismic system with reliable SPFs.

1.4 Scopes of the research

This study focuses on high-rise buildings located on soft soil layers in downtown Bangkok. The full description of case study is explored in later chapters. This thesis examines the behavior of tall buildings with several different heights located on soft soil layers in downtown Bangkok with suitable ground motion records.

1.5 Research methodology

The methodology follows the *Quantification of Building Seismic Performance Factors*, FEMA P695 (FEMA, 2009). FEMA P695 is a method for reliably and reproducibly quantifying and establishing global seismic performance factors of new seismic force resisting systems absent in seismic codes to use in design process. The ground motions used in design and analysis of this study came from a study by Thailand Research Fund. The nonlinear response history analyses were performed by using appropriate ground motion records for Bangkok. To sum up, the author designed the number of buildings with a trial R factor. These sample buildings went through nonlinear static analyses to determine the overstrength factor and ductility of systems. Consequently, sample buildings went through series of nonlinear dynamic analyses or incremental dynamic analyses to obtain collapse fragility curves. The fragility curves would determine whether the performance of this building is satisfied or not by verifying that, with the design by using a trial R factor, the designed buildings would have a low probability of collapse at Maximum Considered Earthquake (MCE) intensity. The ultimate objective of the methodology is to find the value of R that ensures an acceptably low likelihood of structural collapse under MCE motions.

1.6 Outline of thesis

This thesis contains six chapters which are described below. Chapter 1 describes the motivations, goals and scopes of work. Chapter 2 describes the theoretical framework. In this chapter, the methodology in FEMA P695 is explained. Chapter 3 examines the

diagrid structure. A complete study on quantification of SPFs of steel diagrid system is included here. In chapter 4, the structural models are generated with varying parameters associated with seismic performance. CCFT and hinge's development and selection of ground motion records are discussed here. The results are presented and discussed in chapter 5. Finally, summary and recommendations for future research are in chapter 6.



CHAPTER 2

METHODOLOGY

2.1 FEMA P695

2.1.1 Objective

The *Quantification of Building Seismic Performance Factors*, FEMA P695 (FEMA, 2009), describes a method for reliably and reproducibly quantifying and establishing global seismic performance factors (SPFs) of new seismic force resisting systems absent in seismic codes to use in design process. Seismic performance factors (SPFs) consist of response modification coefficient (R), system overstrength factor (Ω_0) and deflection amplification factor (C_d).

The goal of this method is to determine SPFs that will provide equivalent safety against collapse in an earthquake, comparable to the inherent safety against collapse intended by current seismic codes, for buildings with different seismic-force-resisting systems with an acceptably low probability of structural collapse under Maximum Considered Earthquake (MCE) ground motions defined in ASCE 7-05 (ASCE, 2005) with reliable collapse margin ratios (CMR). MCE level ground motion is defined as 1.5 times the Design Basis Earthquake (DBE). As stated in the NEHRP Recommended Seismic Provisions (FEMA, 2004), "If a structure experiences a level of ground motion 1.5 times the design level, the structure should have a low likelihood of collapse," FEMA P695 intends to achieve this performance. The appropriate SPFs are directly associated with the level of uncertainties of the system including: uncertainties of ground motions, accurateness of design objectives, complete test data to quantify structural member strength, and accuracy of nonlinear analysis modeling. The key components of FEMA P695 methodology are summarized in Figure 2.1.

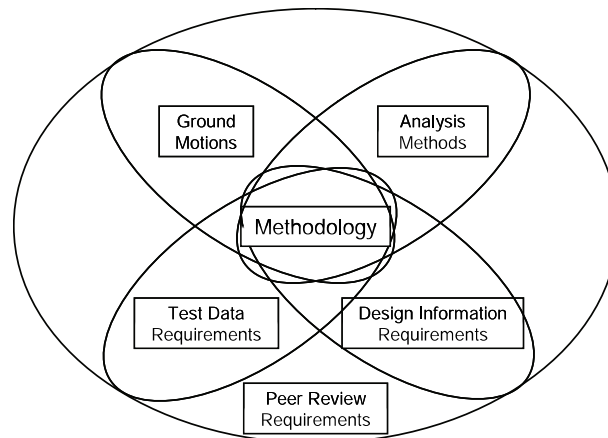


Figure 2.1 Key components of FEMA P695 methodology (FEMA, 2009).

2.1.2 Seismic performance factors

Seismic performance factors (SPFs) are three factors impacting the seismic performance of a specific structural system. Figures 2.2 and 2.3 explain and illustrate SPFs, and how they are used in the methodology. In Figure 2.2, the pushover analysis is performed.

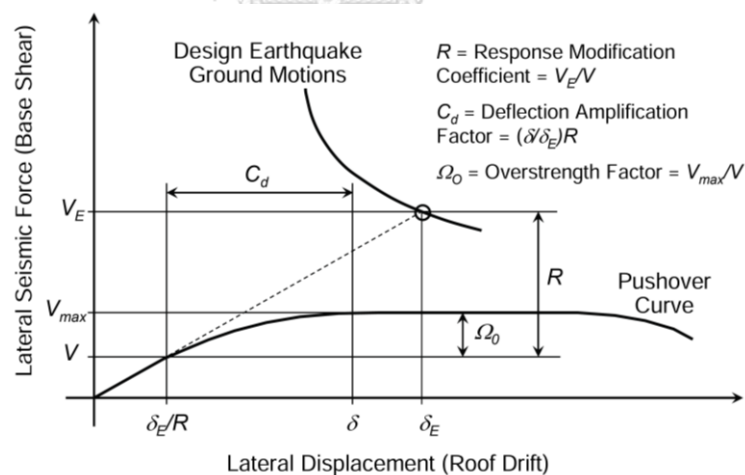


Figure 2.2 Illustration of SPFs in the commentary of the NEHRP recommended provisions (FEMA, 2009).

First, the *response modification coefficient* (R) is the ratio of base shear developed under DBE assuming linearly elastic to design base shear (Eq. 2-1). Second, the *system overstrength factor* (Ω_0) is the ratio of the maximum base shear of the fully-yielded system

to design base shear (Eq. 2-2). Lastly, the *deflection amplification factor* (C_d) is the ratio of the yielded roof displacement to the roof displacement at design base shear (Eq. 2-3).

$$R = \frac{V_E}{V} \quad (2-1)$$

$$\Omega_0 = \frac{V_{\max}}{V} \quad (2-2)$$

$$C_d = \frac{\delta}{\delta_E / R} = \frac{\delta}{\delta_E} R \quad (2-3)$$

where

- V = Required seismic base shear for design from ASCE 7-05
- V_E = Elastic seismic base shear at design basis earthquake (DBE) if the system remains linearly elastic
- V_{\max} = Maximum seismic base shear of the fully-yielded system
- δ = Displacement of the yielded system under DBE
- δ_{\max} = Displacement of the system under DBE if the system remains linearly elastic. Note: δ_E / R represents displacement of the seismic force resisting system at design base shear (V).

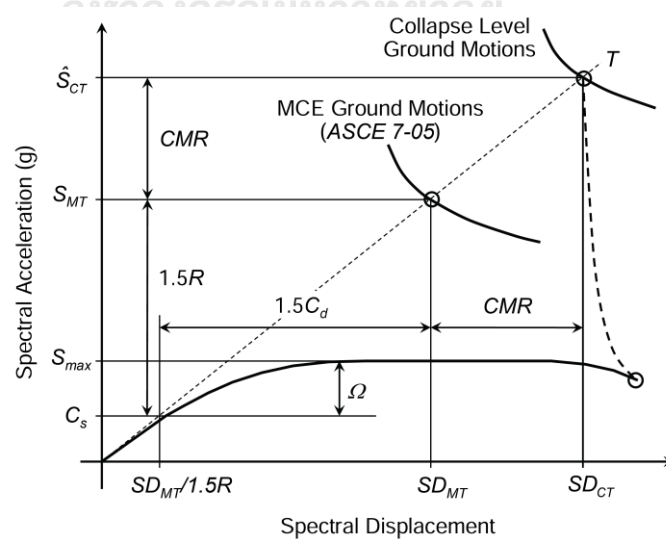


Figure 2.3 Illustration of SPFs in FEMA P695 (FEMA, 2009).

Figure 2.3 demonstrates the definition of SPFs in FEMA P695 and their relationship to MCE motions. R relates S_{MT} to a seismic response coefficient (C_S) by a factor of 1.5 which accounts for the magnification from DBE to MCE level (Eq. 2-4). The overstrength factor (Ω) is a ratio of maximum spectral acceleration of the fully-yielded system (S_{\max}) to C_S (Eq. 2-5).

$$1.5R = \frac{S_{MT}}{C_S} \quad (2-4)$$

$$\Omega = \frac{S_{\max}}{C_S} \quad (2-5)$$

where

S_{MT} = MCE spectral acceleration at the fundamental period of the system, T

S_{\max} = the maximum spectral acceleration of the fully-yielded system (or V_{\max} normalized by W)

W = Seismic weight of building

C_S = Seismic response coefficient for DBE

2.1.3 Collapse margin ratio

The collapse level ground motion is defined in FEMA P695 as the intensity or spectral acceleration that causes a collapse of seismic force resisting system when subjected to a half or fifty percent of applied ground motions. In Figure 2.3, collapse level spectral accelerations are higher than MCE spectral accelerations. Therefore, MCE ground motions result in a lower probability of collapse. Then, the collapse margin ratio (CMR) is a ratio of the median spectral acceleration at collapse level, \hat{S}_{CT} (or corresponding displacement, SD_{CT}), to the spectral acceleration at MCE level, S_{MT} (or corresponding displacement, SD_{MT}), at the fundamental period of the system (T):

$$CMR = \frac{\hat{S}_{CT}}{S_{MT}} = \frac{SD_{CT}}{SD_{MT}} \quad (2-6)$$

In other words, CMR is the amount that S_{MT} must be increased to cause building collapsed by a half or fifty percent of applied ground motions. The probability of collapse

is influenced by many factors: variability of ground motions, accuracy of design objectives, comprehensive test data to quantify structural member strength, and accuracy of nonlinear analysis modeling. These factors are considered together in a collapse fragility curve which relates a probability of collapse to an intensity of ground motion. The definition of collapse fragility curve will be explained later.

FEMA P695 specifies acceptable values of *CMR* that will cause an acceptably low probability of collapse under MCE motions combining with collapse uncertainties by using a collapse fragility curve. If a structure has strict design requirements, a comprehensive experiment results that are used to develop nonlinear members and a complex and precise nonlinear model, a structure can achieve the same performance objective with smaller *CMR* because it has less collapse uncertainty. If a value of *CMR* passes the performance requirements, then a trial value of *R* used to design a structure is acceptable. Otherwise, another value of *R* will be evaluated with the same method or consider other limitations of the system such as a restriction of height.

2.2 Procedure in FEMA P695

FEMA P695 procedure is summarized in Figure 2.4.

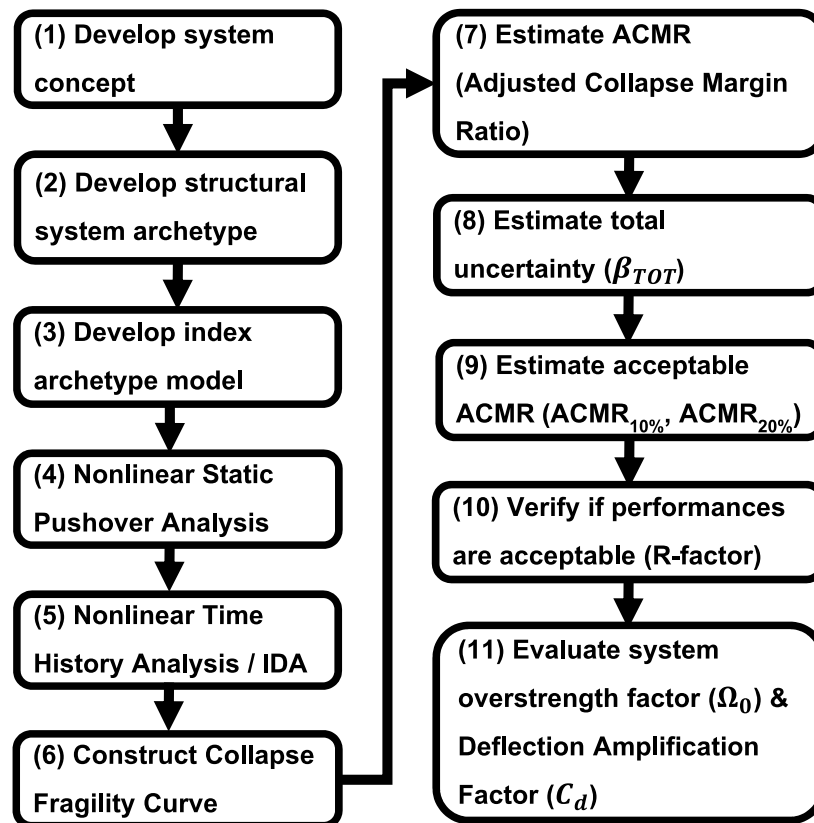


Figure 2.4 Procedure of FEMA P695.

2.2.1 Conceptual development of structural system

The specific type of structural system is determined with detailed design requirements. A value of R is chosen for seismic design process. In this study, the specified structural system is a circular concrete-filled steel tube (CCFT) diagrid system. The sample SPF of composite braced frames are in Table A.1. The trial value of R was chosen as 5.0 since the composite steel and concrete concentrically braced frame has a value of R as 5.0 in ASCE 7-05. The design method is modal response spectrum analysis (RSA) as specified in ASCE 7-05. The design response spectrum is developed by considering a specific site condition of Bangkok and is explained in chapter 4. In this study, seismic design category (SDC) is D, and important factor (I) is 1.0. The occupancy type is II.

2.2.2 Development of performance groups

System behavior is characterized by structural system archetypes. Archetypes define a reference model with allowable configurations of the proposed system. Archetypes are collected into performance groups. Each group represents each major change in behavior within the archetype space. The performance objective is evaluated for each individual and each performance group. As shown in Table 2.1, the basic performance groups are organized to consider:

1. **Basic Structural Configuration.** All permissible configurations that may greatly affect the seismic response are captured. An example is a variation in bracing configurations, such as, x-bracing and chevron bracing.
2. **Gravity Load Level.** A variation in gravity load level can differ an amount of seismic weight of a seismic force resisting system. For example, usage of bearing walls can cause a different gravity load intensity compared to usage of non-bearing walls.
3. **Seismic Design Category.** The full range of SDCs should be included to capture all permissible buildings. Nonetheless, it should be sufficient to check only the highest permissible SDC since higher SDC governs seismic demand.
4. **Period Domain.** Sample buildings should include a range of buildings from short-period to long-period configurations.

Each performance group requires at least three sample buildings. If it is impossible to have three designs within one performance group, this requirement may be waived.

Table 2.1 Generic performance group (FEMA, 2009).

Performance Group Summary					
Group No.	Basic Configuration	Grouping Criteria		Period Domain	Number of Archetypes
		Design Load Level			
		Gravity	Seismic		
PG-1	Type 1	High	Max SDC	Short	≥ 3
PG-2				Long	≥ 3
PG-3			Min SDC	Short	≥ 3
PG-4				Long	≥ 3
PG-5		Low	Max SDC	Short	≥ 3
PG-6				Long	≥ 3
PG-7			Min SDC	Short	≥ 3
PG-8				Long	≥ 3
PG-9	Type 2	High	Max SDC	Short	≥ 3
PG-10				Long	≥ 3
PG-11			Min SDC	Short	≥ 3
PG-12				Long	≥ 3
PG-13		Low	Max SDC	Short	≥ 3
PG-14				Long	≥ 3
PG-15			Min SDC	Short	≥ 3
PG-16				Long	≥ 3
PG-17	Type N	High	Max SDC	Short	≥ 3
PG-18				Long	≥ 3
PG-19			Min SDC	Short	≥ 3
PG-20				Long	≥ 3
PG-21		Low	Max SDC	Short	≥ 3
PG-22				Long	≥ 3
PG-23			Min SDC	Short	≥ 3
PG-24				Long	≥ 3

2.2.3 Development of models

Index archetype models or sample buildings are created to provide a range of typical configurations that can capture significant behaviors of the system. A range of buildings may be characterized by floor plan configurations, heights, and tributary areas. These characteristics of building can impact seismic performance of system. The system concept in section 2.2.1 is applied in design of sample buildings.

2.2.3.1 Fundamental period

The fundamental period of structure (T) is used within the methodology in two ways. First, it establishes the seismic base shear. Second, it defines the ground motion

spectral acceleration from MCE response spectrum for dynamic analyses. As defined in ASCE 7-05, the fundamental period (T) defines as:

$$T = C_u T_a = C_u (C_t h_n^x) \geq 0.25 \text{ seconds} \quad (2-7)$$

where

- h_n = Building height to roof
- C_u = Coefficient value based on response spectrum (Table A.2)
- C_t = Coefficient value based on type of structure (Table A.3)
- x = Coefficient value based on type of structure (Table A.3)

2.2.3.2 Seismic base shear

Index archetypes are designed using the seismic design base shear (V) defined as:

$$V = C_s W \quad (2-8)$$

$$C_s = \frac{S_{DT}}{R} \quad (2-9)$$

where

- C_s = Seismic response coefficient for DBE Response Spectrum from ASCE 7-05

2.2.3.3 Design load combinations

Design of index archetypes should consider gravity and seismic load by using load combinations of section 12.4 of ASCE 7-05. Only seismic load, dead load and live load are considered in this study. Detail description of loads is in Appendix C. Basic seismic load combinations for strength design are:

$$1.2D + Q_E + L \quad (2-10)$$

$$0.9D + Q_E \quad (2-11)$$

where

- D = Structural self-weight and superimposed dead load

L = Reduced design Live load

Q_E = Effect of horizontal seismic forces resulting from RSA

2.2.4 Nonlinear static pushover analysis

Nonlinear static pushover analysis is conducted to validate behavior of nonlinear model and estimate overstrength factor (Ω) and period-based ductility (μ_T) of each building using a pushover curve in Figure 2.5 and Eqs. 2-12 and 2-13. The expected gravity load for analysis is changed from design gravity loads and specified in Eq. 2-14. The expected gravity load is applied prior to pushover load to include a P-Delta effect. The lateral load pattern to push the structure is the first-mode shape of structure.

$$\Omega = V_{\max} / V \quad (2-12)$$

$$\mu_T = \delta_u / \delta_{y,eff} \quad (2-13)$$

$$1.05D + 0.25L \quad (2-14)$$

where

δ_u = Roof displacement used to approximate the ultimate capacity of the seismic force-resisting system as defined in FEMA P695 (Appendix A) at the point of 20% strength loss ($0.8V_{\max}$)

$\delta_{y,eff}$ = Effective yield roof displacement of the seismic force-resisting system as defined in FEMA P695 (Appendix A)

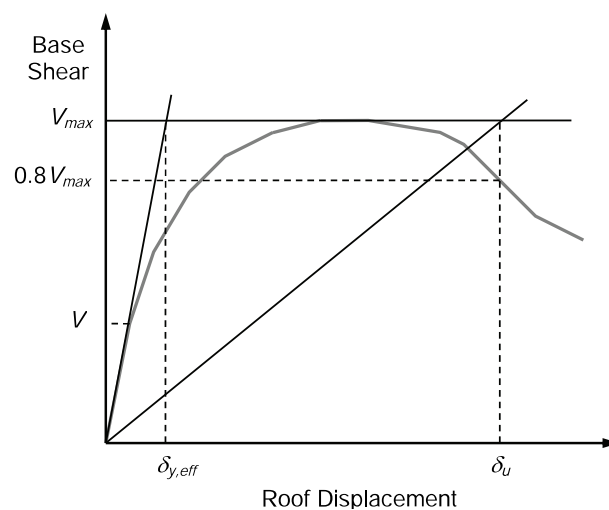


Figure 2.5 Idealized nonlinear static pushover curve (FEMA, 2009).

2.2.5 Incremental dynamic analysis

Incremental dynamic analysis, IDA (Vamvatsioks & Cornell, 2002) is conducted for each sample buildings by conducting several nonlinear response history analysis (NLRHA) using ground motion records. The expected gravity load is applied prior to seismic load to include a P-Delta effect in the same way as pushover analysis (Eq. 2-14).

NLRHA are repeated with ground motion intensities increased until collapse occurred to calculate median collapse capacities (\hat{S}_{CT}) and to calculate *CMR* as shown in Figure 2.6. Figure 2.6 shows an example of Incremental dynamic analysis' results for a building subjected to a set of ground motions with increasing spectral accelerations. In this figure, the governing mechanism is sideways collapse which can be predicted by excessive lateral displacement.

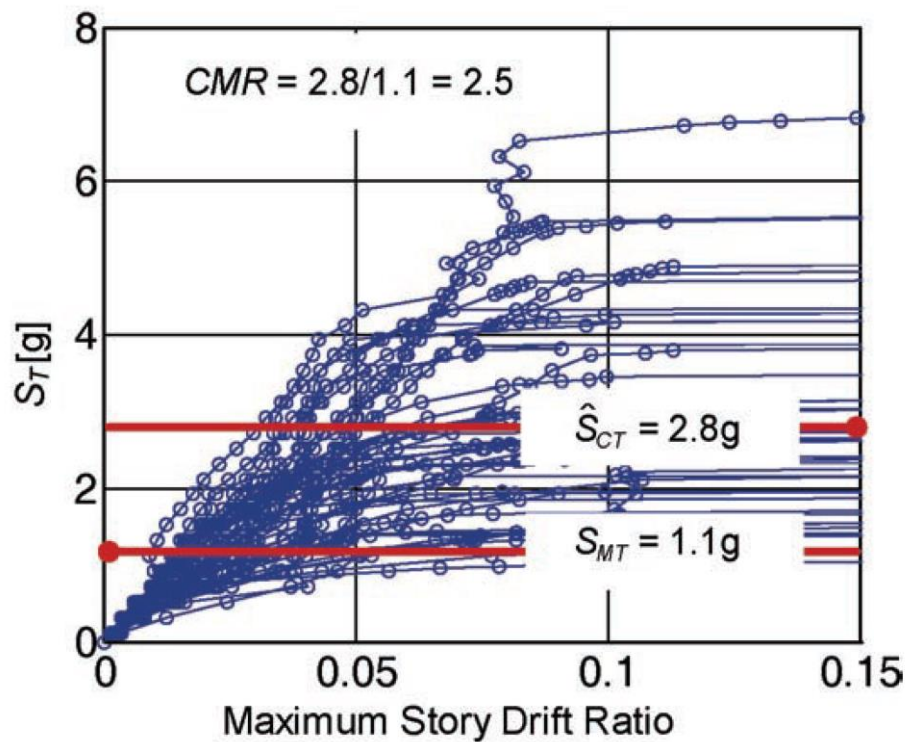


Figure 2.6 Sample incremental dynamic analysis (FEMA, 2009).

2.2.6 Collapse fragility curve

Using collapse data from IDA curves, one can construct a collapse fragility curve which is a cumulative distribution function (CDF), which relates the ground motion intensity to a collapse probability, based on lognormal distribution as shown in Figure 2.7. Note that a number of data points in Figure 2.7 equals to a number of ground motions used in NLRHA. This represents the probability that buildings will form a collapse mechanism given a value of intensity measure in term of spectral acceleration of specific ground motion at collapse level (S_{CT}). Then, CMR is computed by Eq. 2-15.

$$CMR = \frac{\hat{S}_{CT}}{S_{MT}} \quad (2-15)$$

where

S_{CT} = Spectral acceleration of specific ground motion at collapse level

\hat{S}_{CT} = Median value of the estimated spectral acceleration at collapse or at fifty-percent probability of collapse

S_{MT} = the MCE spectral acceleration at the fundamental period of the system (T)

For two-dimensional analyses, all record is applied twice to a structure. First, a ground motion record is oriented in one principal direction and then rotate it to another principal direction. If the structure is symmetric in horizontal directions, the ground motion may not rotate; therefore, reduce numbers of analysis.

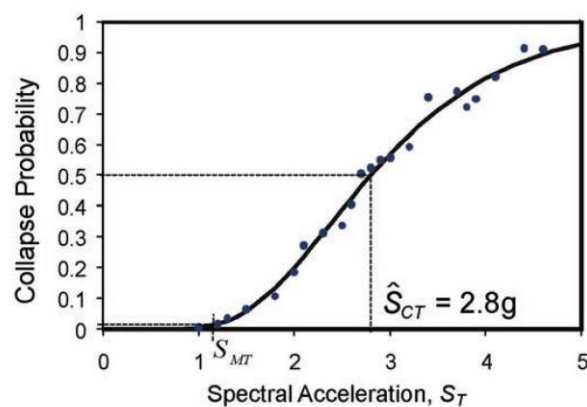


Figure 2.7 Sample collapse fragility curve (FEMA, 2009).

2.2.7 Adjusted collapse margin ratio

Collapse capacity can be significantly influenced by the frequency content or spectral shape of ground motion record. To account for the effects of spectral shape, CMR is modified to the adjusted collapse margin ratio ($ACMR$) by Eq. 2-16. of each sample building.

$$ACMR = CMR \times SSF \quad (2-16)$$

where

CMR = Collapse Margin Ratio

SSF = Spectral Shape Factor is a function of SDC, T , and μ_T provided in Tables A.4-5.

2.2.8 Total system collapse uncertainty

Estimate uncertainties based on quality of each key elements in the collapse assessment process (FEMA, 2009):

1. **Record-to-Record Uncertainty (RTR).** Record-to-record uncertainty is due to variability in the response of index archetypes to different ground motion records. Values of record-to-record variability, β_{RTR} , range from 0.35 to 0.45 typically. A fixed value of $\beta_{RTR} = 0.40$ is assumed in the performance evaluation of systems with period-based ductility greater than 3, $\mu_T \geq 3$. For systems with very limited ductility, values of record-to-record uncertainty can be reduced as follows:

$$\beta_{RTR} = 0.1 + 0.1\mu_T \leq 0.40 \quad (2-17)$$

where β_{RTR} must be greater than or equal to 0.20.

2. **Design Requirements Uncertainty (DR).** Design requirements uncertainty is related to the completeness and robustness of the design requirements, and the level of protection against unanticipated failure modes.
3. **Test Data Uncertainty (TD).** Test data uncertainty is related to the completeness and robustness of the test data used to define the system.

4. **Modeling Uncertainty (MDL).** Modelling uncertainty is related to how well index archetype models represent the full range of structural response characteristics and capture structural collapse behavior.

Each quality rating is calibrated in Tables A.6-8. The total collapse uncertainty (β_{TOT}) is computed using square root of sum of squares (SRSS) of each parameter since these uncertainties are statistically independent:

$$\beta_{TOT} = \sqrt{\beta_{RTR}^2 + \beta_{DR}^2 + \beta_{TD}^2 + \beta_{MDL}^2} \quad (2-18)$$

2.2.9 Acceptable values of $ACMR$

Set the performance objectives based on the acceptable values of $ACMR$: $ACMR_{10\%}$ and $ACMR_{20\%}$. These values are computed based on β_{TOT} in Table A.9. $ACMR_{10\%}$ represents an acceptable value of $ACMR$ for 10% probability of collapse. $ACMR_{20\%}$ represents an acceptable value of $ACMR$ for 20% probability of collapse.

2.2.10 Evaluation of response modification coefficient

Verify that the calculated $ACMR$ is greater than acceptable values of $ACMR$ established by the performance objectives, $ACMR_{10\%}$ and $ACMR_{20\%}$. FEMA P695 set the requirements that acceptable performances are achieved when:

1. The average value of adjusted collapse margin ratio for each performance group exceeds $ACMR_{10\%}$ or the probability of collapse under MCE motions is about 10%, or less, on average across a performance group:

$$\overline{ACMR}_i \geq ACMR_{10\%}$$

2. Individual value of $ACMR$ for each index archetype within a performance group exceeds $ACMR_{20\%}$ or the probability of collapse under MCE motions is about 20%, or less, for each index archetype within a performance group:

$$ACMR_i \geq ACMR_{20\%}$$

If the calculated $ACMR$ satisfies the requirements, the trial R is deemed appropriate. If not, the system needs to be re-defined, and the process is re-iterated until

$ACMR$ is greater than the acceptable values of $ACMR$ by either modifying R or changing the structural system concept in section 2.2.1.

2.2.11 Evaluation of system overstrength factor and evaluation of deflection amplification factor

FEMA P695 computes the overstrength factor (Ω) based on nonlinear static pushover analysis. In general, a unique design of a same system will have different values of Ω . The mean value of each performance group ($\bar{\Omega}_{group}$) is computed for each performance group. The system overstrength factor (Ω_0) is the largest value of mean values of each performance group, and Ω_0 should be conservatively and judgmentally rounded to half unit intervals. Since ASCE 7-05 provides the largest overstrength value of 3.0, the computed overstrength factor has an upper limit of 3.0 in design process.

$$\Omega_0 = \max(\bar{\Omega}_{group}) \quad (2-19)$$

The deflection amplification factor (C_d) is computed based on R and inherent damping of the system as:

$$C_d = \frac{R}{B_I} \quad (2-20)$$

where

B_I = Numerical coefficient found in ASCE 7-05 as set forth in Table A.10 for effective damping, β_I , and period, T

β_I = Component of effective damping of the structure due to the inherent dissipation of energy by elements of the structure, at or just below the effective yield displacement of the seismic force-resisting system in Table A.10 found in ASCE 7-05

CHAPTER 3

DIAGRID STRUCTURES

3.1 Static analysis of diagrid structures

“Diagrid” structure is a new type of braced tube structures. Diagonal members are spread over the facade of the buildings while acting as a perimeter configuration. The diagonal perimeter members are tied together to provide significant overall bending resistance and rigidity. The triangulated sloped column and spandrel beam frame configurations are called “Diagrid” (W. Baker, Besjak, Sarkisian, Lee, & Doo, 2010). These closely spaced diagonal members represent both inclined columns to carry gravity loads and bracing elements to resist lateral forces efficiently. Due to their triangulated configuration, internal forces that arise in the members are mainly axial force, thus, thus minimizing shear racking effects.

In a preliminary stage, one can analysis the diagrid structures by dividing the whole building into a module representing groups of stacking floors. Figure 3.1(a) shows the diagrid module under gravity loads (G) is subjected to the downward vertical force ($N_{G,mod}$) causing the two diagonals being both in compression and the horizontal chord in tension (Mele, Toreno, Brandonisio, & Luca, 2014). Figure 3.1(b) shows the diagrid module under horizontal load (W). The overturning moment (M_w) causes vertical forces at the peak joint of the diagrid modules ($N_{w,mod}$) with direction and intensity of this force depending on the position of the diagrid module, with upward and downward direction and maximum intensity for the modules located on the windward and leeward façades, respectively (Mele et al., 2014). Figure 3.1(c) shows the diagrid module under the global shear (V_w) causing a horizontal force in the apex joint of the diagrid modules ($V_{w,mod}$) which an intensity depends on the position of the module with respect to the direction of wind load (Mele et al., 2014). To be precise, the real triangle module spans over a certain number of stories (floor), and transfer of services loads to the module happens on every floor. This load transfer causes concentrated loads along the diagonal length as shown in

Figure 3.2. Therefore, the moment and shear are expected to present within the module. However, in the actual structure, there is a girder at each floor; this chord (girder) allows for the absorption of the force transferring through the brace, and the moment and shear are minimized in the braces (Mele et al., 2014).

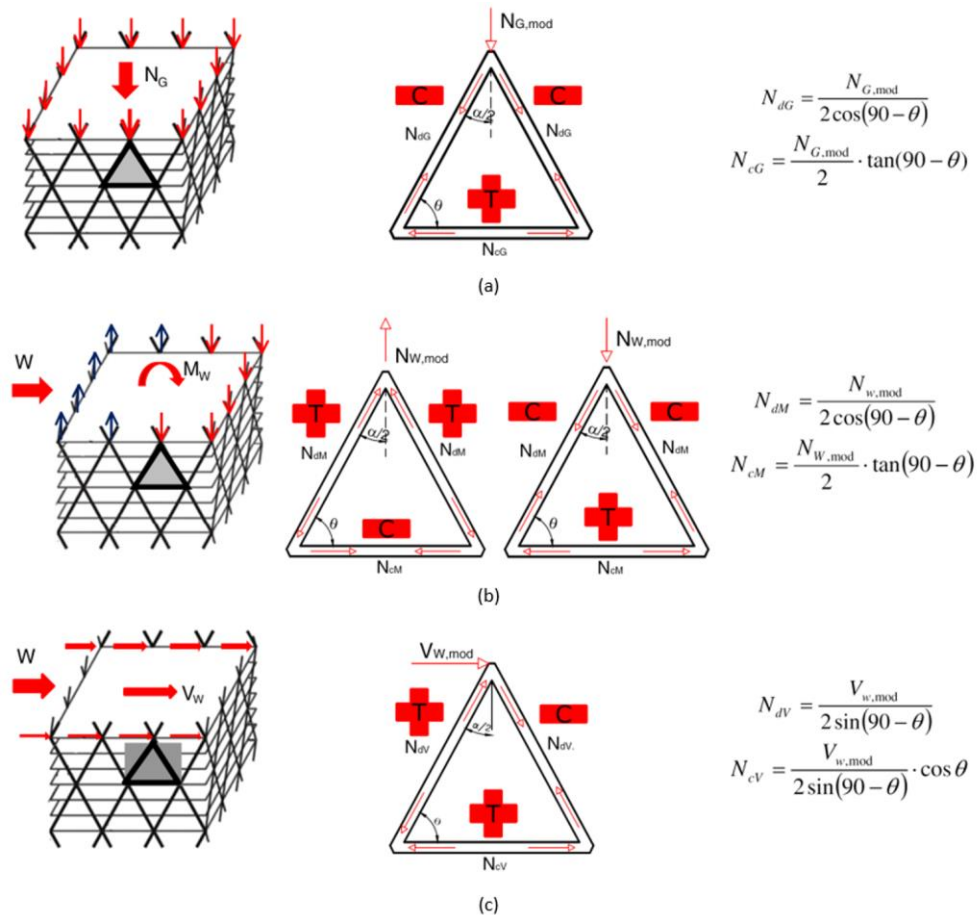


Figure 3.1 Diagrid module: (a) effect of gravity load, (b) effect of overturning moment and (c) effect of shear force (Mele et al., 2014).

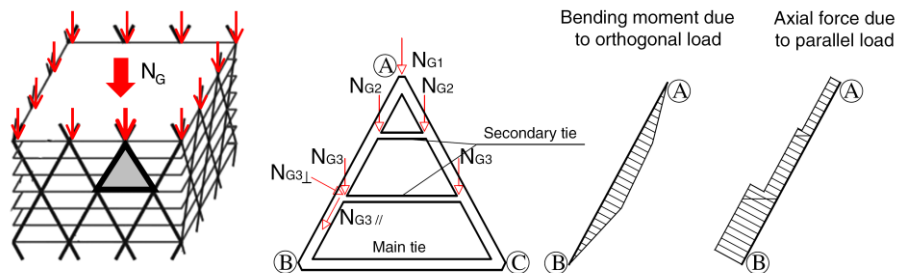


Figure 3.2 Diagrid module: effect of gravity load along the diagonal length (Mele et al., 2014).

3.2 SPFs for steel diagrid

William Baker and his team from Skidmore, Owings & Merrill LLP, studied the seismic performance factors for steel diagrid system (W. Baker et al., 2010). The team followed the procedure in ATC-63 which subsequently published as FEMA P695. They investigated the seismic performance and behavior of steel diagrid framed system in high seismic regions. Typically, steel diagrid framed systems are configured as a dual system for the seismic force-resisting system and their response modification coefficients (R) are selected from 5.5 to 8.0 without further justification since the systems are typically composed of exterior steel diagrid frames in companion with ductile reinforced concrete core-wall frames. However, for standalone exterior diagrid frame, this system is currently classified as an “Undefined System” in ASCE 7-05 provision. Therefore, as an undefined system, it is necessary to establish a methodology to determine appropriate seismic performance factors using a more reliable procedure.

3.2.1 Proposed methodology for steel diagrid framed system

The structural system is considered to have variations in geometrical properties and configurations, such as, a variation of building height-to-width (aspect ratios), and, an angle of sloped columns with intervals of diagrid elements over story heights as shown in Figures 3.3 and 3.4. The total number of models is 300. W. Baker et al. (2010) modeled the diagrid frame as the inclined column. These inclined column elements were modeled using a “Column, Inelastic Fiber section” based on material properties defined as “Inelastic Steel Material, Buckling” in PERFORM-3D modeling space. This definition of section properties captured the tension yielding in a manner of idealized elastic-perfectly plastic yielding while the buckling strength of members was idealized based on the limited compression stress of $0.60F_y$. The force-deformation relationship of typical column element modeling is shown in Figure 3.5 for both axial stress-strain and flexural moment relationships (W. Baker et al., 2010).

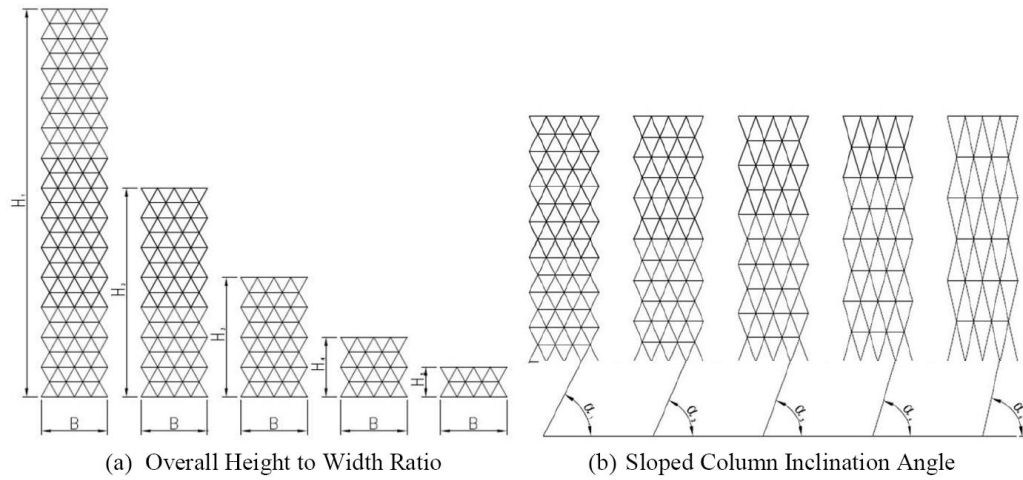


Figure 3.3 Parameters of interest for diagrid (W. Baker et al., 2010).

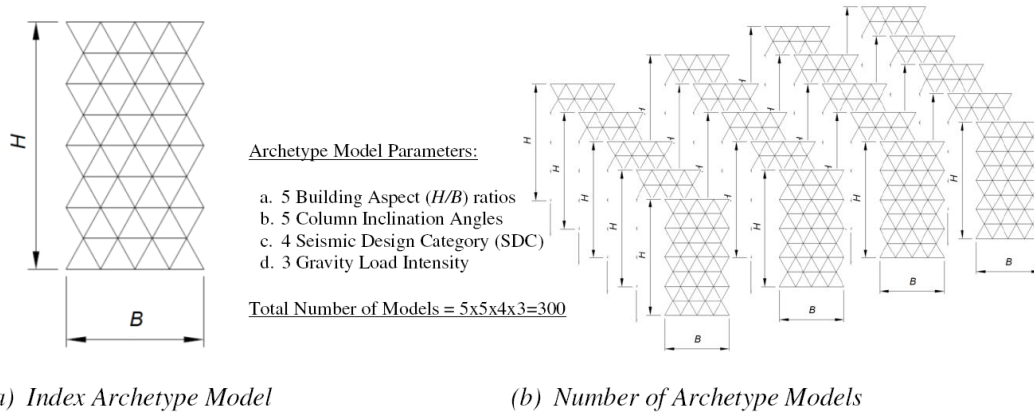


Figure 3.4 Development of archetype models (W. Baker et al., 2010).

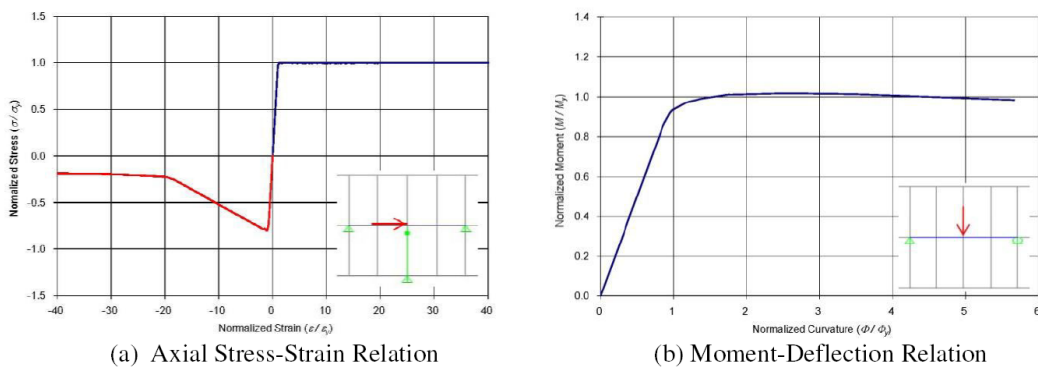


Figure 3.5 Element behavior in analysis model (W. Baker et al., 2010).

3.2.2 Results of steel diagrid framed system

W. Baker et al. (2010) considered the system collapse uncertainties as:

1. Variability between ground motion records $\beta_{RTR} = 0.40$ (for structure with period-based ductility greater than 3, $\mu_T \geq 3$)
2. Uncertainty in the nonlinear structural modeling, $\beta_{MDL} = 0.20$ (the quality rating for modelling is judged good)
3. Quality of test data used to calibrate the element models, $\beta_{TD} = 0.20$ (the quality rating is judged good since a confidence level is high in test results and most important testing issues are addressed).
4. Quality of the structural system design requirements, $\beta_{DR} = 0.20$ (the quality rating is judged good since a confidence level is high in design requirements, and there are reasonable protections against unanticipated failure modes).

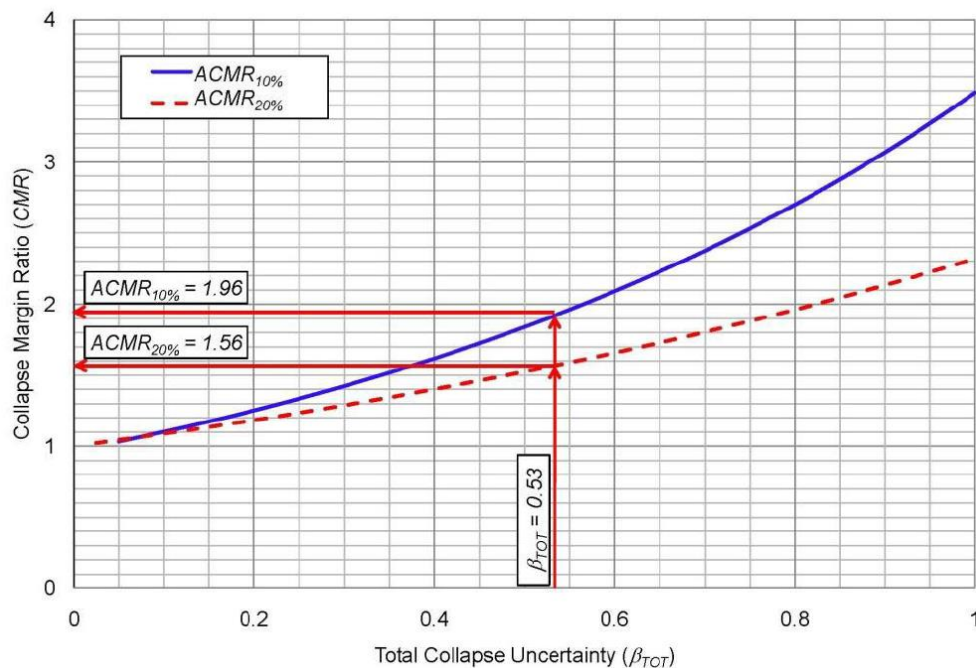


Figure 3.6 Estimation of collapse margin ratio criteria (W. Baker et al., 2010).

Total collapse uncertainty parameter:

$$\beta_{TOT} = \sqrt{0.40^2 + 0.20^2 + 0.20^2 + 0.20^2} = 0.53$$

If the collapse margin ratio, CMR , is calculated as a 1.60 from the nonlinear response history analysis results, the $ACMR$ is calculated as:

$$ACMR = SSF \times CMR = 1.26 \times 1.60 = 2.0$$

With the considered total collapse uncertainty, β_{TOT} , the 10-percent acceptable adjusted collapse margin ratio can be read as 1.96 as shown in Figure 3.6. Since the adjusted collapse margin ratio is greater than the demand required at 10 percent probability of collapse, the performance of a single archetype model is satisfied.

William Baker started the trial value of R from 1.0 to finally 3.64 when the performance no longer met the criteria in FEMA P695. The sample pushover analysis is shown in Figure 3.7. A summary of Results from Figure 3.7 and 3.8 is:

Response Modification Coefficient,	R	=	3.64
Fundamental Period,	T	=	0.8 sec
Base Shear,	V	=	0.11g
	V_{max}	=	0.16g
	$0.80V_{max}$	=	0.13g
Displacement,	$\delta_{y,eff}$	=	3.8 inch
	δ_u	=	14.0 inch
System Overstrength Factor,	$\Omega_0 = \frac{V_{max}}{V} = \frac{0.16}{0.11}$	=	1.5
Period-based ductility,	$\mu_T = \frac{\delta_u}{\delta_{y,eff}} = \frac{14}{3.8}$	=	3.7
Spectral Shape Factor (SDC D_{max}),	$SSF = e^{0.212 \times (1.5 - 0.42)}$	=	1.26
Since,	$\beta_1(0.8) = 0.14 \times (3.7 - 1)^{0.42}$	=	0.212
	$\bar{\epsilon}_0 = 1.5$ for SDC D		
	$\bar{\epsilon}(0.8) = 0.6 \times (1.5 - 0.8)$	=	0.42

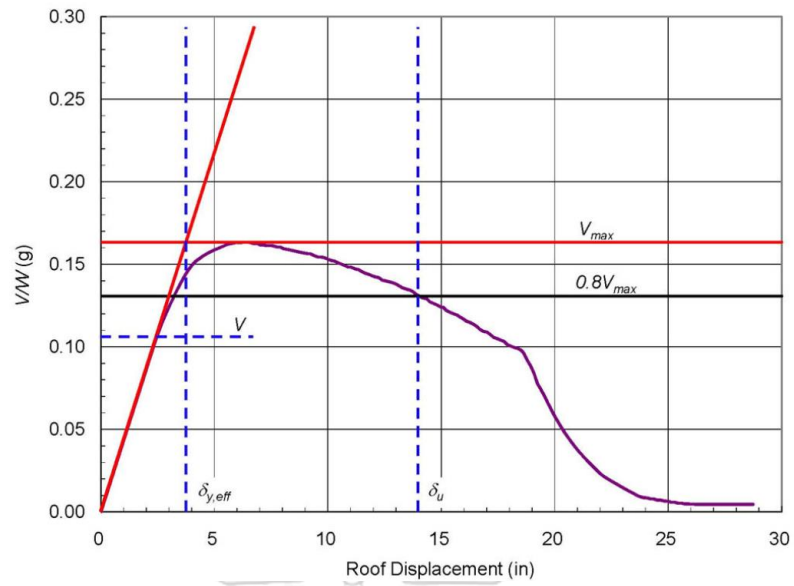


Figure 3.7 Sample nonlinear static pushover curve (W. Baker et al., 2010).

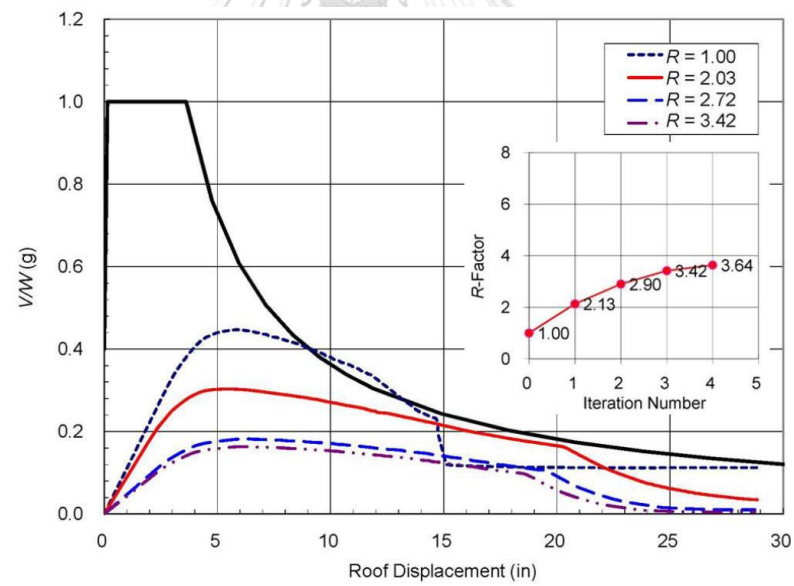


Figure 3.8 Iterative estimation of R-factor (W. Baker et al., 2010).

CHAPTER 4

BUILDINGS AND GROUND MOTIONS

4.1 Performance group

As shown in Table 4.1, the archetype development includes these major grouping criteria: basic configuration, gravity load intensity, seismic design category, and period domain of archetypes. This results in a total of 24 performance groups varying each criterion. FEMA P695 (FEMA, 2009) requires a minimum of 3 archetypes per performance groups to come up with proper mean performance. However, the total of $(3 \times 24 =)$ 72 archetypes is infeasible to complete without computational support in this level of study. The author limits the number of performance groups as shown in Table 4.2:

1. Low Gravity Load is neglected, and consider only one type of load
2. When focusing on tall building, short period is neglected
3. Min SDC is neglected since Max SDC tends to govern seismic demand
4. Finally, to reduce sample size to perform an achievable study, B and C configurations need to be removed.

The only remaining performance group is PG-2 or A-High-Max-Long, shortly, CFT-A group. The total number of archetypes is three. The detail description of archetypes of CFT-A group is explained in the later subsection. In the future study, all neglected archetype needs to be included.

Table 4.1 Index archetype configurations.

Performance Group Summary					
Group No.	Grouping Criteria				Number of Archetypes (3-6 per group)
	Basic Config.	Design Load Level		Period Domain	
		Gravity	Seismic		
PG-1	A	High	Max SDC	Short	≥ 3
PG-2				Long	≥ 3
PG-3			Min SDC	Short	≥ 3
PG-4				Long	≥ 3
PG-5		Low	Max SDC	Short	≥ 3
PG-6				Long	≥ 3
PG-7			Min SDC	Short	≥ 3
PG-8				Long	≥ 3
PG-9	B	High	Max SDC	Short	≥ 3
PG-10				Long	≥ 3
PG-11			Min SDC	Short	≥ 3
PG-12				Long	≥ 3
PG-13		Low	Max SDC	Short	≥ 3
PG-14				Long	≥ 3
PG-15			Min SDC	Short	≥ 3
PG-16				Long	≥ 3
PG-17	C	High	Max SDC	Short	≥ 3
PG-18				Long	≥ 3
PG-19			Min SDC	Short	≥ 3
PG-20				Long	≥ 3
PG-21		Low	Max SDC	Short	≥ 3
PG-22				Long	≥ 3
PG-23			Min SDC	Short	≥ 3
PG-24				Long	≥ 3

Table 4.2 Selected index archetype configurations.

Performance Group Summary					
Group No.	Grouping Criteria				Number of Archetypes (3-6 per group)
	Basic Config.	Design Load Level		Period Domain	
		Gravity	Seismic		
PG-1	A	High	Max SDC	Short	≥ 3
PG-2			Long	≥ 3	
PG-3			Min SDC	Short	≥ 3
PG-4				Long	≥ 3
PG-5		Low	Max SDC	Short	≥ 3
PG-6				Long	≥ 3
PG-7			Min SDC	Short	≥ 3
PG-8				Long	≥ 3
PG-9	B	High	Max SDC	Short	≥ 3
PG-10				Long	≥ 3
PG-11			Min SDC	Short	≥ 3
PG-12				Long	≥ 3
PG-13		Low	Max SDC	Short	≥ 3
PG-14				Long	≥ 3
PG-15			Min SDC	Short	≥ 3
PG-16				Long	≥ 3
PG-17	C	High	Max SDC	Short	≥ 3
PG-18				Long	≥ 3
PG-19			Min SDC	Short	≥ 3
PG-20				Long	≥ 3
PG-21		Low	Max SDC	Short	≥ 3
PG-22				Long	≥ 3
PG-23			Min SDC	Short	≥ 3
PG-24				Long	≥ 3

4.2 Earthquake ground motions

The uniform hazard spectrum (UHS) at MCE level for rock site at downtown Bangkok was first determined. Then, conditional mean spectra (CMS) (J. W. Baker, 2011) at period of interest, called conditioning period, equal 0.2, 0.5, 1, 1.5, 2 and 3 seconds were constructed and ground motions from corresponding magnitude and distance at rock sites were selected to match these CMS spectra. These ground motions and corresponding CMS are shown in Appendix C. The rock ground motions were simulated to propagate through soft soil layers underneath Bangkok by software SHAKE (Jirasakjamroonsri, Poovarodom, & Warnitchai, 2018) and soft soil ground motions were obtained. UHS for soft soil at downtown Bangkok of four cases: DBE with damping ratio of 2.5 and 5 percent and MCE with damping ratio of 2.5 and 5 percent are shown in Figures 4.1 and 4.2. The spectral value at 0 second follows values from CMS 0.5s, and values after 3.0 second follow value from CMS 3.0s. The design of archetype building used DBE level earthquake which is $2/3$ of this soft-soil MCE UHS spectrum. Spectral acceleration from this MCE spectrum for damping ratio of 2.5% at the fundamental period of a sample building is denoted by S_{MT} and used to compute CMR in Eq. 2-15. For each sample building, two sets of the CMS soft-soil ground motions conditioned at period closet to the period of the first and second modes of building were used in nonlinear response history analysis (NLRHA). Each component of ground motions was applied to the structure one direction at a time in analysis process.

Ground motions used in dynamic analyses (NLRHA) were modified. The duration of ground motions was shortened by selecting the durations of 5 to 95 percent based on Arias intensity (Arias, 1970) (Appendix C). The second order baseline correlation (Chiu, 1997) (Appendix C) was used to modify ground motion records, so the ground displacement was limited. By performing these modifications, the running time analysis was reduced such that many IDA can be performed with provided computational effort. The study by Chandramohan (Chandramohan, Lin, Baker, & Deierlein, 2013) shows that by using Arias intensity, the solution of systems may not be different from the whole

duration of record if the collapse failure is based on the intensity (spectral acceleration) of ground motions in incremental dynamic analysis framework. The detail descriptions of full records and analysis ground motions are in Appendix C. The computer software PRISM (Jeong, Lee, & Jang, 2017) was used to generate time history and response spectra in Appendix C. The time integration method was Newmark with $\beta = 0.25$ and $\gamma = 0.5$.

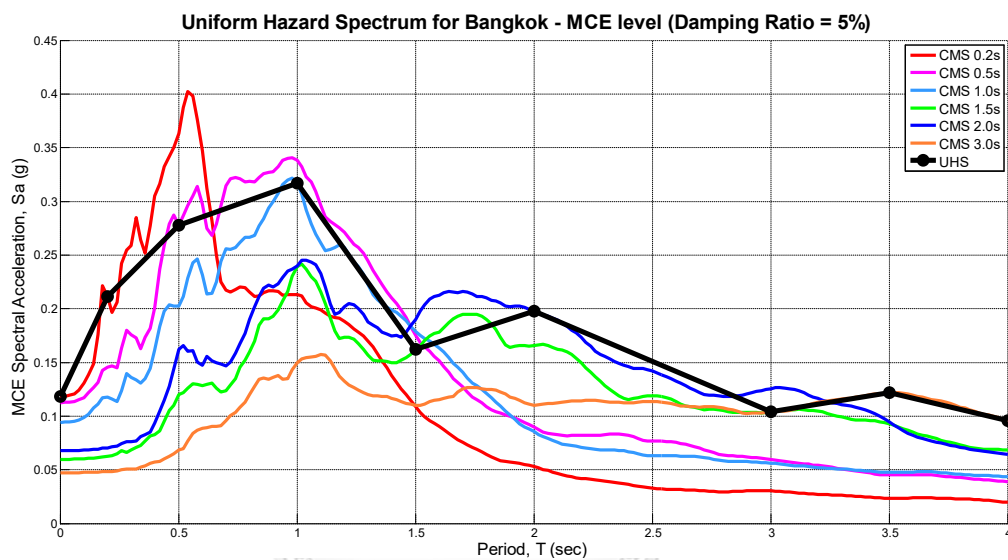


Figure 4.1 Response spectra at MCE level for Bangkok with damping ratio of 5%.

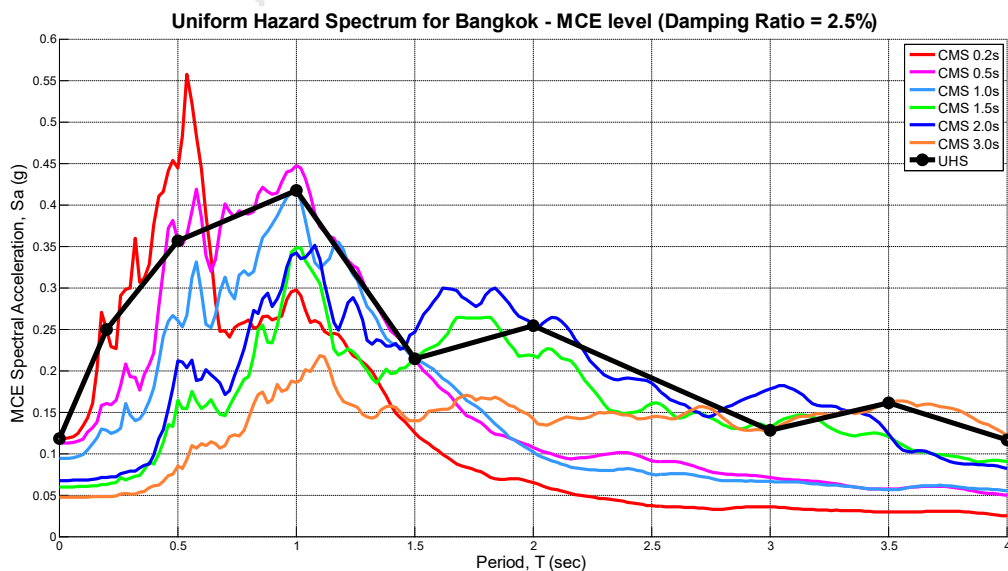


Figure 4.2 Response spectra at MCE level for Bangkok with damping ratio of 2.5%.

Table 4.3 Bangkok response spectrums.

Level (DR)	S_a (0 s)	S_a (0.2 s)	S_a (0.5 s)	S_a (1 s)	S_a (1.5 s)	S_a (2 s)	S_a (3 s)	S_a (3.5 s)	S_a (4 s)
DBE (5%)	0.079	0.141	0.185	0.211	0.108	0.132	0.69	0.081	0.064
MCE (5%)	0.118	0.211	0.278	0.317	0.162	0.198	0.104	0.122	0.096
DBE (2.5%)	0.079	0.167	0.238	0.279	0.143	0.170	0.086	0.108	0.081
MCE (2.5%)	0.118	0.250	0.357	0.418	0.214	0.254	0.129	0.161	0.122

4.3 Description of buildings

The total number of archetypes is three. Each archetype varies based on its height. The three buildings used in this study are 18, 24, and 36 stories. The foundation was assumed to be pin-support. The configuration A is the circular concrete-filled steel tube (CCFT) diagrid with an inclination of 74.5 degrees. All diagrid sections were designed to be compact and highly ductile as specified in section 3.3. The archetypes were designed by RSA method with trial SPFs by using software ETABS (CSI, 2015). In this study, R is 5.0. In NLRHA, each building was subjected to two sets (6 pairs or 12 records) of CMS ground motions whose conditioning periods are closed to the periods of the first and second modes of the building. For two-dimensional analysis, one direction (EW or NS) of ground motions was applied. Therefore, there is a total of (12x3=) 36 IDA curves. The summary of archetype profile is shown in Table 4.4. The modal periods were solved by using Ritz vectors. The story plan of buildings is symmetric in x and y directions and shows in Figure 4.4. All building models are shown in Figures 4.5 to 4.7. The detail descriptions of sample buildings are in Appendix C. The damping ratio of sample buildings is calculated using Eq. 4-1 and in Figure 4.3. Since all heights are higher than 64 meters, damping ratios of all buildings are 2.5 percent. The name of archetype comes

from building's story and R used in design. For example, 18R5 means an 18-story building designed with $R = 5.0$.

$$\zeta_{critical} = \frac{0.2}{\sqrt{H}} \leq 0.05 \quad (4-1)$$

where

H = The height of the roof, excluding mechanical penthouses, above the grade plane, in meter. (For MCE level, the value need not be taken less than 0.025.)

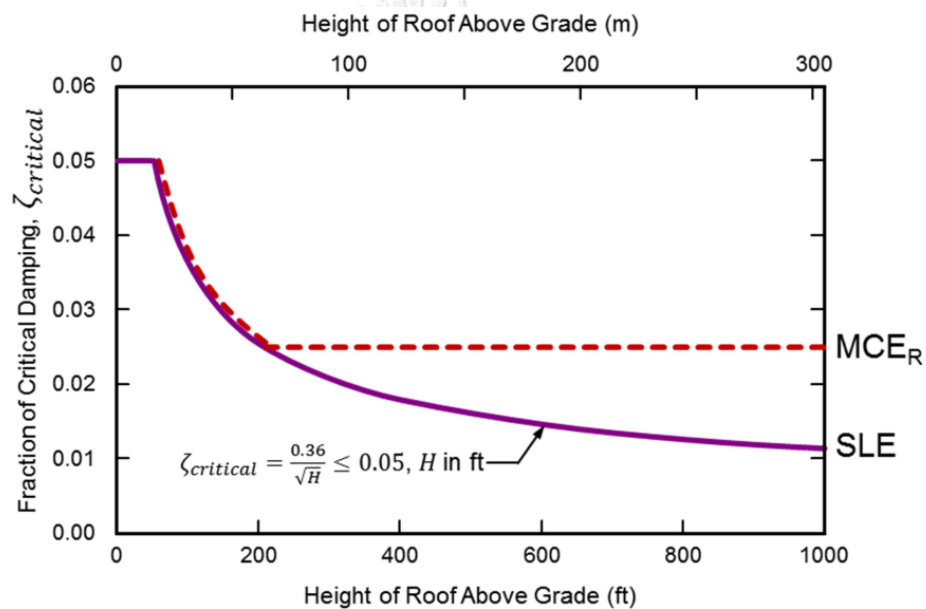


Figure 4.3 Equivalent viscous damping versus building height based on Eq. 4-1 (PEER, 2017).

Table 4.4 Summary of archetype descriptions.

Archetype ID	No. of Stories	Height (m)	Key Archetype Design Parameters							S_{MT} (g)
			SDC	R	T (sec)	T_1 (sec)	T_2 (sec)	C_s (g)	CMS set	
CFT-A (74.5-degree inclination)										
18R5	18@3.6m	64.8	D	5	1.67	1.57	0.83	0.030	1.5s, 0.5s	0.227
24R5	24@3.6m	86.4	D	5	2.06	1.98	1.00	0.033	2.0s, 1.0s	0.2465
36R5	36@3.6m	129.6	D	5	2.79	3.03	1.37	0.021	3.0s, 1.5s	0.155

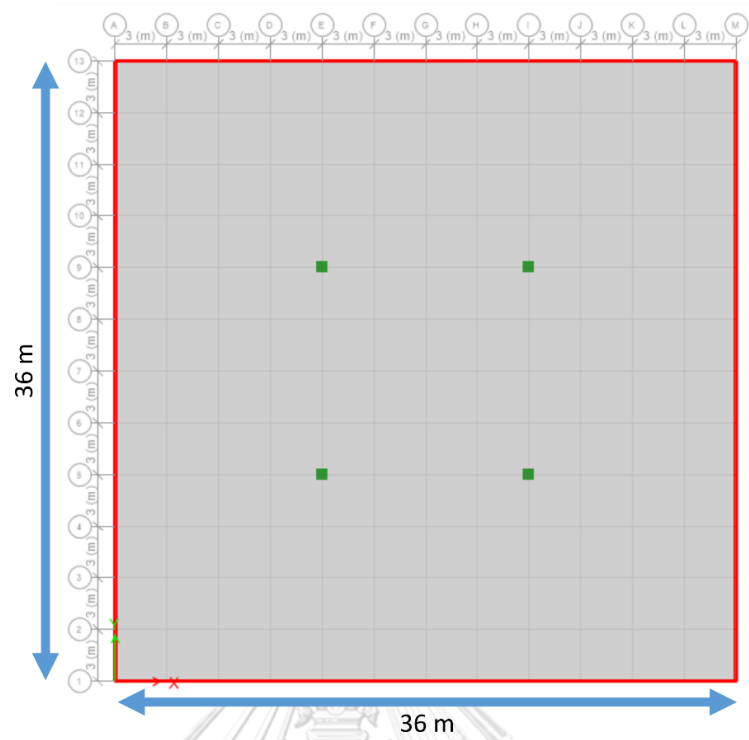


Figure 4.4 Plan view of all buildings in FEM models (CSI, 2015).

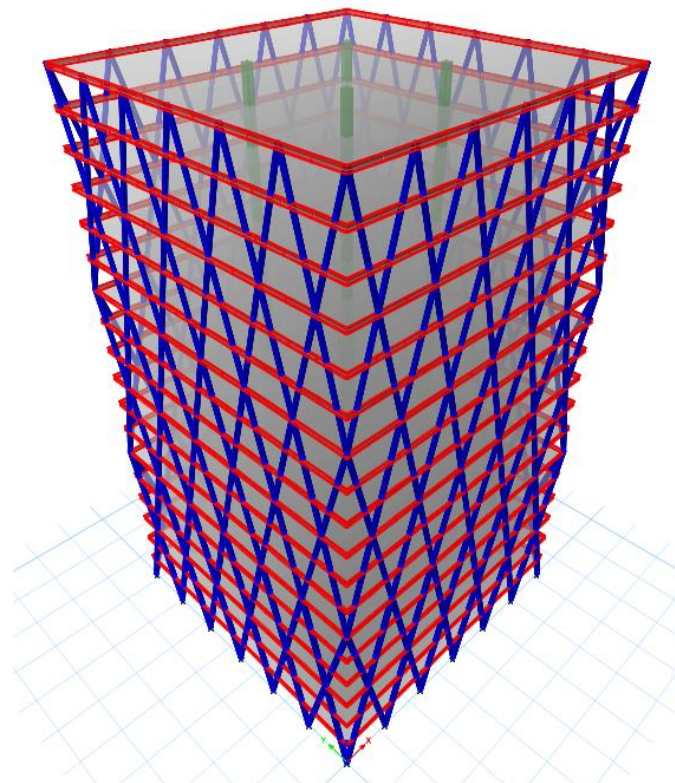


Figure 4.5 3D view of 18R5 in FEM model (CSI, 2015).

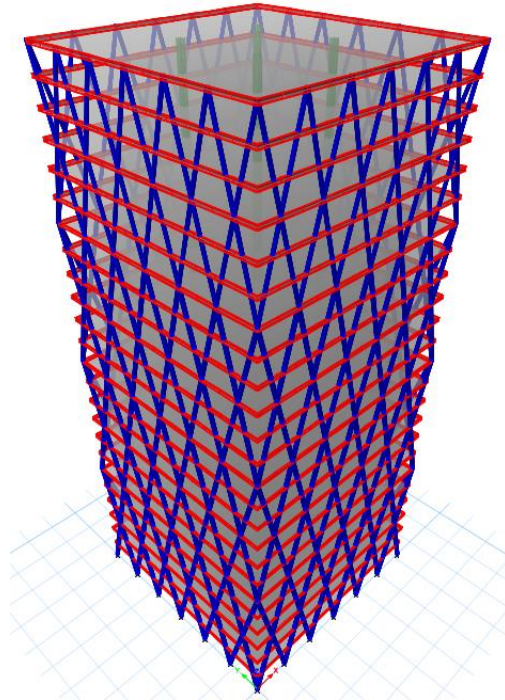


Figure 4.6 3D view of 24R5 in FEM model (CSI, 2015).

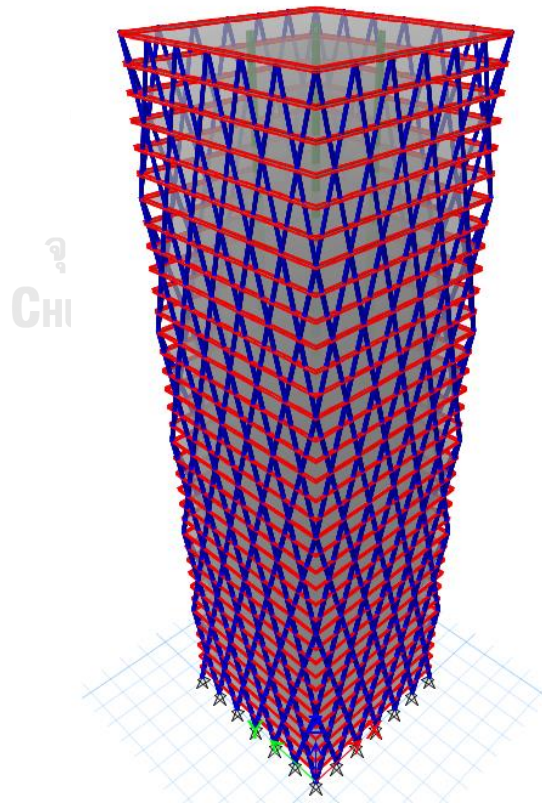


Figure 4.7 3D view of 36R5 in FEM model (CSI, 2015).

4.4 Fiber section of CCFT braces

To develop nonlinear components of archetypes, composite braces of diagrid are defined by nonlinear axial-flexural fiber section hinge. The fiber hinges were developed based on stress-strain curves of steel and concrete. The sections of diagrid were chosen to be compact based on the compactness requirement of AISC 360-10 (AISC, 2010b), and the strength of section were also designed according to the specification of AISC 360-10. The sections of diagrid were chosen to be highly ductile based on the ductility requirement of AISC 341-10 (AISC, 2010a). Furthermore, the expected strength of steel sections was based on AISC 341-10. All these requirements are in Appendix B. Fiber discretization of a CCFT cross section is shown in Figure 3.9. In every hinge, the number of fibers is 21 consisting of 12 steel fibers and 9 concrete fibers.

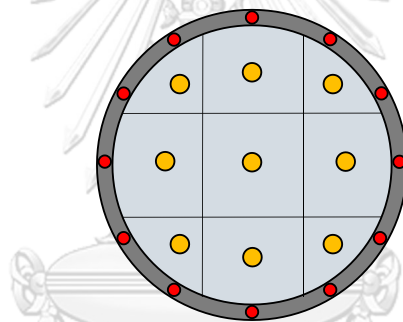


Figure 4.8 Fiber discretization of CCFT cross section.

4.4.1 Steel material

Steel material was modeled by elastic-perfectly-plastic model as shown in Figure 4.9. The steel grade is pipe ASTM A53b with yield strength F_y of 241 MPa and the expected strength is 1.6 times the nominal yield strength, or 386 MPa (Table B.3). The yield strain is at 0.0019, and the ultimate strain is assumed to be 0.23; then, strain at rupture is assumed to be at 0.251. For steel tube with infilled concrete, the local buckling of all designed sections was neglect when considering the study of local buckling effect (Denavit & Hajjar, 2014). The stress-strain is now identical in both tension and compression.

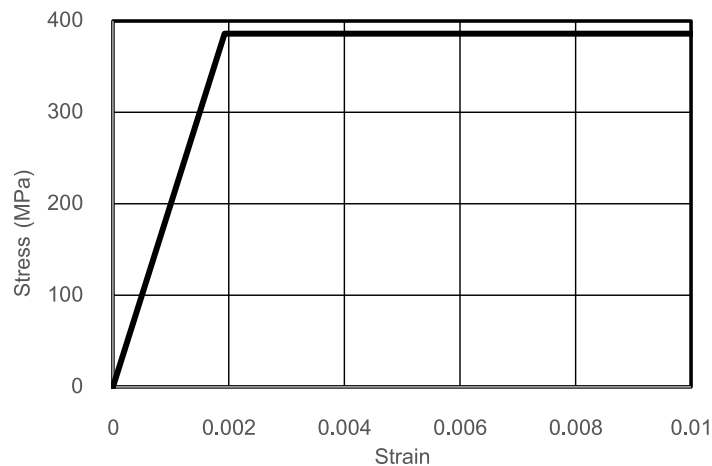


Figure 4.9 Elastic-perfectly-plastic steel material with expected strength equal to 1.6 times nominal yield strength of 241 MPa.

4.4.2 Concrete material

The concrete model followed Denavit and Hajjar (Denavit & Hajjar, 2014) which was adapted from Chang and Mander (Chang & Mander, 1994) by using the monotonic backbone curve following Tsai's equation (Tsai, 1988). The detail description of concrete model is in Appendix B. The tensile strength of concrete was assumed equal to zero in this study. The pre-peak and post-peak behavior of concrete is controlled by ratio of diameter to thickness of steel tube. The stress-strain relation is shown in Figure 4.10. The ultimate strain is assumed to be 0.05. All concrete has a specific compressive strength (f'_c) of 6 ksi or 42 MPa.

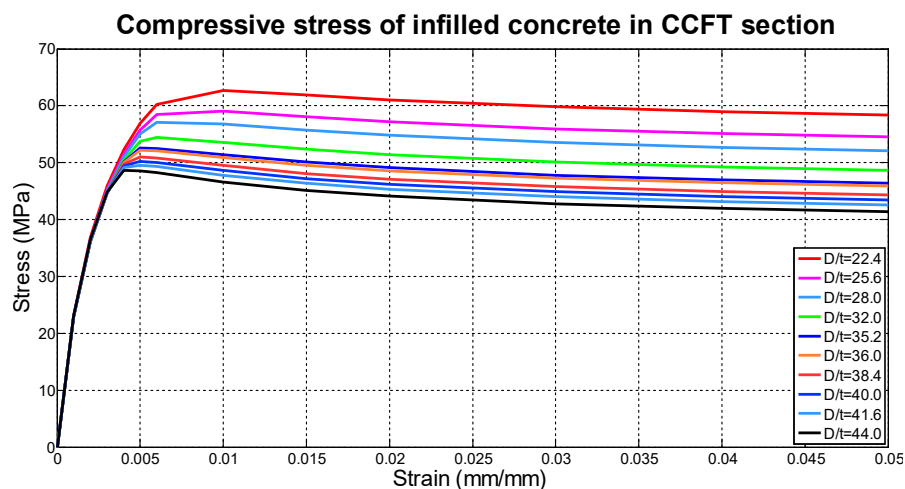


Figure 4.10 Stress-strain relation of confined concrete in CCFT based on D/t ratio.

4.4.3 Diagrid module

Diagrid module represents two triangulated trusses spanning over six stories as shown in Figure 4.11. The braces are made of a circular concrete-filled tube (CCFT). The beams are typical steel wide flange. The axial-flexural fiber hinge is assigned at the middle of braces or relative length of 0.5. The hinge length equals to the length of member such that when the members fail in axial stress, there is no axial stress left in the whole member. The inclination of this study is 74.5 degree.

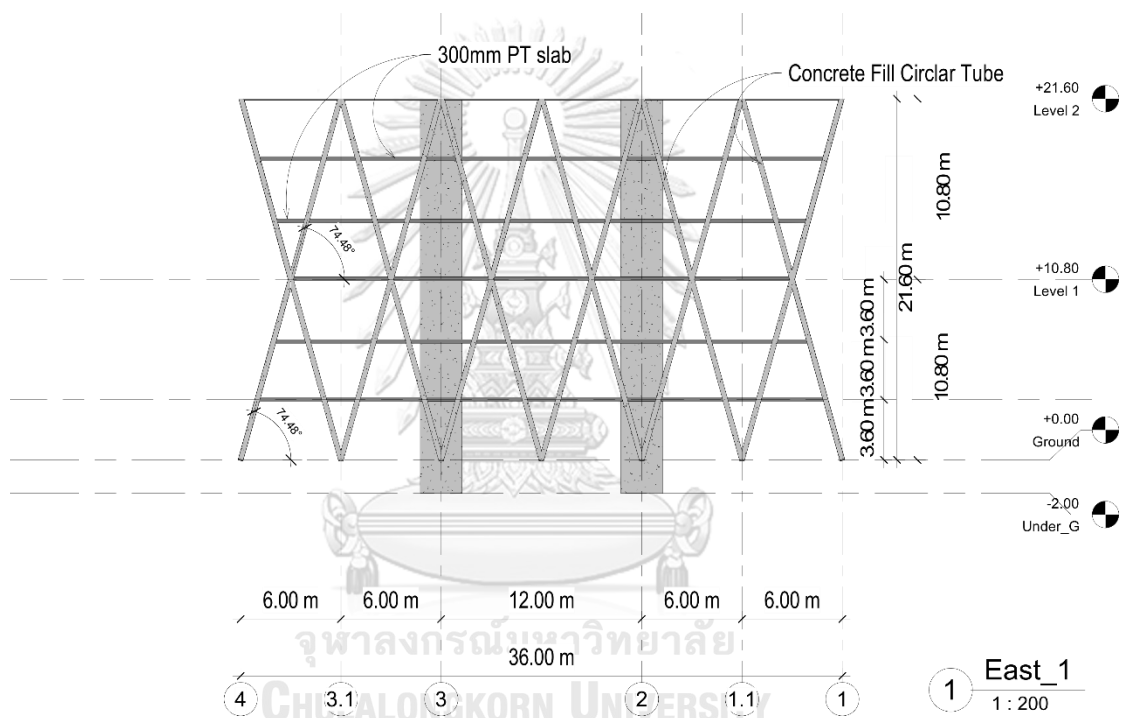


Figure 4.11 Sample 6-story diagrid module.

CHAPTER 5

RESULTS

5.1 Pushover analysis

For each building, pushover analysis was using the first-mode shape as lateral load pattern to push the structure. First, a gravity load of $1.05DL+1.05SDL+0.25LL$ is applied by using nonlinear analysis considering P-Delta effect (Figure 5.1). Next, pushover analysis is conducted by using first-mode shape as lateral load pattern (Figure 5.2). The analysis was considered complete when a base shear is dropped to 80% of maximum base shear or until the step size is less than $5E-5$. Only one direction is considered since the models are symmetry in x and y directions. The overstrength parameter, Ω , and period-based ductility, μ_T , then computed for each building as in section 2.2.4. Then, SSF for each building was computed based on Table A.5 in case of SDC D. The summary of pushover static analyses is in Table 5.1. The pushover curves are shown in Figures 5.3 to 5.5.

Steps in pushover analysis:

1. Apply nonlinear gravity load case: $1.05(DL+SDL)+0.25LL$
2. Apply pushover load with load type as: 1st mode shape including P-Delta effect.
3. Load application is displacement control with monitored displacement at roof's joint.
4. The target displacement is assumed to be at least 2% of building height.
5. Increase the target displacement until the pushover curve passes through the peak point and falls.
6. The building is assumed to collapse, and analysis is stopped when (a) base shear fall until 80% of maximum base shear or (b) after the peak point, the solution's step size is shown to be smaller than $5E-5$ sec (solution needs to be in negative slope).

General

Load Case Name: push_gravity [Design...]

Load Case Type: Nonlinear Static [Notes...]

Exclude Objects in this Group: Not Applicable

Mass Source: Previous

Initial Conditions

Zero Initial Conditions - Start from Unstressed State

Continue from State at End of Nonlinear Case (Loads at End of Case ARE Included)

Nonlinear Case: []

Loads Applied

Load Type	Load Name	Scale Factor
Load Pattern	Dead	1.05
Load Pattern	SuperDL	1.05
Load Pattern	Liveload	0.25

[Add] [Delete]

Other Parameters

Modal Load Case: Modal

Geometric Nonlinearity Option: P-Delta

Load Application: Full Load [Modify/Show...]

Results Saved: Final State Only [Modify/Show...]

Nonlinear Parameters: Default [Modify/Show...]

Figure 5.1 Nonlinear gravity loads applied (CSI, 2015).

General

Load Case Name: push_mode1 [Design...]

Load Case Type: Nonlinear Static [Notes...]

Exclude Objects in this Group: Not Applicable

Mass Source: Previous

Initial Conditions

Zero Initial Conditions - Start from Unstressed State

Continue from State at End of Nonlinear Case (Loads at End of Case ARE Included)

Nonlinear Case: push_gravity

Loads Applied

Load Type	Load Name	Scale Factor
Mode	1	1

[Add] [Delete]

Other Parameters

Modal Load Case: Modal

Geometric Nonlinearity Option: P-Delta

Load Application: Displacement Control [Modify/Show...]

Results Saved: Multiple States [Modify/Show...]

Nonlinear Parameters: User Defined [Modify/Show...]

Figure 5.2 Performing pushover by pushing in first mode direction (CSI, 2015).

Table 5.1 Pushover static results.

ID	T (s)	T_1 (s)	W (kN)	V_{max} (kN)	$V_{dyn-str}$ (kN)	Ω	δ_u (m)	$\delta_{y,eff}$ (m)	μ_T	SSF
18R5	1.67	1.57	262077	125779	6705	18.8	3.301	0.499	6.62	1.54
24R5	2.06	1.98	358475	151724	10190	14.9	4.105	0.669	6.13	1.52
36R5	2.79	3.03	555088	133510	9952	13.4	7.529	0.823	9.15	1.61

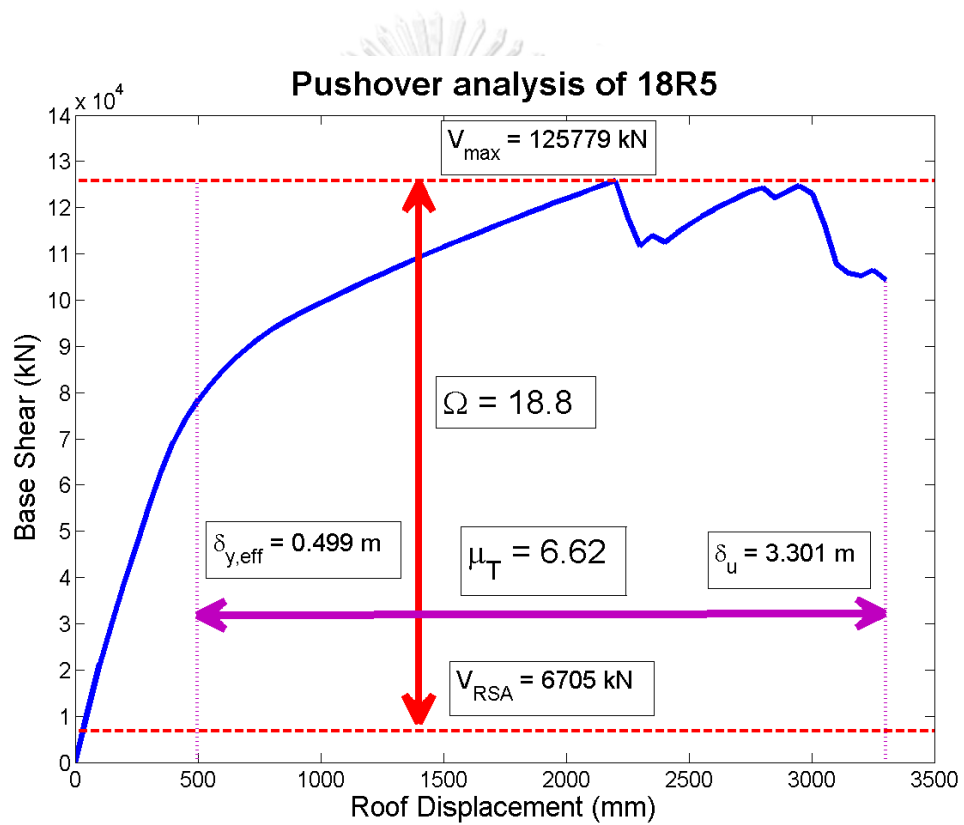


Figure 5.3 Pushover curve of 18R5.

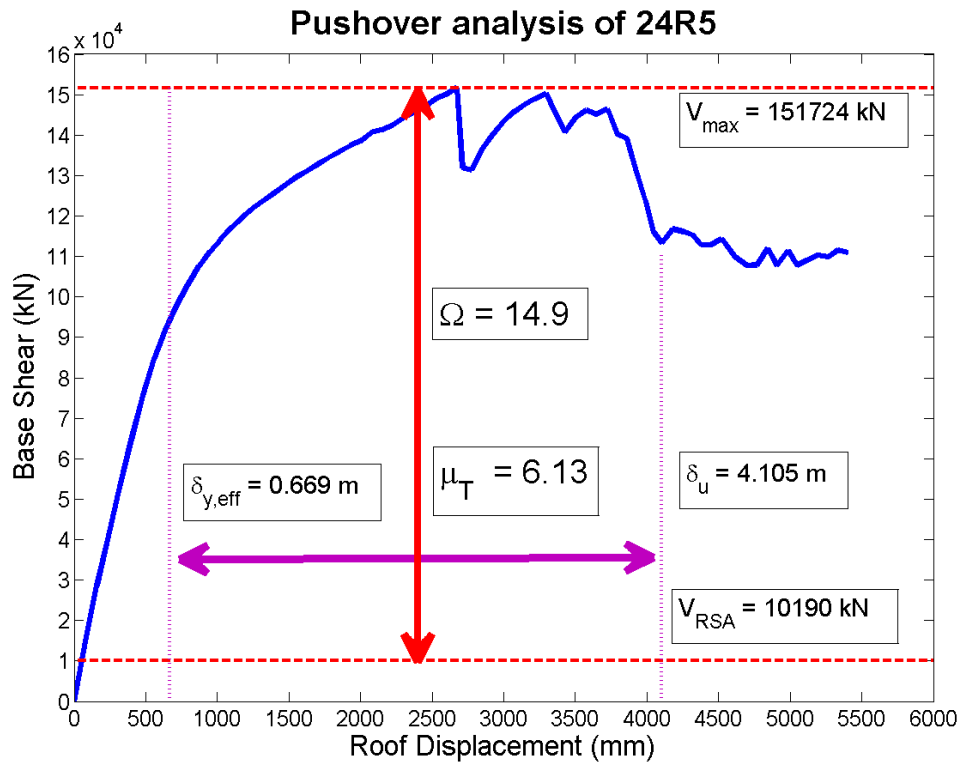


Figure 5.4 Pushover curve of 24R5.

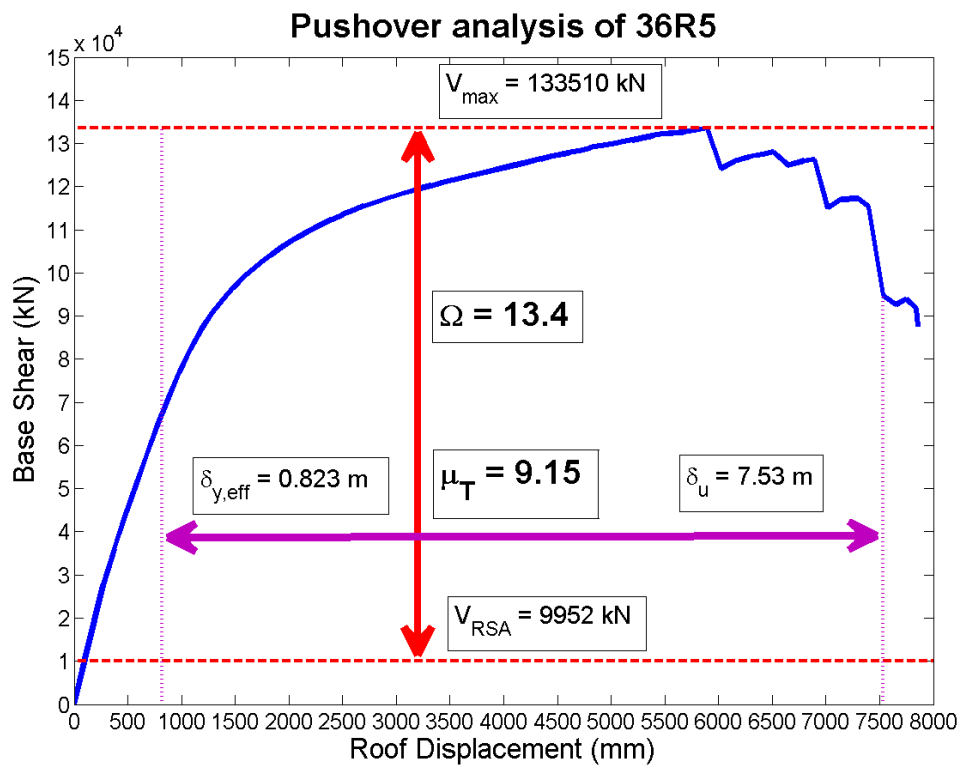


Figure 5.5 Pushover curve of 36R5.

From analysis, all buildings have a similar value of overstrength factor and period-based ductility. All buildings do not show a limited ductility defined as period-based ductility less than 3. All buildings show a high value of overstrength; the detailed sources of overstrength are explained in Appendix D.

5.2 Nonlinear response history analysis

The modal type for dynamic analysis was solved by Ritz vectors with applied loads: *all gravity load, all translational and rotational movement* (Figure 5.6). First, the models were subjected to nonlinear time history of gravity load of $1.05(DL+SDL)+0.25LL$ represented by ramp function (Figures 5.7 to 5.8). Subsequently, the nonlinear response history analyses (NLRHA) were performed with ground motions on translational x direction (Figures 5.9 to 5.10). NLRHA were performed with increasing scale factor to ultimately perform incremental dynamic analyses (IDA) or pushover dynamic analyses. For each scale factor, NLRHA provided scaled spectral acceleration and corresponding maximum inter-story drift ratio of models. NLRHA were performed repeatedly with ground motions scaled by increasing scaling factors until the inter-story drift ratio exceeded 3% which is a recommended limit level for MCE_R shaking (PEER, 2017) for damage measure.

General

Modal Case Name: Ritz [Design...]

Modal Case Sub Type: Ritz [Notes...]

Exclude Objects in this Group: Not Applicable

Mass Source: MsSrc1

P-Delta/Nonlinear Stiffness

Use Preset P-Delta Settings [iterative based on loads] [Modify/Show...]

Use Nonlinear Case (Loads at End of Case NOT Included)

Nonlinear Case: []

Loads Applied

Load Type	Load Name	Maximum Cycles	Target Dyn. Par. Ratio, %
Acceleration	UX	0	99
Acceleration	UY	0	99
Acceleration	UZ	0	99

[Add] [Delete]

Other Parameters

Maximum Number of Modes: 12

Minimum Number of Modes: 1

Figure 5.6 Modal analysis with Ritz vectors based on gravity loads and horizontal accelerations (CSI, 2015).

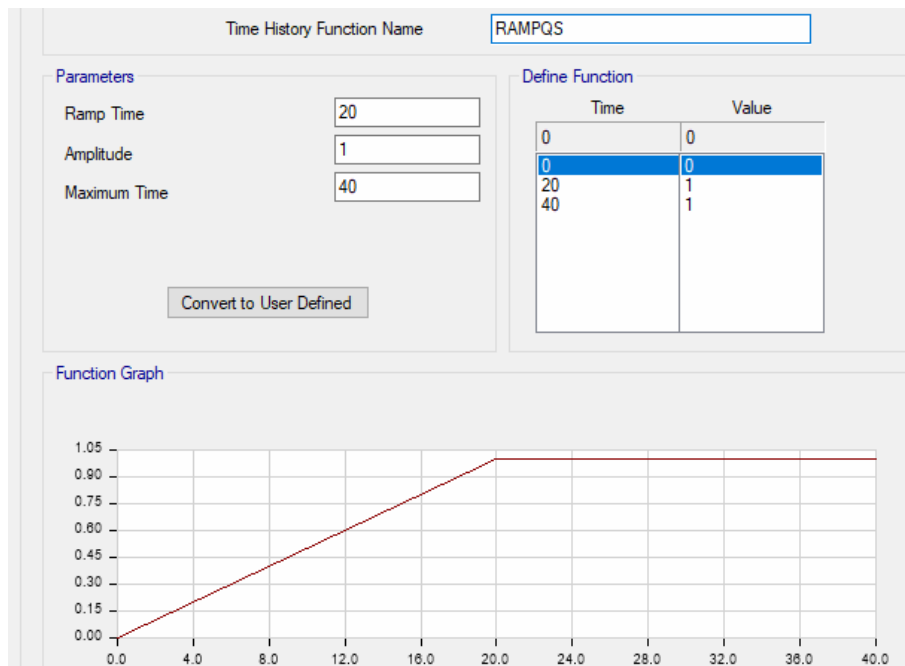


Figure 5.7 RAMPQS function for static load pattern (CSI, 2015).

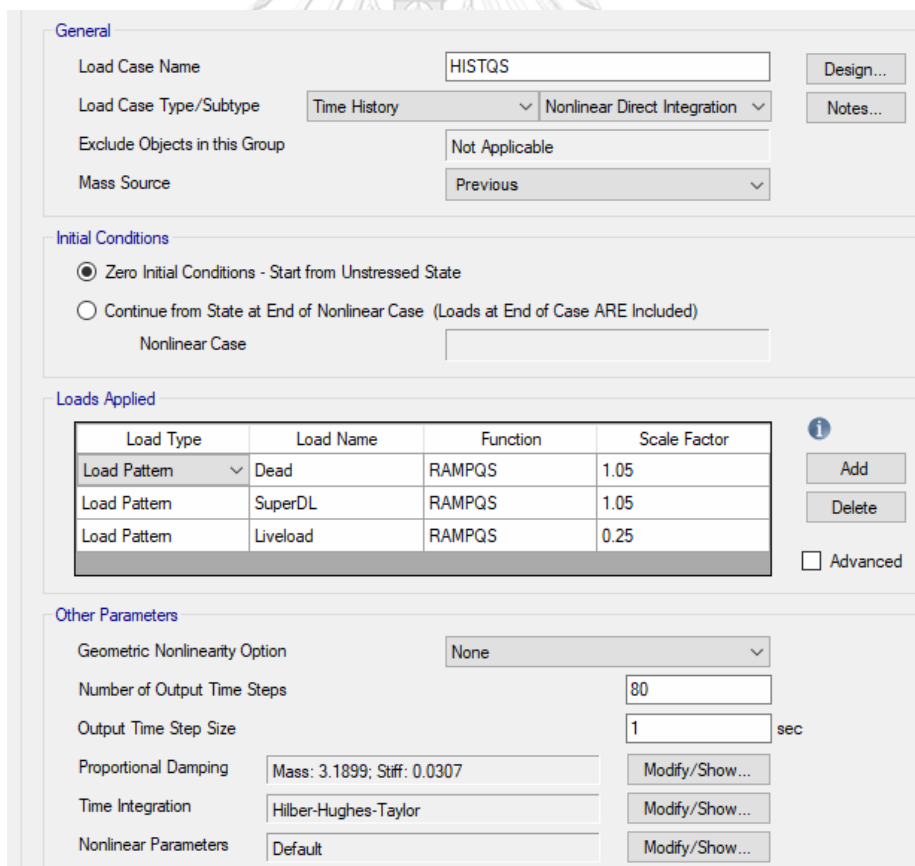


Figure 5.8 Initial nonlinear gravity loads for response history analysis (CSI, 2015).

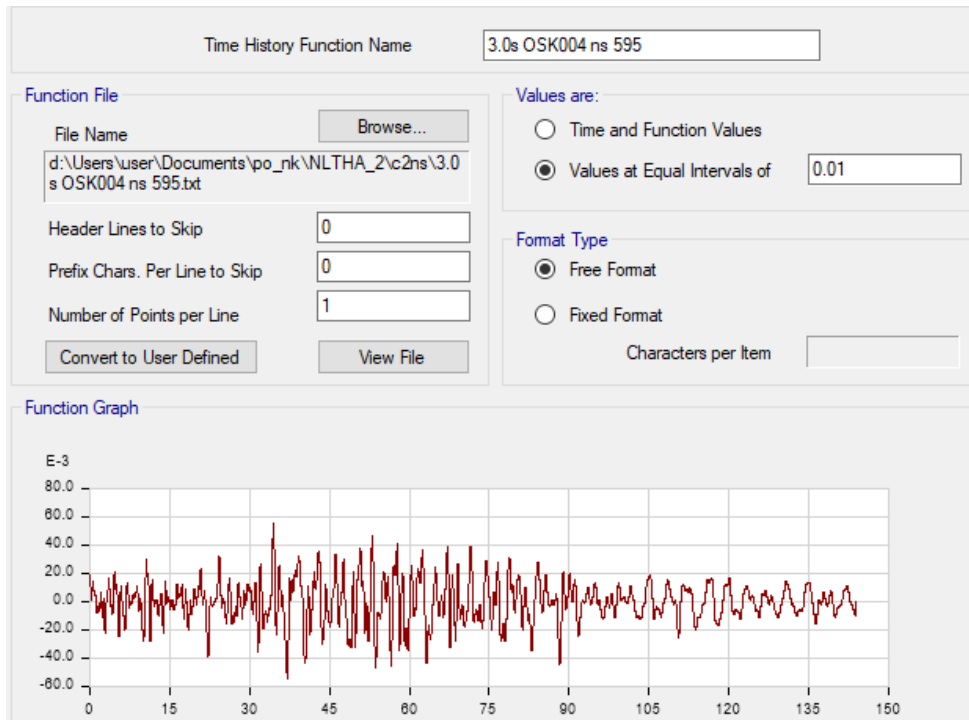


Figure 5.9 Sample time history function (CSI, 2015).

General

Load Case Name: c2ns sf4 [Design...]

Load Case Type/Subtype: Time History [Nonlinear Direct Integration] [Notes...]

Exclude Objects in this Group: Not Applicable

Mass Source: Previous

Initial Conditions

Zero Initial Conditions - Start from Unstressed State

Continue from State at End of Nonlinear Case (Loads at End of Case ARE Included)

Nonlinear Case: HISTQS

Loads Applied

Load Type	Load Name	Function	Scale Factor
Acceleration	U1	3.0s OSK004 ns 595	1544.8

[Add] [Delete] [Advanced]

Other Parameters

Geometric Nonlinearity Option: P-Delta

Number of Output Time Steps: 1439

Output Time Step Size: 0.1 sec

Proportional Damping: Mass: 0.0766; Stiff: 0.0008 [Modify/Show...]

Time Integration: Hilber-Hughes-Taylor [Modify/Show...]

Nonlinear Parameters: User Defined [Modify/Show...]

Figure 5.10 Sample NLRHA (CSI, 2015)

5.3 Incremental dynamic analysis

Incremental dynamic analyses (IDA) were performed to compute CMR of individual buildings. For each building, the selected ground motion records consist of a total of 2 CMS sets or 6 pairs or 12 records based on a first and second period compared to conditional periods of ground motions. Since the buildings were designed to be symmetric in x and y directions, only one direction of acceleration on building needed to be considered; therefore, twelve ground motion records were analyzed for each building individually. In this study, the damage measure is inter-story drift ratio and when it exceeds 3%, the building fails life safety (LS) performance level, and collapse is assumed to occur (PEER, 2017). For each building, NLRHA were performed repeatedly with selected ground motions scaled by increasing scale factors of ground accelerations until the corresponding inter-story drift ratio exceeded 3%. In summary, one building has 12 IDA curves due to 12 ground motions. IDA curves for each building are shown in Figures 5.11 to 5.13.

Steps in incremental dynamic analysis:

1. Create a Ramp function for nonlinear gravity load case
2. Perform nonlinear response history analysis of gravity load: $1.05(DL+SDL)+0.25LL$ applied as a Ramp function. The constant modal damping for all modes is 99% as recommended in CSI manual (CSI, 2015). The time integration method is Hilber-Hughes-Taylor.
3. Then, perform nonlinear response history analysis of one ground acceleration in X direction (one direction in this study). Choose arbitrary scale factor for ground motion. For example, scale factor is chosen as 4g; this represents 4 times the intensity of MCE level. P-Delta effect need to be included. The constant modal damping for all modes is 2.5%. The time integration method is Hilber-Hughes-Taylor.
4. In this study, the minimum solution substep size is chosen as 5E-5 sec. If the substep size yields this size, the building is assumed to occur, and the analysis is stopped.

5. After conducting NLRHA for a ground motion, check the corresponding maximum inter-story drift of building.
 - a) if drift ratio is greater than 3%, the next scaling factor must be reduced.
 - b) If drift ratio is less than 3%, the next scaling factor must be increased.
 - c) If drift ratio is within $3 \pm 0.2\%$, the analysis stops. Obtain the required spectral acceleration that causes this drift ratio to collapse level (S_{CT}) and go to step (8).
6. Reperform NLRHA until obtain the result of step 5(c) or obtain 2 solutions that are relatively close to 3% drift (one less than 3% and one greater than 3%). In this study, after one obtains 2 solutions that are between 3% drift, one may compute the required spectral acceleration at collapse S_{CT} by linear interpolation between the point before and after 3% drift.
7. Repeat steps 3-6 for other ground motions.
8. Compute the geometric mean of all spectral acceleration that causes collapse S_{CT} ; obtain \hat{S}_{CT} .

$$\hat{S}_{CT} = \text{average}(\ln(S_{CT,i}))$$
9. Compute collapse margin ratio as a ratio of geometric mean of spectral accelerations to MCE spectral acceleration of building.

$$CMR = \frac{\hat{S}_{CT}}{S_{MT}}$$

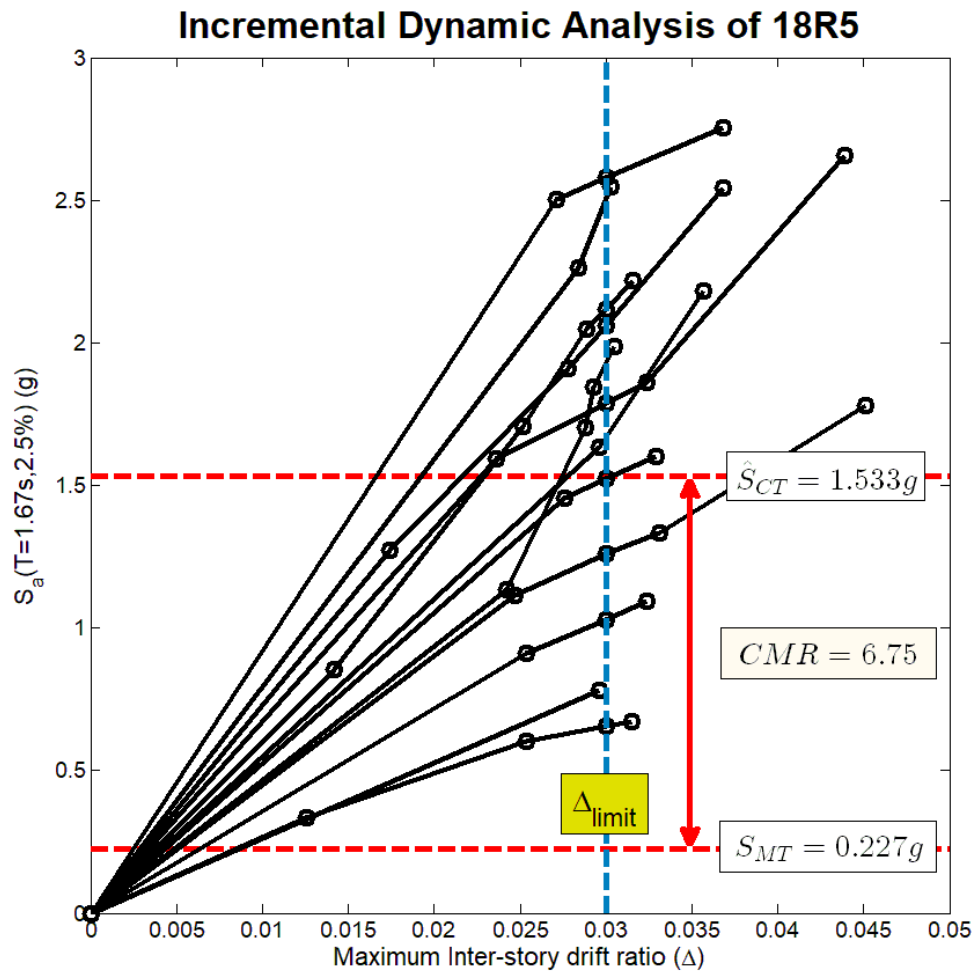


Figure 5.11 IDA results of 18R5.

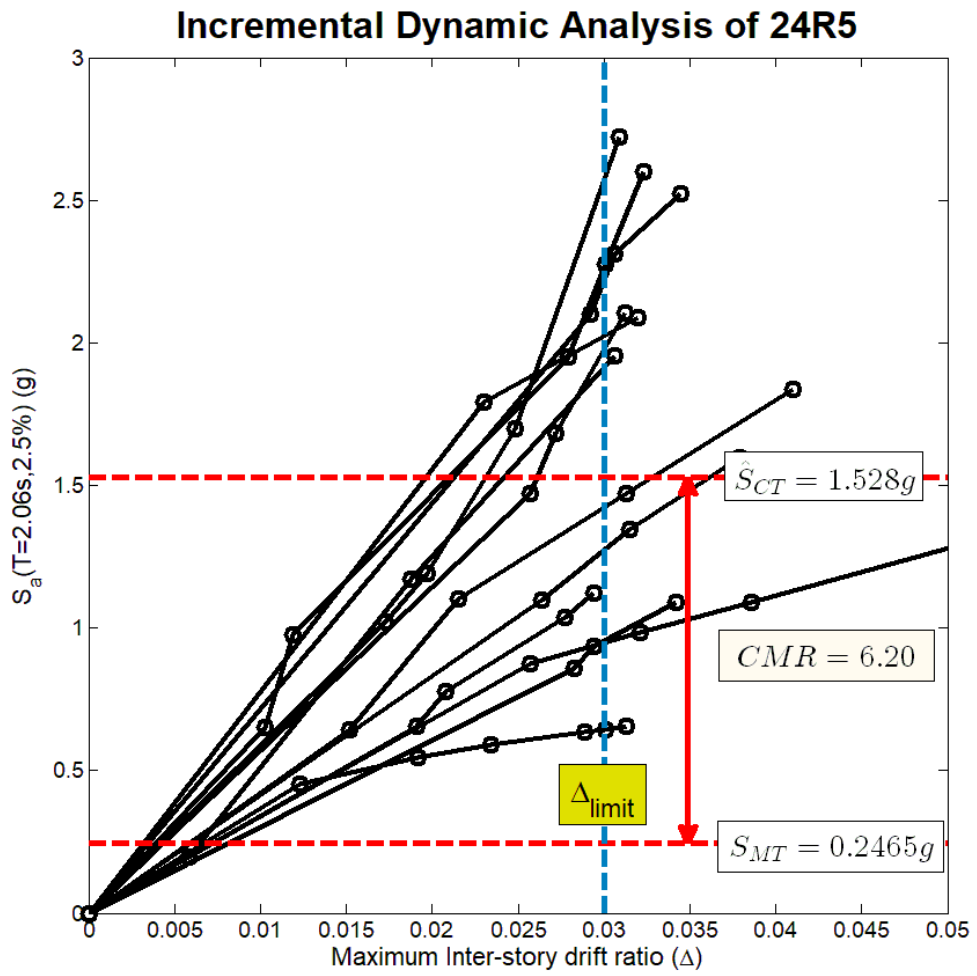


Figure 5.12 IDA results of 24R5.

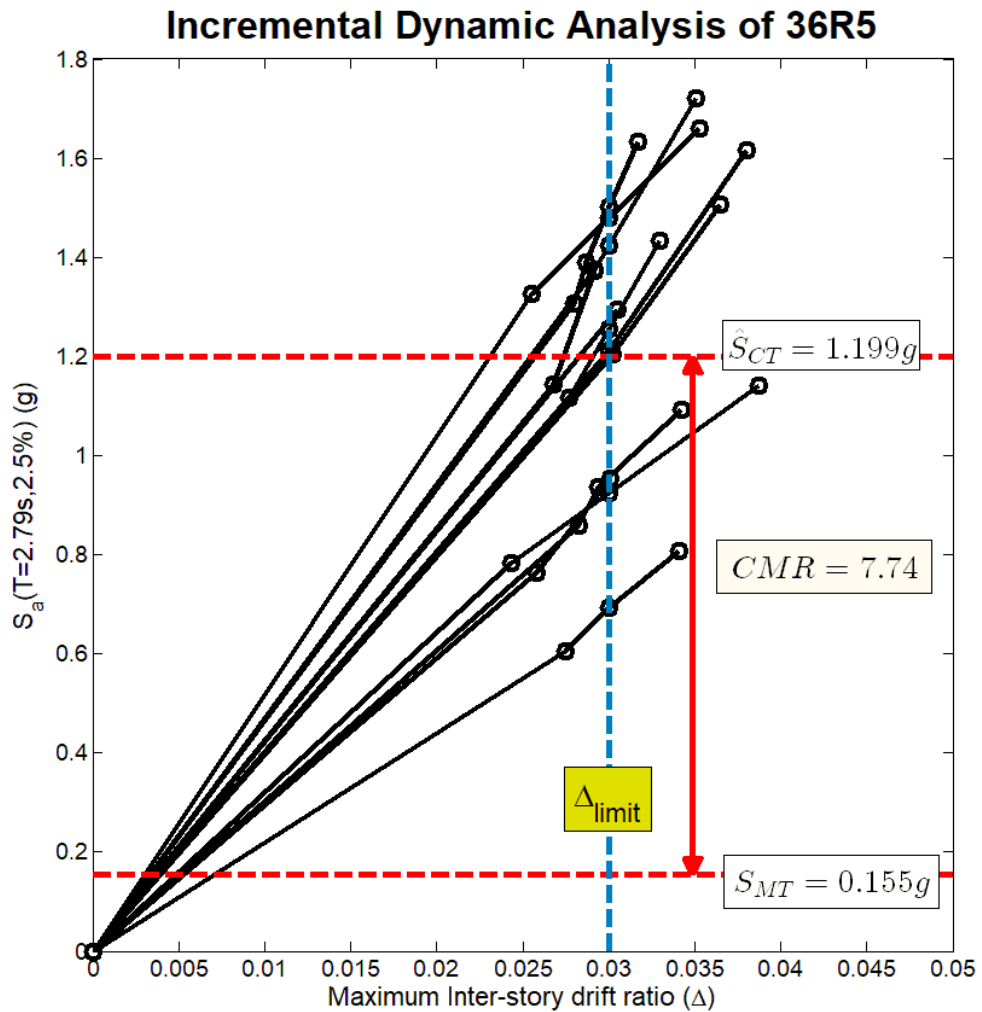


Figure 5.13 IDA results of 36R5.

The results show that all buildings have a high value of collapse margin ratio. With the given limit state, all buildings show a high level of seismic performance and require a very high spectral acceleration to collapse them. Due to variations of ground motions, results may be different if one chooses different ground motions to conduct incremental dynamic analysis.

5.4 Collapse uncertainty

These are assumptions used to estimate uncertainties of the system to evaluate seismic performance factors:

- Uncertainty in variability of ground motions, $\beta_{RTR} = 0.40$ (since the period-based ductility of *all sample building* is greater than 3; $\mu_T \geq 3$).
- Uncertainty in accuracy of design objectives, $\beta_{DR} = 0.20$ (since the failure modes of nonlinear members were limited to only tension and compression failure due to compact and ductile section of members with moderate confidence in design requirements. The sample buildings were designed based on current design code. The quality rating was justified to be (B) Good).
- Uncertainty in comprehensive test data to develop structural members, $\beta_{TD} = 0.20$ (since the nonlinear model was developed from reliable and accurate fiber model. The quality rating was justified to be (B) Good).
- Uncertainty in ability of nonlinear analysis modeling, $\beta_{MDL} = 0.35$ (limited numbers of sample building but the model comprehensively reflects the main modes of failure: tension and compression failure of diagrid. The quality rating was justified to be (C) Fair).

Total system collapse uncertainty is computed as a SRSS of four uncertainties:

$$\beta_{TOT} = \sqrt{\beta_{RTR}^2 + \beta_{DR}^2 + \beta_{TD}^2 + \beta_{MDL}^2}$$

$$\beta_{TOT} = \sqrt{0.40^2 + 0.20^2 + 0.20^2 + 0.35^2} = 0.60$$

The acceptable values of *ACMR* of 10% and 20% probability of collapse were computed from Table A.8.

Table 5.2 Collapse uncertainties of archetypes

ID	Variability of Ground Motions (β_{RTR})	Quality of Design Requirements (β_{DR})	Quality of Test Data (β_{TD})	Quality of Nonlinear Modeling (β_{MDL})	Total System Collapse Uncertainty (β_{TOT})	Group Criteria $ACMR_{10\%}$	Individual Criteria $ACMR_{20\%}$
All	0.40	0.20	0.20	0.35	0.60	2.16	1.66

5.5 Collapse fragility curve

The collapse probability data points from IDA together with the fragility curves based on a lognormal cumulative distribution function (CDF) as defined in FEMA P695 are shown in Figures 5.14 to 5.16. From data points, one can follow the empirical CDF or combinatorial probability (Chompoothawach, 2009) which represents the equally like outcome for each sample. For FEMA P695 method, the lognormal CDFs are defined by using the mean (μ) equal to $\ln(\hat{S}_{CT})$ and the standard deviation (σ) equal to β_{RTR} .

Steps in constructing collapse fragility curve:

1. First, spectral acceleration data from each IDA curve are used to construct empirical CDF. This method will produce an equally like outcome or combinatorial probability. By order of magnitude, each spectral acceleration at collapse from each ground motion will increase a probability of collapse by $1/n$.
 - a) Rank value of spectral acceleration at collapse from each ground motion from smallest to largest.
 - b) Then, assign a probability of each point by order and increase by $1/n$; i.e., the first point has a probability of collapse of $1/n$; the next point has a probability of collapse of $2/n$. Finally, the final point will have a probability of collapse of 1.0.
2. Second, FEMA P695 uses a lognormal CDFs to construct collapse fragility curve. There are two parameters required to construct CDFs.

- a) Mean value (μ): geometric mean of S_{CT} : the average value of natural logarithm of S_{CT} ; $\hat{S}_{CT} = \text{average}(\ln(S_{CT,i}))$.
- b) Standard deviation (σ): β_{RTR} as computed by Eq. 2-17.
3. By plotting collapse fragility curve, one can interpret the probability of collapse of this building given the spectral acceleration value. Moreover, it visualizes a concept of CMR.

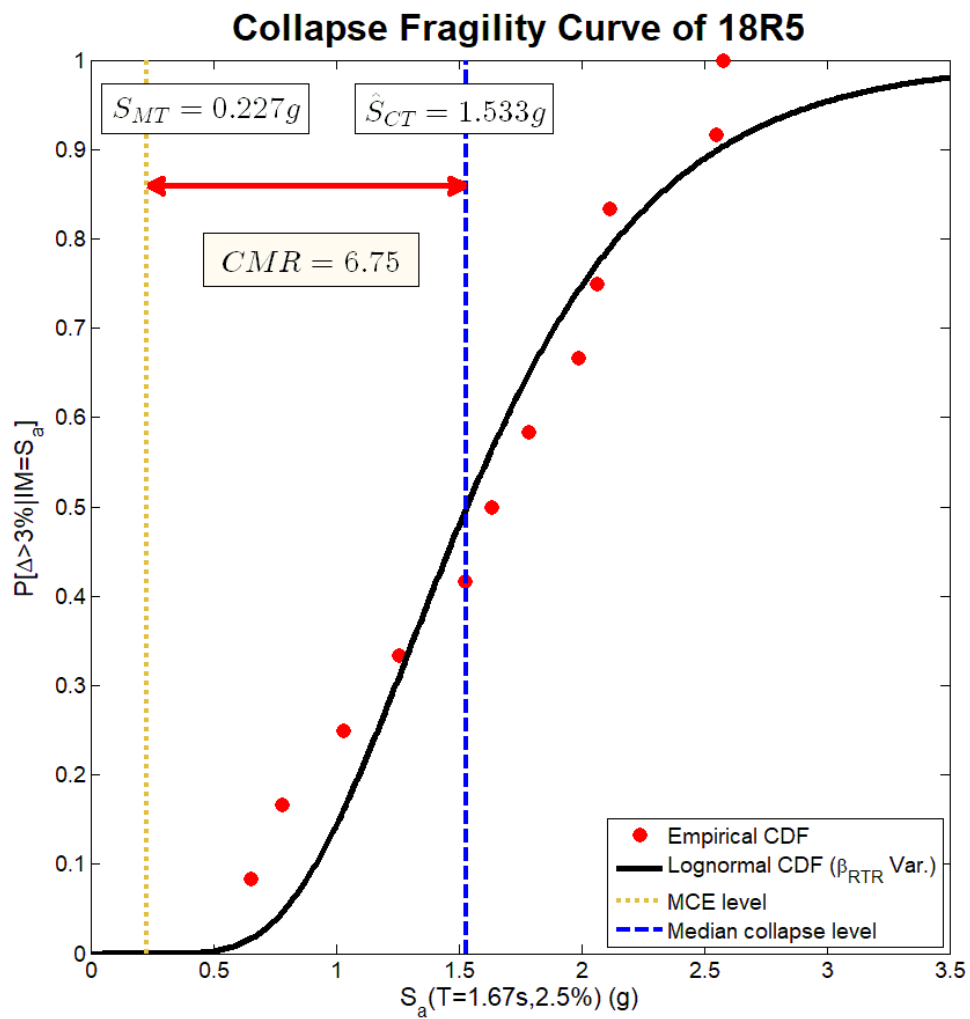


Figure 5.14 Collapse fragility curve of 18R5.

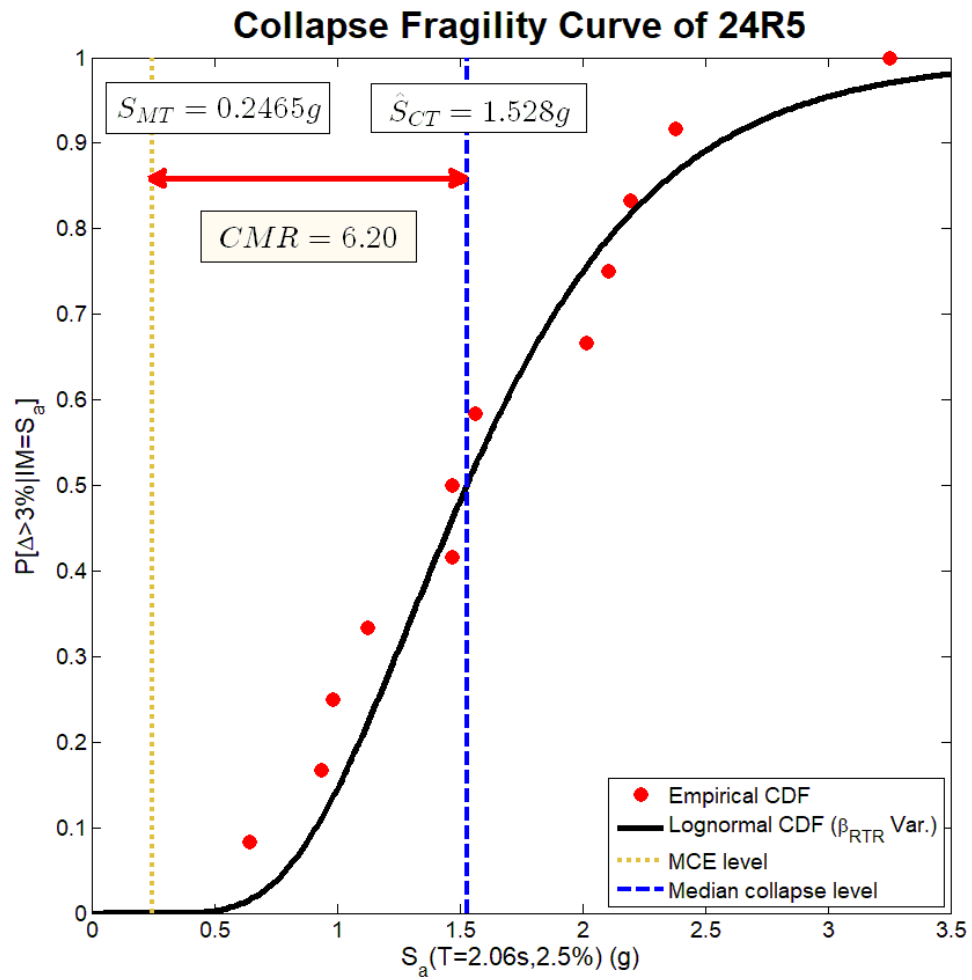


Figure 5.15 Collapse fragility curve of 24R5.

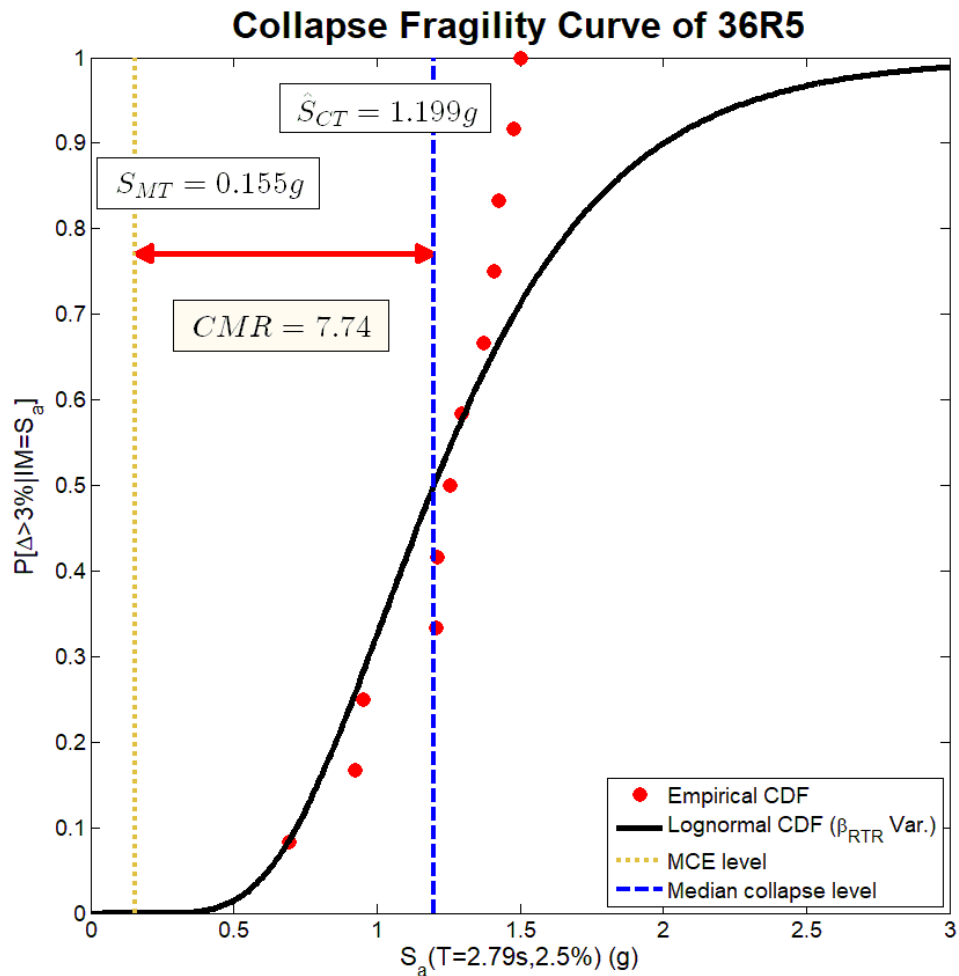


Figure 5.16 Collapse fragility curve of 36R5.

CHULALONGKORN UNIVERSITY

The lognormal CDF constructed from FEMA P695 method shows a good fitting to empirical CDF of sample buildings. Nonetheless, for 36R5, since many ground motions cause similar collapse level spectral accelerations, using an empirical CDF causes a graph to be steep. Using different ground motions for 36R5 can make the curve less steep. These collapse fragility curves are helpful to visualize how spectral acceleration of ground motion events relate to the probability of collapse of buildings. Without calculation, one can interpret roughly a probability of collapse at MCE level spectral acceleration. In this case, all sample buildings have a very low probability of collapse.

5.6 Seismic performance factors

To evaluate the response modification coefficient (R), $ACMR$ of sample building and average value of $ACMR$ across the performance group must be checked. $ACMR$ can be computed as a product of CMR and SSF . To verify that seismic performance of sample buildings are acceptable or has a low probability of collapse at MCE intensity, values of $ACMR$ have to be greater than the acceptance value of adjusted collapse margin ratio at 10% and 20% ($ACMR_{10\%}$ & $ACMR_{20\%}$) computed in section 5.4.

In Table 5.3, seismic performances of sample buildings designed by using $R = 5$ have been verified, and $ACMR$ is greater than the criteria for individual and average values; therefore, seismic performances of sample buildings are deemed acceptable. A value of R can be used as 5.0.

Next, the system overstrength factor (Ω_0), according to FEMA P695, needs to be greater than the average value across performance group and rounded up. In this study, Ω_0 needs to be greater than 13. Nonetheless, this value cannot be greater than 3.0 since the upper bound value prescribed in ASCE 7 is 3.0; therefore, the recommended value of Ω_0 to use in design is 3.0.

Finally, the deflection amplification factor (C_d) is evaluated by Eq. 2-20. For system with effective damping less than 5%, a damping coefficient, B_I , is less than 1.0. This will produce a C_d value which is greater than R . This contradicts with values provided in ASCE 7. In ASCE 7, values of C_d have never been specified to be greater than R . Therefore, a value of C_d should be used as a value of R ; C_d can be used as 5.0.

Table 5.3 Summary of collapse margins and comparison to acceptance criteria

ID	Analysis results							Acceptance Check	
	Ω	μ_T	SSF	S_{MT} (g)	\hat{S}_{CT} (g)	CMR	ACMR	Acceptable ACMR	Pass/Fail
18R5	18.8	6.62	1.54	0.227	1.533	6.75	10.40	1.66	Pass
24R5	14.9	6.13	1.52	0.2465	1.528	6.20	9.42	1.66	Pass
36R5	13.4	9.15	1.61	0.155	1.199	7.74	12.46	1.66	Pass
Average	<u>15.7</u>						<u>10.76</u>	2.16	Pass



CHAPTER 6

CONCLUSIONS

6.1 Summary

This study investigated the seismic performance of CCFT diagrid buildings: 18, 24 and 36-story located in Bangkok. Each building was subjected to 2 sets of CMS ground motions based on first and second modal periods. Using methodology in FEMA P695, it is found that the appropriate SPFs for the regular floor plan buildings using circular concrete-filled steel tube diagrid located at the exterior frame are as follows: $R = C_d = 5.0$ and $\Omega_0 = 3.0$. These values are based on the assumed uncertainties. If the quality ratings were judged to be higher than assumed, then a higher value of R may be plausible.

These SPFs are correlated with the values provided for composite concentrically braced frames in ASCE 7-05. CCFT diagrid systems can use the same SPFs values as the traditional composite braced frame systems. The result is consistent with the study by W. Baker et al. (2010) that steel diagrid systems can use the same SPFs values as steel braced frame systems.

The daigrd structure designed with load combinations in ASCE 7-05 (2005) provided an extra overstrength factor to the building because a load combination 1.2DL+1.0LL with higher gravity load governs the design of diagrid structure, while the gravity load used in pushover analysis for computing the overstrength factor is 1.05DL+0.25LL which is lower than design gravity load. Another main source of overstrength of pushover is the redistribution of force. After one member reaches its maximum capacity, an additional force will flow into other members that still have a capacity to support load. Due to a configuration of diagrid, when design a diagrid, the govern members are the one located in a first story of each module; on the other hand, members in the last story of each module have a low demand to capacity ratio (DCR).

The outcome of this study is very limited since only one performance group of sample buildings was examined. The SPFs obtained from this study can only be applied

to similar buildings used in this study. To obtain more reliable SPFs applicable to more cases, more performance groups of sample buildings need to be analyzed.

6.2 Recommendations for future research

Further studies may involve the followings:

1. More angles of inclinations of diagrid module need to be investigated. The range of angle may be 60-70 degrees.
2. More buildings with different heights need to be considered. Either supertall buildings (60-story or higher) or short buildings (10-story or less) should be considered.
3. Other sets of ground motions should be used. Increase ground motions to 4-6 CMS sets of ground motions per sample building will highly cover more scenarios and the accuracy of results.
4. Different gravity systems (beam and column) configurations may affect the performance of diagrid structures.
5. Different range of diagrid module may affect the global performance of diagrid structures: 4-story or 8-story should be considered.
6. influence of vertical ground motions to seismic performance of diagrid module needs to be investigated;
7. And irregular buildings should also be investigated.

REFERENCES

- AISC. (2010a). *Seismic Provisions for Structural Steel Buildings (AISC 341-10)*. Chicago, IL: American Institute of Steel Construction
- AISC. (2010b). *Specification for Structural Steel Buildings (AISC 360-10)*. Chicago, IL: American Institute of Steel Construction.
- Arias, A. (1970). *A measure of earthquake intensity*. Cambridge, MA: M.I.T. Press.
- ASCE. (2005). *Minimum Design Loads for Buildings and Other Structures (ASCE 7-05)*. Reston, VA: American Society of Civil Engineers.
- ASCE. (2016). *Minimum Design Loads for Buildings and Other Structures (ASCE 7-16)*. Reston, VA: American Society of Civil Engineers.
- Baker, J. W. (2011). Conditional Mean Spectrum: Tool for Ground-Motion Selection. *Journal of Structural Engineering*, 137(3), 322-331. doi:doi:10.1061/(ASCE)ST.1943-541X.0000215
- Baker, W., Besjak, C., Sarkisian, M., Lee, P., & Doo, C.-S. (2010). Proposed Methodology to Determine Seismic Performance Factors for Steel Diagrid Framed Systems *Council on Tall Buildings and Urban Habitat*
- Chandramohan, R., Lin, T., Baker, J., & Deierlein, G. (2013). *Influence of Ground Motion Spectral Shape and Duration on Seismic Collapse Risk*. Paper presented at the 10th International Conference on Urban Earthquake Engineering, Tokyo, Japan.
- Chang, G. A., & Mander, J. B. (1994). *Seismic Energy Based Fatigue Damage Analysis of Bridge Columns: Part 1 - Evaluation of Seismic Capacity*. Retrieved from Buffalo, NY:
- Chiu, H.-C. (1997). *Stable Baseline Correction of Digital Strong-Motion Data* (Vol. 87).
- Chompothawach, T. (2009). *Seismic Fragility of a case study building in Thailand*. (Master of Engineering), Chulalongkorn University.
- CSI. (2015). ETABS, Integrated Building Design Software (Version 15.2.2). Berkeley, California Computers and Structures, Inc.

- Denavit, M. D., & Hajjar, J. F. (2014). *Characterization of Behavior of Steel-Concrete Composite Members and Frames with Applications for Design*. Retrieved from Urbana, IL:
- FEMA. (2004). *NEHRP Recommended Provisions for Seismic Regulations for New Buildings and Other Structures (FEMA 450)*. Retrieved from Washington, D.C.:
- FEMA. (2009). *Quantification of Building Seismic Performance Factors Report No. FEMA P695*. Retrieved from Washington, D.C.:
- Jeong, S.-H., Lee, K.-H., & Jang, W.-S. (2017). PRISM for Earthquake Engineering (Version 2.0.1). Incheon, South Korea: Earthquake Engineering Research Group, Department of Architectural Engineering, INHA University Retrieved from <http://sem.inha.ac.kr/prism/>
- Jirasakjamroonsri, A., Poovarodom, N., & Warnitchai, P. (2018). Seismic site characteristics of shallow sediments in the Bangkok Metropolitan Region, and their inherent relations. *Bulletin of Engineering Geology and the Environment*. doi:10.1007/s10064-017-1220-3
- Mele, E., Toreno, M., Brandonisio, G., & Luca, A. D. (2014). Diagrid Structures for Tall Buildings: Case Studies and Design Considerations. *The Structural Design of Tall and Special Buildings*, 23, 124-145. doi:10.1002/tal.1029
- Moon, K.-S., Cornor, J. J., & Fernandez, J. E. (2007). Diagrid Structural Systems for Tall Buildings: Characteristics and Methodology for Preliminary Design. *The Structural Design of Tall and Special Buildings*, 16, 205-230. doi:10.1002/tal.311
- PEER. (2017). *Guidelines for Performance-Based Seismic Design of Tall Buildings* (May 2017 ed.). Berkeley, CA: Pacific Earthquake Engineering Research Center
- Sadraddin, H. (2015). *Fragility Assessment of High-Rise Reinforced Concrete Buildings*. (Master of Science in Engineering), Western Michigan University.
- Tsai, W. T. (1988). Uniaxial Compressional Stress-Strain Relation of Concrete. *Journal of Structural Engineering*, 114(9), 2133-2136. doi:doi:10.1061/(ASCE)0733-9445(1988)114:9(2133)

Vamvatsioks, D., & Cornell, C. A. (2002). Incremental Dynamic Analysis. *Earthquake Engineering and Structural Dynamics*, 31(3), 24. doi:10.1002/eqe.141





APPENDICES

จุฬาลงกรณ์มหาวิทยาลัย
CHULALONGKORN UNIVERSITY



Table A.1 SPFs of composite braced frames in ASCE 7-05 (ASCE, 2005).

Seismic Force-Resisting System	Response Modification Coefficient, R	System Overstrength Factor, Ω_0	Deflection Amplification Factor, C_d
BUILDING FRAME SYSTEMS			
Composite steel and concrete concentrically braced frames	5	2	4½
Ordinary composite steel and concrete braced frames	3	2	3

Table A.2 Coefficient C_u (ASCE, 2005).**TABLE 12.8-1 COEFFICIENT FOR UPPER LIMIT ON CALCULATED PERIOD**

Design Spectral Response Acceleration Parameter at 1 s, S_{D1}	Coefficient C_u
≥ 0.4	1.4
0.3	1.4
0.2	1.5
0.15	1.6
≤ 0.1	1.7

where I and R are as defined in Section 12.8.1.1 and

S_{D1} = the design spectral response acceleration parameter at a period of 1.0 s, as determined from Section 11.4.4

T = the fundamental period of the structure (s) determined in Section 12.8.2

T_L = long-period transition period (s) determined in Section 11.4.5

S_1 = the mapped maximum considered earthquake spectral response acceleration parameter determined in accordance with Section 11.4.1

Table A.3 Coefficient C_t and x (ASCE, 2005).

12.8.2 Period Determination. The fundamental period of the structure, T , in the direction under consideration shall be established using the structural properties and deformational characteristics of the resisting elements in a properly substantiated analysis. The fundamental period, T , shall not exceed the product of the coefficient for upper limit on calculated period (C_u) from Table 12.8-1 and the approximate fundamental period, T_a , determined from Eq. 12.8-7. As an alternative to performing an analysis to determine the fundamental period, T , it is permitted to use the approximate building period, T_a , calculated in accordance with Section 12.8.2.1, directly.

12.8.2.1 Approximate Fundamental Period. The approximate fundamental period (T_a), in s, shall be determined from the following equation:

$$T_a = C_t h_n^x \quad (12.8-7)$$

where h_n is the height in ft above the base to the highest level of the structure and the coefficients C_t and x are determined from Table 12.8-2.

TABLE 12.8-2 VALUES OF APPROXIMATE PERIOD PARAMETERS C_t AND x

Structure Type	C_t	x
Moment-resisting frame systems in which the frames resist 100% of the required seismic force and are not enclosed or adjoined by components that are more rigid and will prevent the frames from deflecting where subjected to seismic forces:		
Steel moment-resisting frames	0.028 (0.0724) ^a	0.8
Concrete moment-resisting frames	0.016 (0.0466) ^a	0.9
Eccentrically braced steel frames	0.03 (0.0731) ^a	0.75
All other structural systems	0.02 (0.0488) ^a	0.75

^aMetric equivalents are shown in parentheses.

Pushover Plot (FEMA, 2009)

Figure A.1 shows a sample pushover curve and explanations of the maximum base shear, V_{max} and the ultimate displacement, δ_u . V_{max} is the maximum base shear the pushover curve, and δ_u is the roof displacement at 20% strength loss ($0.8V_{max}$). $\delta_{y,eff}$ is an effective roof displacement used to approximate full yield of the seismic force resisting system:

$$\delta_{y,eff} = C_0 \frac{V_{max}}{W} \left[\frac{g}{4\pi^2} \right] (\max(T, T_1))^2$$

where

C_0 = Coefficient relates fundamental-mode (SDOF) displacement to roof displacement. The coefficient C_0 is based on Equation C3-4 of ASCE/SEI 41-06 as follows: or using table in ASCE 7-05. C_0 can read from Table 3-2 in ASCE 41-06. For other buildings, with any load pattern, C_0 is 1.5 for buildings with 10 or more stories.

V_{max}/W = the maximum base shear normalized by building weight

g = the gravity constant

T = the fundamental period

T_1 = the fundamental period of the archetype model computed using modal analysis

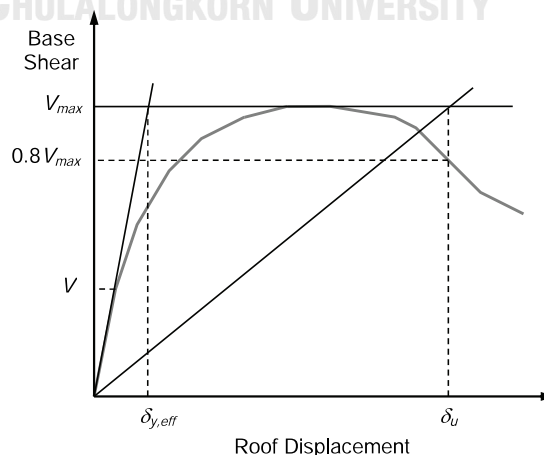


Figure A.1 Idealized nonlinear static pushover curve (FEMA, 2009).

Table A.4 Spectral shape factor (SSF) for archetype designed for SDC B, C, or Dmin (FEMA, 2009).

T (sec.)	Period-Based Ductility, μ_T							
	1.0	1.1	1.5	2	3	4	6	≥ 8
≤ 0.5	1.00	1.02	1.04	1.06	1.08	1.09	1.12	1.14
0.6	1.00	1.02	1.05	1.07	1.09	1.11	1.13	1.16
0.7	1.00	1.03	1.06	1.08	1.10	1.12	1.15	1.18
0.8	1.00	1.03	1.06	1.08	1.11	1.14	1.17	1.20
0.9	1.00	1.03	1.07	1.09	1.13	1.15	1.19	1.22
1.0	1.00	1.04	1.08	1.10	1.14	1.17	1.21	1.25
1.1	1.00	1.04	1.08	1.11	1.15	1.18	1.23	1.27
1.2	1.00	1.04	1.09	1.12	1.17	1.20	1.25	1.30
1.3	1.00	1.05	1.10	1.13	1.18	1.22	1.27	1.32
1.4	1.00	1.05	1.10	1.14	1.19	1.23	1.30	1.35
≥ 1.5	1.00	1.05	1.11	1.15	1.21	1.25	1.32	1.37

Table A.5 Spectral shape factor (SSF) for archetype designed for SDC Dmax (FEMA, 2009).

T (sec.)	Period-Based Ductility, μ_T							
	1.0	1.1	1.5	2	3	4	6	≥ 8
≤ 0.5	1.00	1.05	1.1	1.13	1.18	1.22	1.28	1.33
0.6	1.00	1.05	1.11	1.14	1.2	1.24	1.3	1.36
0.7	1.00	1.06	1.11	1.15	1.21	1.25	1.32	1.38
0.8	1.00	1.06	1.12	1.16	1.22	1.27	1.35	1.41
0.9	1.00	1.06	1.13	1.17	1.24	1.29	1.37	1.44
1.0	1.00	1.07	1.13	1.18	1.25	1.31	1.39	1.46
1.1	1.00	1.07	1.14	1.19	1.27	1.32	1.41	1.49
1.2	1.00	1.07	1.15	1.2	1.28	1.34	1.44	1.52
1.3	1.00	1.08	1.16	1.21	1.29	1.36	1.46	1.55
1.4	1.00	1.08	1.16	1.22	1.31	1.38	1.49	1.58
≥ 1.5	1.00	1.08	1.17	1.23	1.32	1.4	1.51	1.61

Construction of collapse fragility curves

After performing Incremental Dynamic Analysis (IDA), the next step is to use those computed spectral accelerations and corresponding maximum interstory drift ratio to construct a fragility curve. The procedure for constructing the curve refers to *Fragility Assessment of High-Rise Reinforced Concrete Buildings* Thesis by Hezha Sadraddin (Sadraddin, 2015). The sample of a fragility is shown in Figure A.2 by Chompothawach (Chompothawach, 2009). Figure A.2(a) illustrates the IDA curves providing spectral accelerations and corresponding maximum interstory drift ratio. Figure A.2(b) illustrates the probability of collapse given the specific spectral acceleration from Figure A.2(a). For example, in this study, the collapse defines at the maximum interstory drift ratio of 4 percent; the 100 percent probability of collapse occurs at a spectral acceleration of 1.720g as shown in Figure A.2(a). After completing the fragility curve, if one examines the spectral acceleration of 0.425g, this spectral acceleration will be corresponding to 1/20 or 5 percent of collapse.

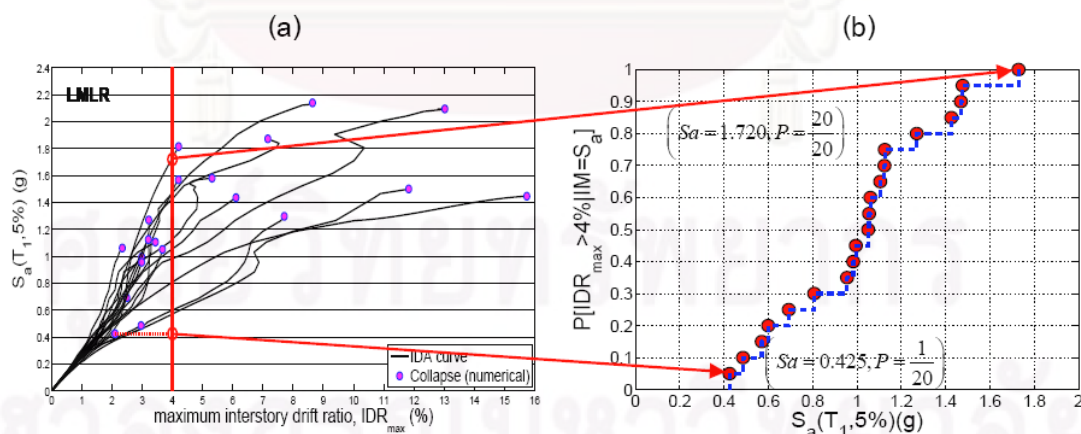


Figure A.2 Fragility curve constructing from spectral acceleration and maximum inter-story drift ratio (Chompothawach, 2009).

Procedure for Constructing Fragility Curves (Sadraddin, 2015)

1. Create the IDA curves for all ground motions. Determine the value of Intensity Measure (IM) or X , in this case, the spectral acceleration, S_a , which is the function of fundamental period and five-percent damping, of the buildings' response from the IDA curves.
2. Choose type of distribution function. In this case, the lognormal distribution is used. Therefore, the chosen parameter, spectral acceleration, is taken by natural logarithm to become $\ln(x)$, where x is the specific spectral acceleration.
3. Compute the mean and the standard deviation for $\ln(x)$:

$$\mu = \frac{\sum_{i=1}^n \ln(x_i)}{n}$$

$$\sigma = \sqrt{\frac{\sum_{i=1}^n (\ln(x_i) - \mu)^2}{n-1}}$$

where,

μ = mean of $\ln(x)$

σ = standard deviation of $\ln(x)$

x = specified parameter for IM, in this case, Spectral Acceleration, S_a

4. Calculate s of the lognormal data:

$$s = \frac{\ln(x) - \mu}{\sigma}$$

5. Define the random variable, X which is less than or equal to the specific value, x . Define the Cumulative Distribution Function (CDF) represents the probability of a random variable, X . The Probability Density Function (PDF) defines as the derivative of the CDF. This PDF will be expressed as the normal distribution which will represent the probability distribution in this study.

$$P(X \leq x) = F_X(x) = \int_{-\infty}^x f_X(x) dx$$

$$f_x(x) = \frac{d}{dx} F_x(x) = \frac{1}{\sigma_x \sqrt{2\pi}} \exp \left[-\frac{1}{2} \left(\frac{x - \mu_x}{\sigma_x} \right)^2 \right]$$

In this study, we are interested in the lognormal value, so the PDF will become:

$$f_x(\ln x) = \frac{1}{\sigma_x \sqrt{2\pi}} \exp \left[-\frac{1}{2} \left(\frac{\ln x - \mu_x}{\sigma_x} \right)^2 \right]$$

6. Introduce the parameter s in the equation and call this variable, ϕ :

$$\phi(s) = f_s(s) = \frac{1}{\sqrt{2\pi}} \exp \left[-\frac{1}{2} (s)^2 \right]$$

In normal distribution domain, the mean equals to zero, and standard deviation equals to one.

7. The CDF is now expressed as:

$$P(X \leq x) = F_x(x) = \phi \frac{\ln(X) - \mu}{\sigma}$$

8. If we only interested in the probability under the damage level (D), the probability will become:

$$P(\leq D) = \phi \frac{\ln(x) - \mu}{\sigma}$$

where,

D = the damage level (the drift limit)

9. Plot fragility curve with probability at vertical axis and spectral acceleration (IM) at horizontal axis.

Table A.6 Quality rating of design requirements (FEMA, 2009).

Completeness and Robustness	Confidence in Basis of Design Requirements		
	High	Medium	Low
High. Extensive safeguards against unanticipated failure modes. All important design and quality assurance issues are addressed.	(A) Superior $\beta_{DR} = 0.10$	(B) Good $\beta_{DR} = 0.20$	(C) Fair $\beta_{DR} = 0.35$
Medium. Reasonable safeguards against unanticipated failure modes. Most of the important design and quality assurance issues are addressed.	(B) Good $\beta_{DR} = 0.20$	(C) Fair $\beta_{DR} = 0.35$	(D) Poor $\beta_{DR} = 0.50$
Low. Questionable safeguards against unanticipated failure modes. Many important design and quality assurance issues are not addressed.	(C) Fair $\beta_{DR} = 0.35$	(D) Poor $\beta_{DR} = 0.50$	--

Table A.7 Quality rating of test data (FEMA, 2009).

Completeness and Robustness	Confidence in Test Results		
	High	Medium	Low
High. Material, component, connection, assembly, and system behavior well understood and accounted for. All, or nearly all, important testing issues addressed.	(A) Superior $\beta_{TD} = 0.10$	(B) Good $\beta_{TD} = 0.20$	(C) Fair $\beta_{TD} = 0.35$
Medium. Material, component, connection, assembly, and system behavior generally understood and accounted for. Most important testing issues addressed.	(B) Good $\beta_{TD} = 0.20$	(C) Fair $\beta_{TD} = 0.35$	(D) Poor $\beta_{TD} = 0.50$
Low. Material, component, connection, assembly, and system behavior fairly understood and accounted for. Several important testing issues not addressed.	(C) Fair $\beta_{TD} = 0.35$	(D) Poor $\beta_{TD} = 0.50$	--

Table A.8 Quality rating of index archetype models (FEMA, 2009).

Representation of Collapse Characteristics	Accuracy and Robustness of Models		
	High	Medium	Low
High. Index models capture the full range of the archetype design space and structural behavioral effects that contribute to collapse.	(A) Superior $\beta_{MDL} = 0.10$	(B) Good $\beta_{MDL} = 0.20$	(C) Fair $\beta_{MDL} = 0.35$
Medium. Index models are generally comprehensive and representative of the design space and behavioral effects that contribute to collapse.	(B) Good $\beta_{MDL} = 0.20$	(C) Fair $\beta_{MDL} = 0.35$	(D) Poor $\beta_{MDL} = 0.50$
Low. Significant aspects of the design space and/or collapse behavior are not captured in the index models.	(C) Fair $\beta_{MDL} = 0.35$	(D) Poor $\beta_{MDL} = 0.50$	--



Table A.9 Acceptable values of adjusted collapse margin ratio (FEMA, 2009).

Total System Collapse Uncertainty	Collapse Probability				
	5%	10% (ACMR _{10%})	15%	20% (ACMR _{20%})	25%
0.275	1.57	1.42	1.33	1.26	1.20
0.300	1.64	1.47	1.36	1.29	1.22
0.325	1.71	1.52	1.40	1.31	1.25
0.350	1.78	1.57	1.44	1.34	1.27
0.375	1.85	1.62	1.48	1.37	1.29
0.400	1.93	1.67	1.51	1.40	1.31
0.425	2.01	1.72	1.55	1.43	1.33
0.450	2.10	1.78	1.59	1.46	1.35
0.475	2.18	1.84	1.64	1.49	1.38
0.500	2.28	1.90	1.68	1.52	1.40
0.525	2.37	1.96	1.72	1.56	1.42
0.550	2.47	2.02	1.77	1.59	1.45
0.575	2.57	2.09	1.81	1.62	1.47
0.600	2.68	2.16	1.86	1.66	1.50
0.625	2.80	2.23	1.91	1.69	1.52
0.650	2.91	2.30	1.96	1.73	1.55
0.675	3.04	2.38	2.01	1.76	1.58
0.700	3.16	2.45	2.07	1.80	1.60
0.725	3.30	2.53	2.12	1.84	1.63
0.750	3.43	2.61	2.18	1.88	1.66
0.775	3.58	2.70	2.23	1.92	1.69
0.800	3.73	2.79	2.29	1.96	1.72
0.825	3.88	2.88	2.35	2.00	1.74
0.850	4.05	2.97	2.41	2.04	1.77
0.875	4.22	3.07	2.48	2.09	1.80
0.900	4.39	3.17	2.54	2.13	1.83
0.925	4.58	3.27	2.61	2.18	1.87
0.950	4.77	3.38	2.68	2.22	1.90

Damping Coefficient (ASCE, 2005)

Where the period of the structure is greater than or equal to T_0 , the damping coefficient described in ASCE 7-05 shall be as prescribed in Table A.10. When the period of the structure is less than T_0 , the damping coefficient is computed by a linear interpolation between a value of 1.0 at 0-s in Table A.10.

Effective Damping at design displacement:
$$\beta_{mD} = \beta_I + \beta_{Vm} \sqrt{\mu_D} + \beta_{HD}$$

Effective damping at maximum displacement:
$$\beta_{mM} = \beta_I + \beta_{Vm} \sqrt{\mu_M} + \beta_{HM}$$

where

- μ_D = Effective ductility demand on the seismic force-resisting system in the direction of interest due to the design earthquake
- μ_M = Effective ductility demand on the seismic force-resisting system in the direction of interest due to the maximum considered earthquake
- β_{HD} = Component of effective damping of the structure in the direction of interest due to post-yield hysteretic behavior of the seismic force-resisting system and elements of the damping system at effective ductility demand, μ_D
- β_{HM} = Component of effective damping of the structure in the direction of interest due to post-yield hysteretic behavior of the seismic force-resisting system and elements of the damping system at effective ductility demand, μ_M
- β_I = Component of effective damping of the structure due to the inherent dissipation of energy by elements of the structure, at or just below the effective yield displacement of the seismic force-resisting system
- β_{Vm} = Component of effective damping of the mth mode of vibration of the structure in the direction of interest due to viscous dissipation of energy by the damping system, at or just below the effective yield displacement of the seismic force-resisting system

Table A.10 Damping coefficient (ASCE, 2005)

Effective damping, β (percentage of critical)	$B_{V+1}, B_{1D}, B_R, B_{1M}, B_{mD}$, or B_{mM} (where period of the structure $\geq T_0$)
≤ 2	0.8
5	1.0
10	1.2
20	1.5
30	1.8
40	2.1
50	2.4
60	2.7
70	3.0
80	3.3
90	3.6
≥ 100	4.0



Compactness

The strength of concrete-filled tube is computed based on the steel specification (AISC 360-10) (AISC, 2010b). Since the Round section can easily achieve compact criteria, the author will use only compact section. In Table C.1, the compactness requirement of the section is:

Round filled composite members:
$$\frac{D}{t} \leq 0.15 \frac{E}{F_y}$$

Table B.1 Compactness of steel section (AISC, 2010b).

TABLE I1.1A Limiting Width-to-Thickness Ratios for Compression Steel Elements in Composite Members Subject to Axial Compression For Use with Section I2.2				
Description of Element	Width-to-Thickness Ratio	λ_p Compact/ Noncompact	λ_r Noncompact/ Slender	Maximum Permitted
Walls of Rectangular HSS and Boxes of Uniform Thickness	b/t	$2.26 \sqrt{\frac{E}{F_y}}$	$3.00 \sqrt{\frac{E}{F_y}}$	$5.00 \sqrt{\frac{E}{F_y}}$
Round HSS	D/t	$\frac{0.15E}{F_y}$	$\frac{0.19E}{F_y}$	$\frac{0.31E}{F_y}$

Strength

The tensile strength of axially loaded filled composite braces includes only the area of steel section; the area of confined concrete is neglected in the design. A gross area of section equals to area of steel in this case. The area of reinforcing steel is neglected in this steel and equals to zero. The design tensile strength of a circular concrete-filled steel tube (CCFT) brace is (AISC, 2010b):

$$\phi_t P_n = \phi_t (F_y A_g + A_{sr} F_{ysr}) \quad , \phi_t = 0.90$$

The compressive strength of axially loaded filled composite braces accounts the compressive strength of confined concrete filled inside the steel section (AISC, 2010b). A gross area of section equals to the area of steel plus concrete.

$$\phi_c P_n = \phi_c P_n \quad , \phi_c = 0.75$$

$$\text{When } \frac{P_{no}}{P_e} \leq 2.25 , \quad P_n = P_{no} (0.658^{\frac{P_{no}}{P_e}})$$

$$\text{When } \frac{P_{no}}{P_e} > 2.25 , \quad P_n = 0.877 P_e$$

For compact sections,

$$P_{no} = P_p = F_y A_s + C_2 f'_c (A_c + A_{sr} \frac{E_s}{E_c})$$

$$C_2 = 0.85 \text{ for rectangular sections and } 0.95 \text{ for round sections}$$

$$P_e = \frac{\pi^2 EI_{eff}}{(KL)^2}$$

$$EI_{eff} = E_s I_s + E_s I_{sr} + C_3 E_c I_c$$

$$C_3 = \text{coefficient for calculation of effective rigidity of filled composite compression member}$$

$$= 0.6 + 2 \frac{A_s}{A_c + A_s} \leq 0.9$$

$$E_c = w_c^{1.5} \sqrt{f'_c} \text{ ksi } (0.043 w_c^{1.5} \sqrt{f'_c} \text{ MPa})$$

$$w_c = 150 \text{ lbs/ft}^3 (2400 \text{ kg/m}^3) \text{ assumed}$$

$$E_s = 29,000 \text{ ksi } (200,000 \text{ MPa}) \text{ assumed}$$

$$A_s = \text{designed area with designed thickness}$$

$$A_{sr} = \text{area of reinforcing steel, equal to zero in this study}$$

$$t_d = 0.93 t_{no} , \text{ designed thickness is } 93\% \text{ of nominal thickness}$$

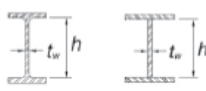

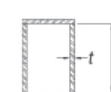
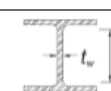
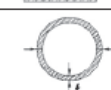


Ductility

Steel seismic provision (AISC 341-10) (AISC, 2010a) requires composite columns and braces to be highly ductile members. Since the Round section can easily achieve highly ductile criteria, the author will only use highly ductile steel section in this study. The ductility requirement of this section is as shown in Table C.2:

Round filled composite members:

$$\frac{D}{t} \leq 0.076 \frac{E}{F_y}$$

Table B.2 Ductility of steel section (AISC, 2010a).

TABLE D1.1 (CONTINUED) Limiting Width-to-Thickness Ratios for Compression Elements For Moderately Ductile and Highly Ductile Members					
	Description of Element	Width-to-Thickness Ratio	Limiting Width-to-Thickness Ratio		Example
			λ_{hd} Highly Ductile Members	λ_{md} Moderately Ductile Members	
Stiffened Elements	Webs of rolled or built-up I-shaped sections used as beams or columns ^{f,g}	h/t_w	For $C_a \leq 0.125$ $2.45\sqrt{E/F_y}(1 - 0.93C_a)$	For $C_a \leq 0.125$ $3.76\sqrt{E/F_y}(1 - 2.75C_a)$	
	Side plates of boxed I-shaped sections used as beams or columns	h/t	For $C_a > 0.125$ $0.77\sqrt{E/F_y}(2.93 - C_a)$ $\geq 1.49\sqrt{E/F_y}$ where $C_a = \frac{P_u}{\phi_c P_y}$ (LRFD) $C_a = \frac{\Omega_c P_a}{P_y}$ (ASD)	For $C_a > 0.125$ $1.12\sqrt{E/F_y}(2.33 - C_a)$ $\geq 1.49\sqrt{E/F_y}$ where $C_a = \frac{P_u}{\phi_c P_y}$ (LRFD) $C_a = \frac{\Omega_c P_a}{P_y}$ (ASD)	
	Webs of built-up box sections used as beams or columns	h/t			
	Webs of H-Pile sections	h/t_w	$0.94\sqrt{E/F_y}$	not applicable	
	Walls of round HSS	D/t	$0.038E/F_y$	$0.044E/F_y$ ^[e]	
Composite Elements	Walls of rectangular filled composite members	b/t	$1.4\sqrt{E/F_y}$	$2.26\sqrt{E/F_y}$	
	Walls of round filled composite members	D/t	$0.076E/F_y$	$0.15E/F_y$	

Brace Strength

Since the requirements for highly ductile member are more restricted than compact section, the value for ductility requirement governs the selection of section. The expected yield strength value combined with previous design strength equations further define the nonlinear hinge in composite braces. The expected strength of steel sections defines in Table B.3.

Round Section

Type of steel: ASTM A53/A53M: $R_y = 1.6$ and $R_t = 1.2$
 A53 Gr. B: Yield Strength = 35 ksi (241 MPa)
 Tensile Strength = 60 ksi (415 MPa)

Table B.3 Expected strength of steel material (AISC, 2010a).

TABLE A3.1 R_y and R_t Values for Steel and Steel Reinforcement Materials		
Application	R_y	R_t
Hot-rolled structural shapes and bars: <ul style="list-style-type: none"> • ASTM A36/A36M • ASTM A1043/1043M Gr. 36 (250) • ASTM A572/572M Gr. 50 (345) or 55 (380), ASTM A913/A913M Gr. 50 (345), 60 (415), or 65 (450), ASTM A588/A588M, ASTM A992/A992M • ASTM A1043/A1043M Gr. 50 (345) • ASTM A529 Gr. 50 (345) • ASTM A529 Gr. 55 (380) 	1.5 1.3 1.1 1.2 1.2 1.1	1.2 1.1 1.1 1.1 1.2 1.2
Hollow structural sections (HSS): <ul style="list-style-type: none"> • ASTM A500/A500M (Gr. B or C), ASTM A501 	1.4	1.3
Pipe: <ul style="list-style-type: none"> • ASTM A53/A53M 	1.6	1.2
Plates, Strips and Sheets: <ul style="list-style-type: none"> • ASTM A36/A36M • ASTM A1043/1043M Gr. 36 (250) • A1011/A1011M HSLAS Gr. 55 (380) • ASTM A572/A572M Gr. 42 (290) • ASTM A572/A572M Gr. 50 (345), Gr. 55 (380), ASTM A588/A588M • ASTM 1043/1043M Gr. 50 (345) 	1.3 1.3 1.1 1.3 1.1 1.2	1.2 1.1 1.1 1.0 1.2 1.1
Steel Reinforcement: <ul style="list-style-type: none"> • ASTM A615, ASTM A706 	1.25	1.25

Monotonic Steel Stress-Strain Relation with Local Buckling (Denavit & Hajjar, 2014)

Under compression, the compressive response of CCFT section can be modified to account for local buckling. The beginning of local buckling is assumed to start when the compressive strain reaches a local buckling value, ϵ_{lb} . Then, there is a linear strength degradation with a slope of a local buckling modulus, K_{slb} . After local buckling occurs, the stress will be a constant ultimate residual stress, F_{ulb} .

$$\epsilon_u = 120 \frac{F_y}{E_s}$$

$$K_{slb} = -\frac{E_s}{30}$$

$$R = \frac{D F_y}{t E_s}$$

$$\epsilon_{lb@compression} = -0.2139 R^{-1.413} \frac{F_y}{E_s}$$

$$F_{ulb} = 0.17 \frac{F_{lb}}{R} \leq F_{lb}$$

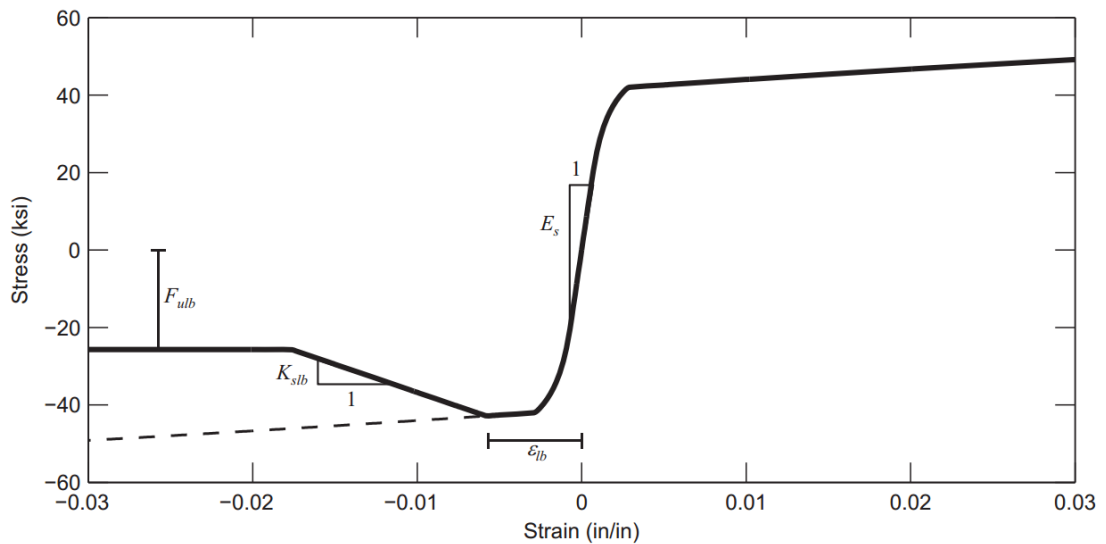


Figure B.1 Monotonic steel stress-strain relationship including local buckling (Denavit & Hajjar, 2014).

Monotonic Concrete Stress-Strain relation for analysis purpose (Denavit & Hajjar, 2014)

The compressive strain at peak stress for unconfined concrete:

$$\varepsilon'_c = \frac{(f'_c)^{0.25} [ksi]}{710}$$

Concrete Compressive Pre-Peak Shape Factor ($\varepsilon_c \leq \varepsilon'_{cc}$):

$$r_{n,pre} = \frac{f'_c [ksi]}{0.75} - 1.9$$

Concrete Compressive Post-Peak Shape Factor ($\varepsilon_c > \varepsilon'_{cc}$):

$$r_{n,post} = 0.4 + 0.016 \frac{D}{t} \frac{f'_c}{F_y}$$

Confinement Pressure (f_l):

$$f_l = \frac{2\alpha_\theta F_y}{\frac{D}{t} - 2}$$

$$\alpha_\theta = 0.138 - 0.00174 \frac{D}{t} \geq 0$$

where D = the outer diameter of section (inch)

t = the thickness of tube (inch)

Peak Stress in Compression f'_{cc} :

For CCFT where a symmetric state of confinement ($f_{l1} = f_{l2}$) may be assumed,

$$f'_{cc} = f'_c \left(-1.254 + 2.254 \sqrt{1 + 7.94 \frac{f_l}{f'_c}} - 2 \frac{f_l}{f'_c} \right)$$

Strain at peak stress ε'_{cc} :

$$\varepsilon'_{cc} = \varepsilon'_c \left(1 + 5 \left(\frac{f'_{cc}}{f'_c} - 1 \right) \right)$$

Tsai's Equation to compute stress from strain and shape factor

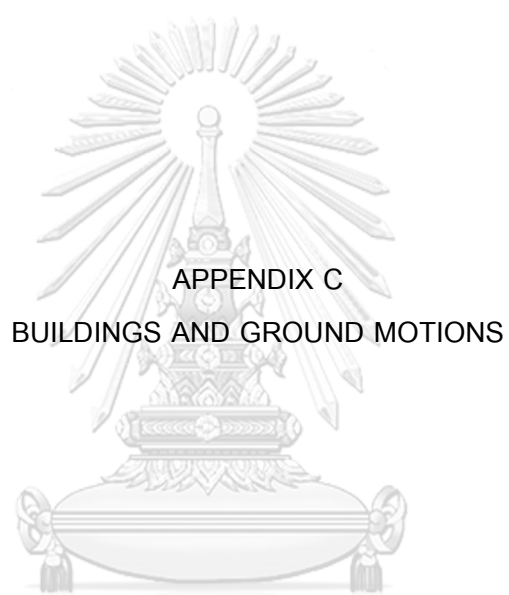
$$D(x) = \begin{cases} 1 + \left(n - \frac{r}{r-1} \right) x + \frac{x^r}{r-1} & \text{for } r \neq 1 \\ 1 + (n-1 + \ln(x))x & \text{for } r = 1 \end{cases} \quad \text{where } r = \begin{cases} r_{n,pre} & \varepsilon_c \leq \varepsilon'_{cc} \\ r_{n,post} & \varepsilon_c \geq \varepsilon'_{cc} \end{cases}$$

$$x = \frac{\varepsilon_c}{\varepsilon'_{cc}} \quad y = \frac{f_c}{f'_{cc}} \quad n = \frac{E_c \varepsilon'_{cc}}{f'_{cc}}$$

$$y = \frac{nx}{D(x)} \quad \varepsilon_c = \varepsilon'_{cc} x \quad f_c = f'_{cc} y$$

where

- ε_c = Strain
- ε'_c = Strain at peak stress in compression of unconfined concrete
- ε'_{cc} = Strain at peak stress in compression of confined concrete
- f_c = Stress
- f'_c = Specific compressive strength of concrete of unconfined concrete
- f'_{cc} = Peak stress in compression of confined concrete
- E_c = Initial modulus of elasticity
- x = Normalized strain
- y = Normalized stress
- n = Normalized modulus



APPENDIX C
BUILDINGS AND GROUND MOTIONS

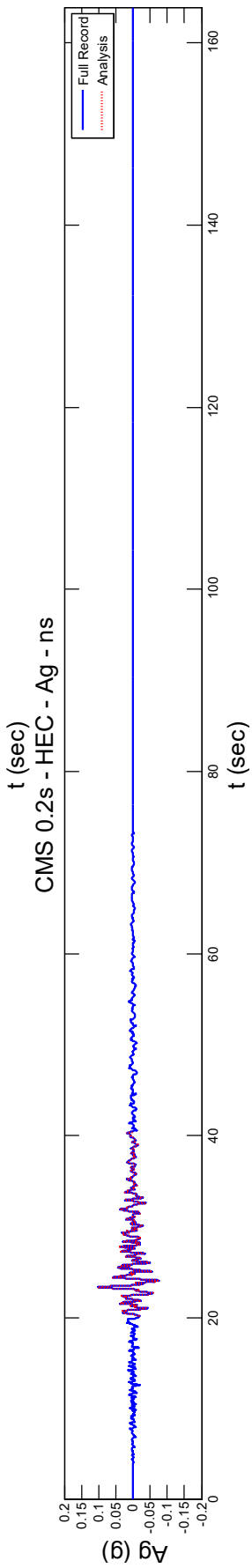
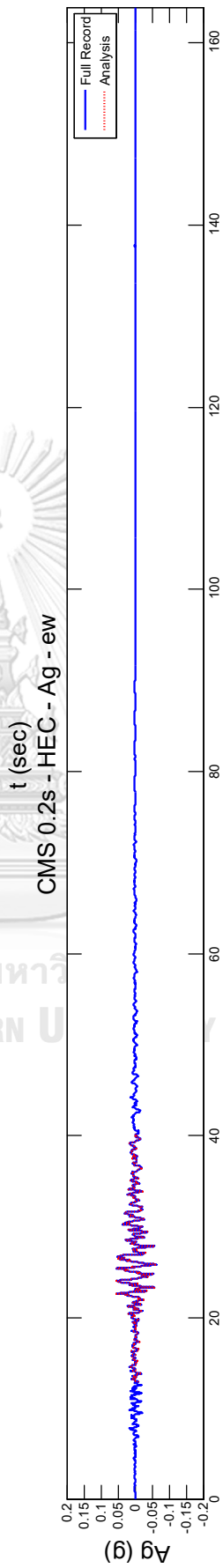
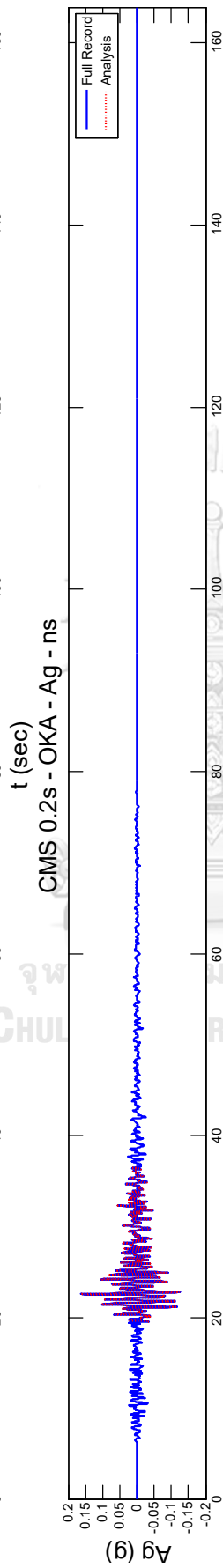
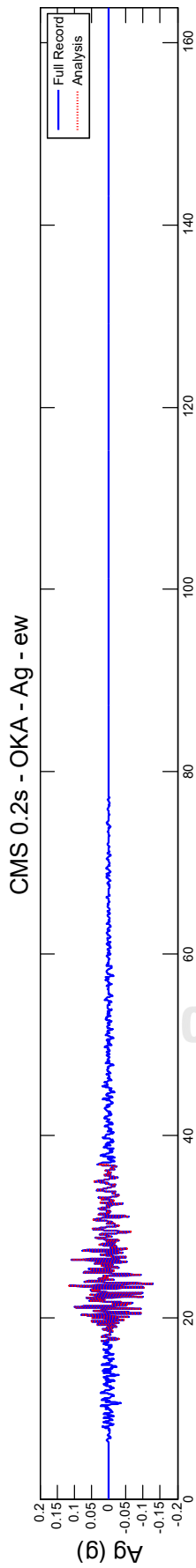
จุฬาลงกรณ์มหาวิทยาลัย
CHULALONGKORN UNIVERSITY

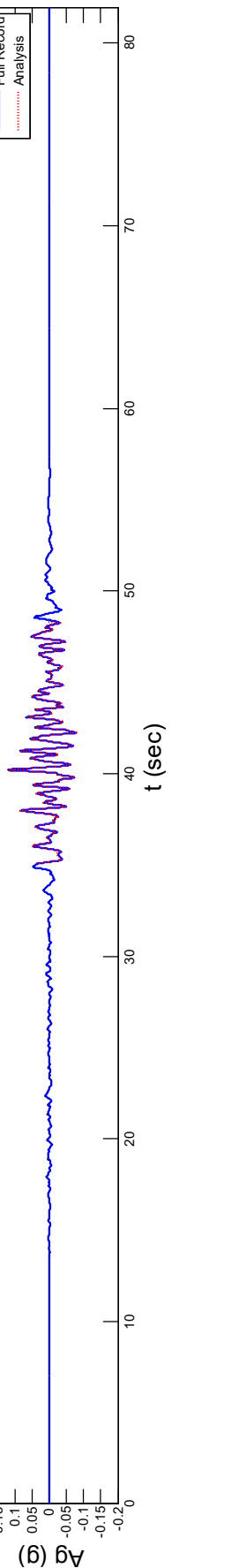
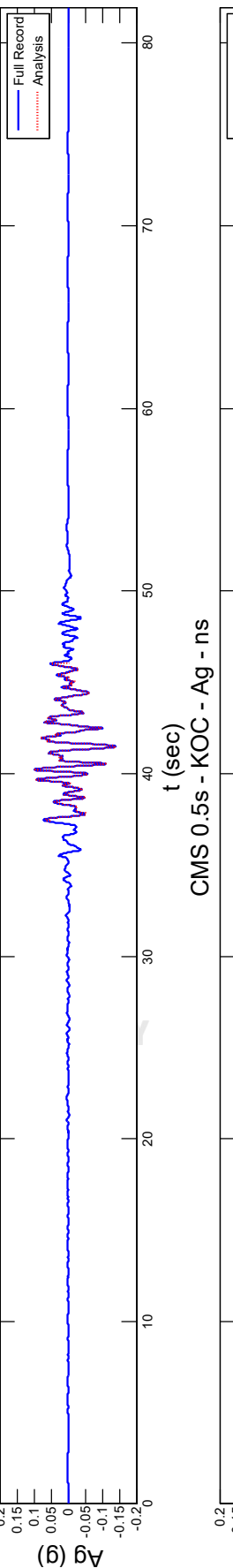
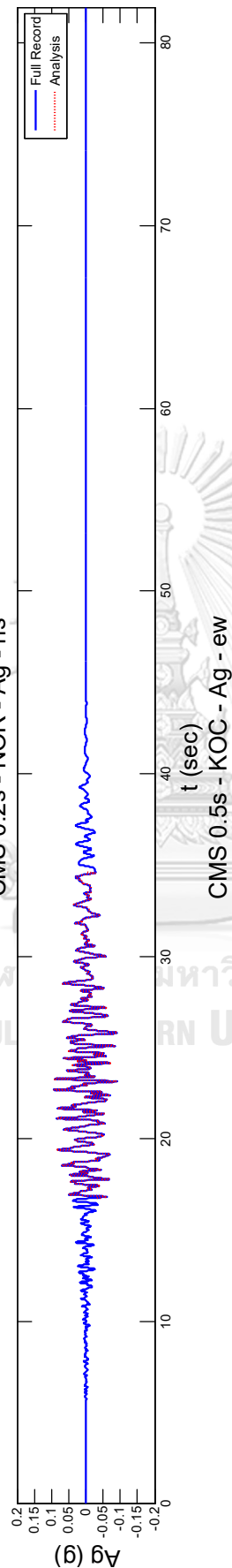
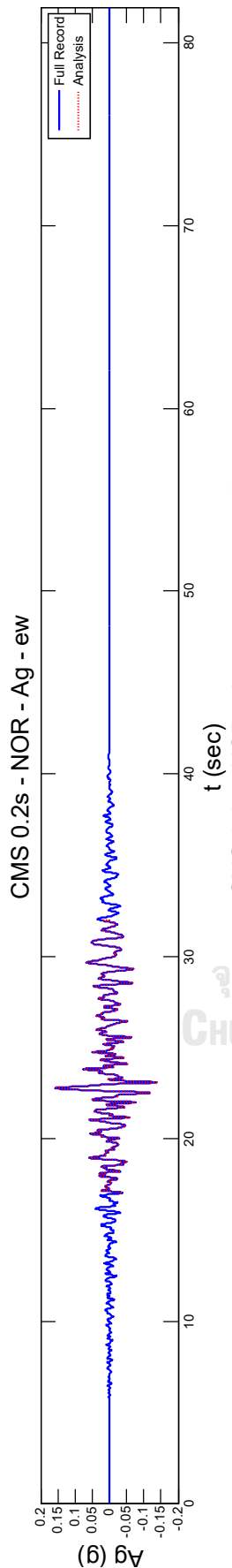
Ground Motions for Response Spectrum and analysis

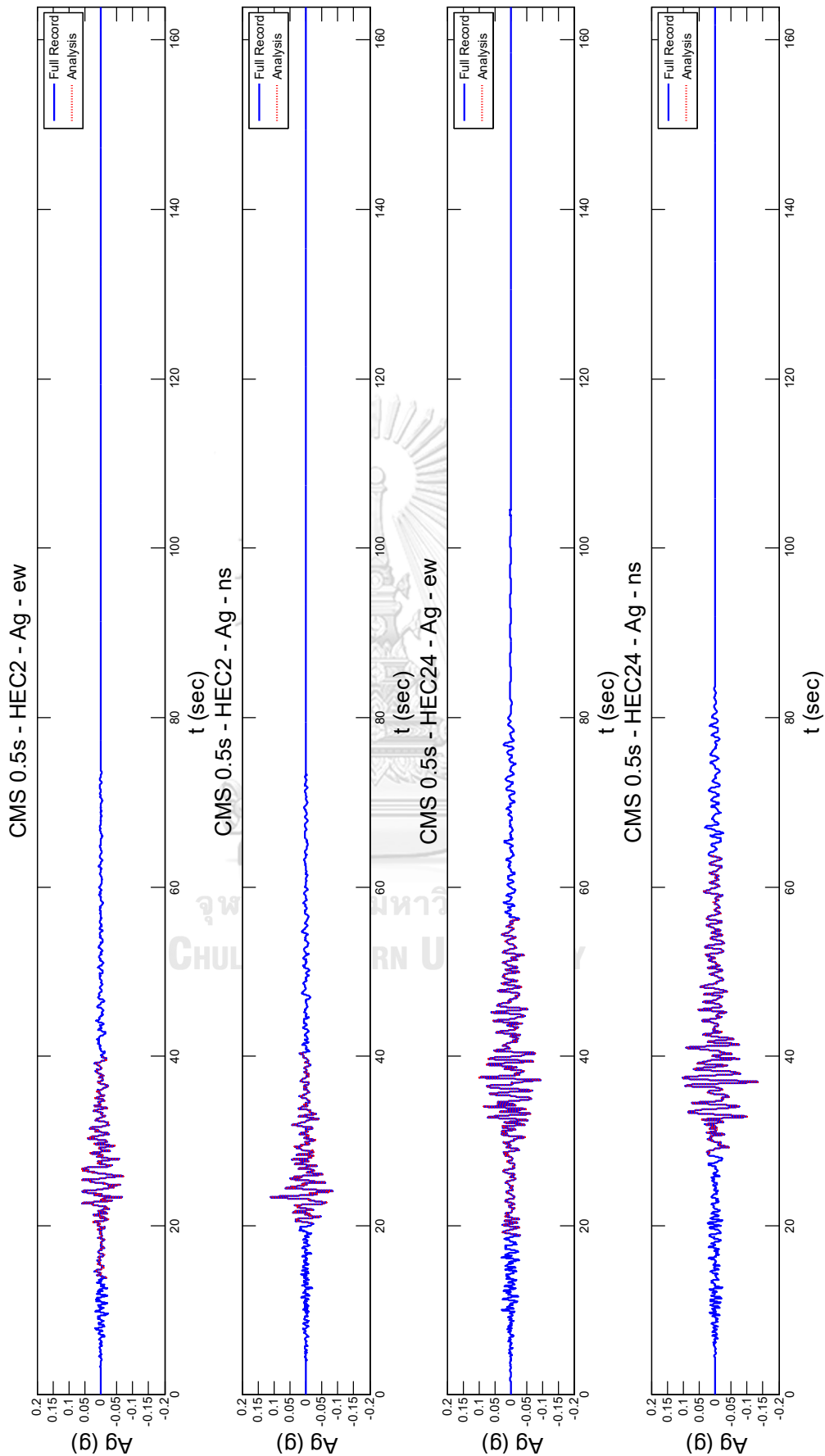
Bold = name of record for analysis purpose

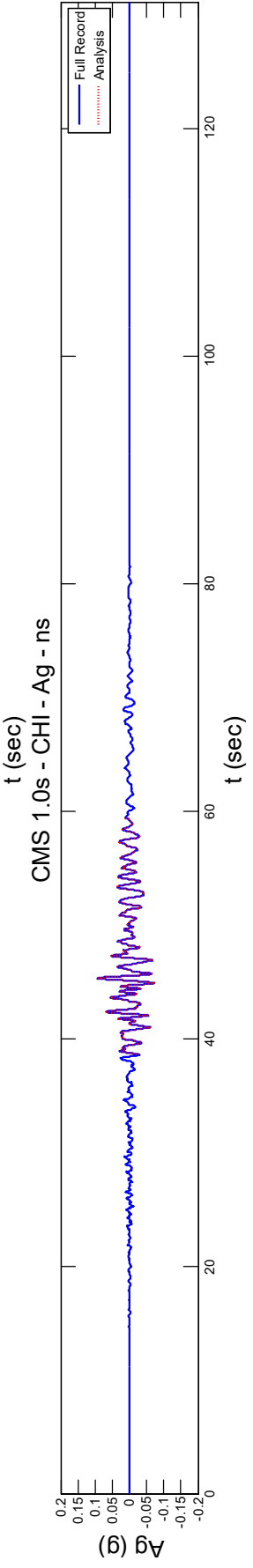
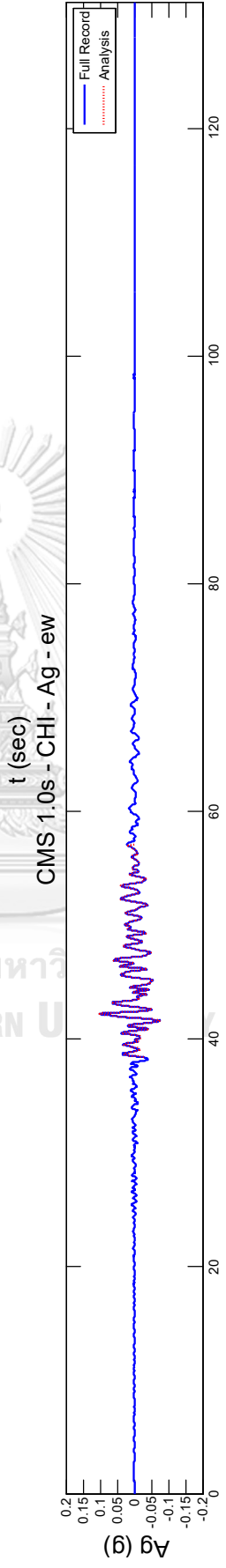
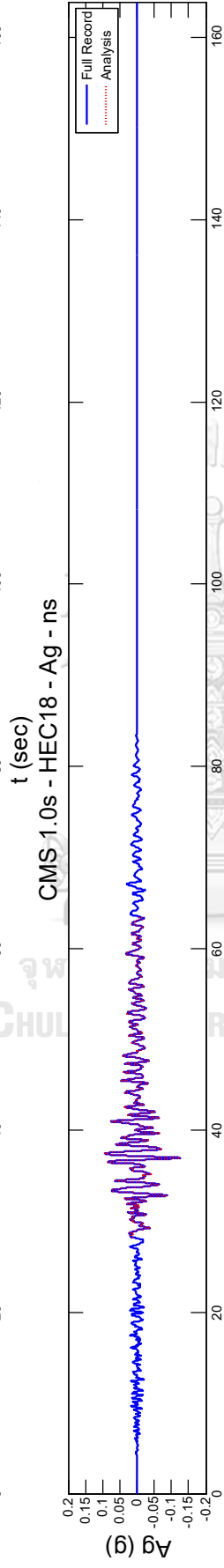
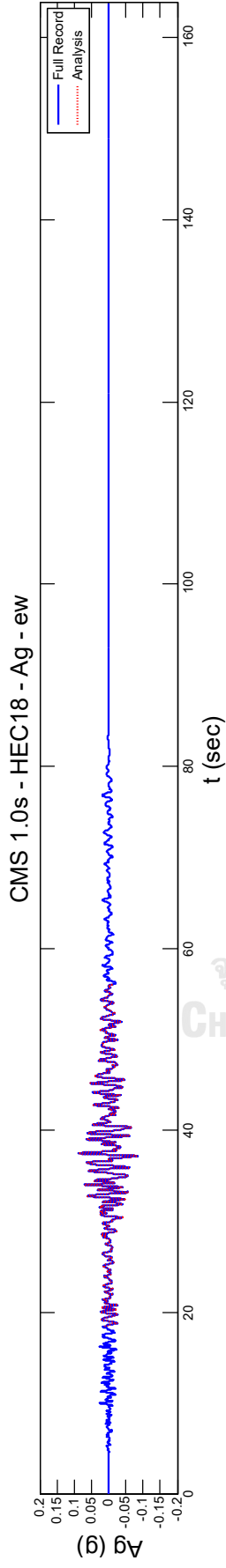
CMS	Event	Station	Comp	PGA(g)	CMS	Event	Station	Comp	PGA(g)
0.2s	Kobe - Japan	OKA	EW	0.129	1.5s	Tokachi- oki	YMT015	EW	0.062
			NS	0.163				NS	0.066
	Hector Mine	Anza – Tripp	EW	0.062		Tohoku	SIG007	EW	0.064
		Flats Training [HEC]	NS	0.102				NS	0.052
	Northridge- 01	Rancho	EW	0.159		Tohoku	HKD06	EW	0.054
		Cucamonga – Deer Can [NOR]	NS	0.093				NS	0.061
0.5s	Kocaeli- Turkey	Tekirdag [KOC]	EW	0.140	2.0s	Tohoku	HKD048	EW	0.077
			NS	0.120				NS	0.063
	Hector Mine	Anza-Tripp	EW	0.069		Tohoku	SIG007 [SIG0072]	EW	0.065
		Flats Training [HEC2]	NS	0.112				NS	0.053
	Hector Mine	Pacoima	EW	0.099		Tokachi- oki	FKS02	EW	0.071
		Kagel Canyon [HEC24]	NS	0.136				NS	0.075
1.0s	Hector Mine	Pacoima	EW	0.087	3.0s	Tohoku	OSK004	EW	0.068
		Kagel Canyon [HEC18]	NS	0.124				NS	0.055
	Chi-Chi- Taiwan	TAP078 [CHI]	EW	0.102		Tohoku	HKD006	EW	0.043
			NS	0.093				NS	0.047
	Hector Mine	Anza – Tripp	EW	0.061		W. Coast of Nortern Sumatera	PYAY	EW	0.041
		Flats Training [HEC17]	NS	0.099				NS	0.028

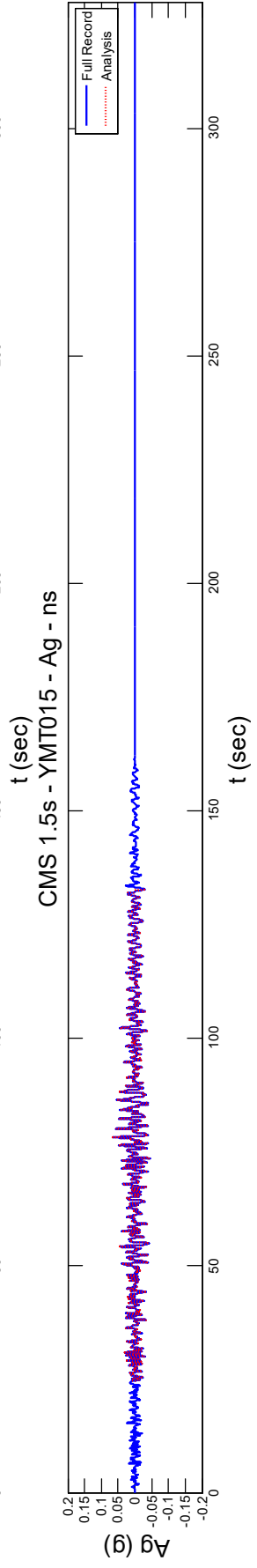
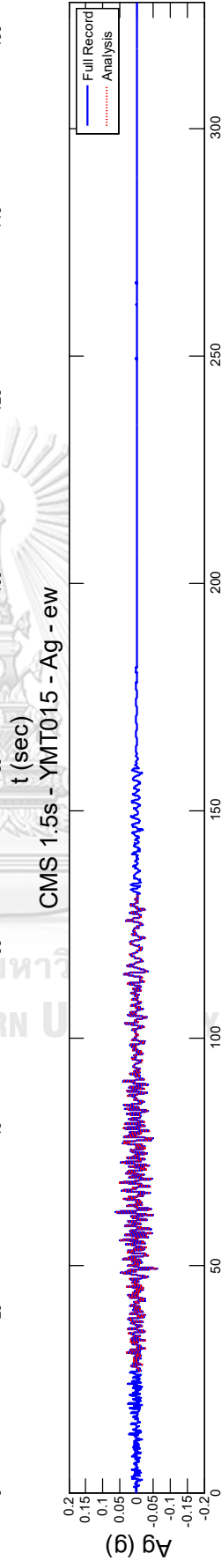
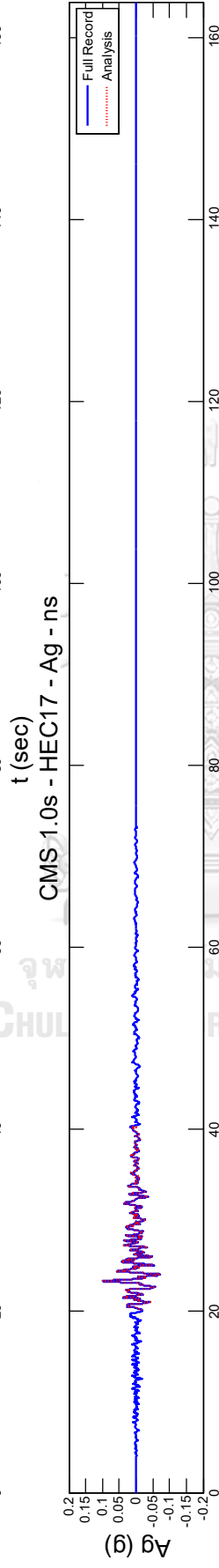
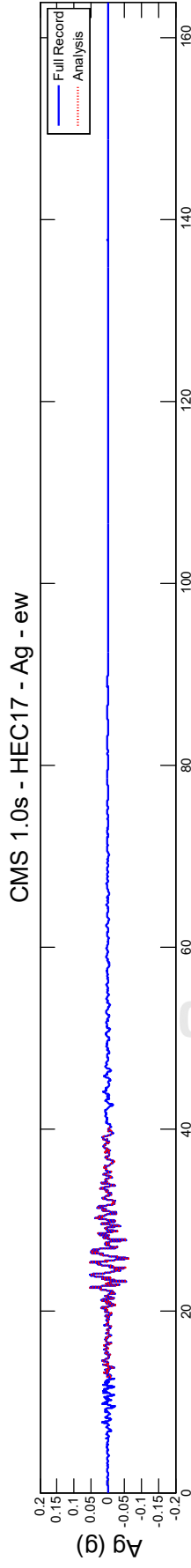
ID	Event	Year	Station	M _w	Mechanism	R _{epi} (km)	Scale Factor	Comp.	PGA (g)	PGV (mm/s)	PGD (mm)	Record Length (s)	Δt (s)
0.2s/1	Kobe-Japan	1995	OKA	6.9	Strike-Slip	86.9	0.8891	EW	0.129	100	27.5	163.82	0.02
								NS	0.163	127	25.4		
0.2s/2	Hector Mine	1999	Anza-Tripp	7.13	Strike-Slip	102.4	1.1524	EW	0.062	139	87.8	163.835	0.005
			Flats Training					NS	0.102	142	59.6		
0.2s/3	Northridge	1994	Rancho	6.69	Reverse	80	1.0221	EW	0.159	84.8	7.45	81.91	0.01
	-01		Cucamonga					NS	0.093	124	26.9		
			-Deer Can										
0.5s/1	Kocaeli-Turkey	1999	Tekirdag	7.51	Strike-Slip	165	1.3575	EW	0.140	185	66.8	81.91	0.01
								NS	0.120	161	48.7		
0.5s/2	Hector Mine	1999	Anza-Tripp	7.13	Strike-Slip	102.4	1.3186	EW	0.069	158	100	163.835	0.005
			Flats Training					NS	0.112	161	68.9		
0.5s/3	Hector Mine	1999	Pacoima	7.13	Strike-Slip	186.3	1.2584	EW	0.099	146	66.4	103.83	0.01
			Kagel Canyon					NS	0.136	215	125		
1.0s/1	Hector Mine	1999	Pacoima	7.13	Strike-Slip	186.3	1.054	EW	0.087	129	55.9	163.83	0.01
			Kagel Canyon					NS	0.124	192	105		
1.0s/2	Chi-Chi-Taiwan	1999	TAP078	7.62	Reverse-Oblique	120	0.7251	EW	0.102	219	151	163.835	0.004
								NS	0.093	154	93.3		
1.0s/3	Hector Mine	1999	Anza-Tripp	7.13	Strike-Slip	102.4	1.1045	EW	0.061	133	84.3	131.068	0.005
			Flats Training					NS	0.099	136	56.9		
1.5s/1	Tokachi-oki	2003	YMT015	8.3	Thrust	550	3.66	EW	0.062	147	240	327.67	0.01
								NS	0.066	158	520		
1.5s/2	Tohoku	2011	SIG007	9.0	Thrust	689	1.85	EW	0.064	206	433	327.67	0.01
								NS	0.052	226	748		
1.5s/3	Tohoku	2011	HKD06	9.0	Thrust	663	2.38	EW	0.054	265	829	327.67	0.01
								NS	0.061	233	802		
2.0s/1	Tohoku	2011	HKD048	9.0	Thrust	655	2.33	EW	0.077	208	3072	327.67	0.01
								NS	0.063	175	1118		
2.0s/2	Tohoku	2011	SIG007	9.0	Thrust	689	1.90	EW	0.065	215	1099	327.67	0.01
								NS	0.053	215	1668		
2.0s/3	Tokachi-oki	2003	FKS02	8.3	Thrust	550	4.36	EW	0.071	197	8655	327.67	0.01
								NS	0.075	223	1916		
3.0s/1	Tohoku	2011	OSK004	9.0	Thrust	747	2.35	EW	0.068	287	785	327.67	0.01
								NS	0.055	232	476		
3.0s/2	Tohoku	2011	HKD06	9.0	Thrust	663	1.73	EW	0.043	177	684	327.67	0.01
								NS	0.047	190	848		
3.0s/3	W. Coast of Northern Sumatra	2004	PYAY	9.0	Thrust	1625	2.58	EW	0.041	355	1930	327.67	0.01
								NS	0.028	275	1598		

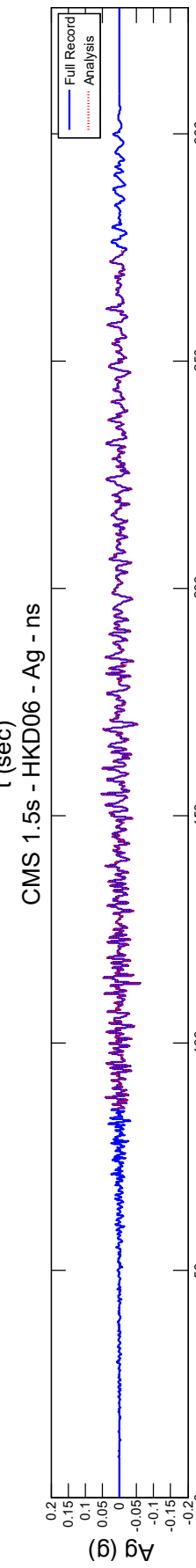
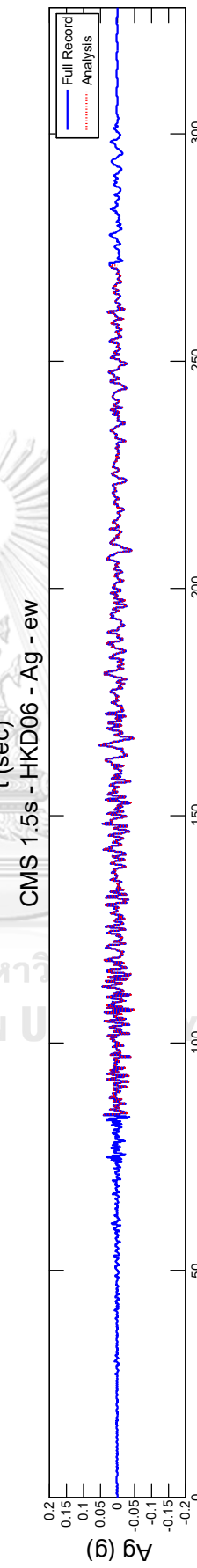
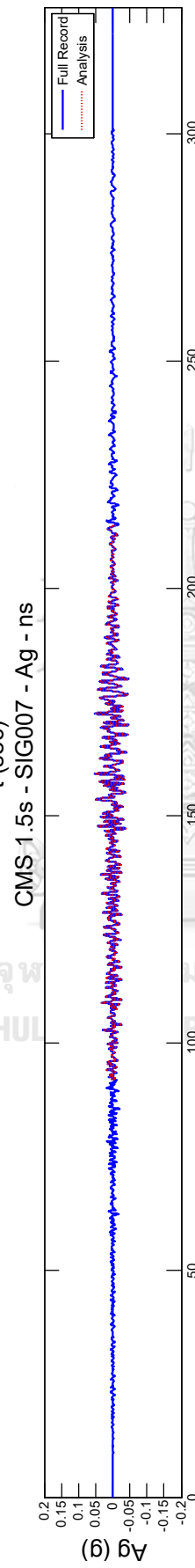
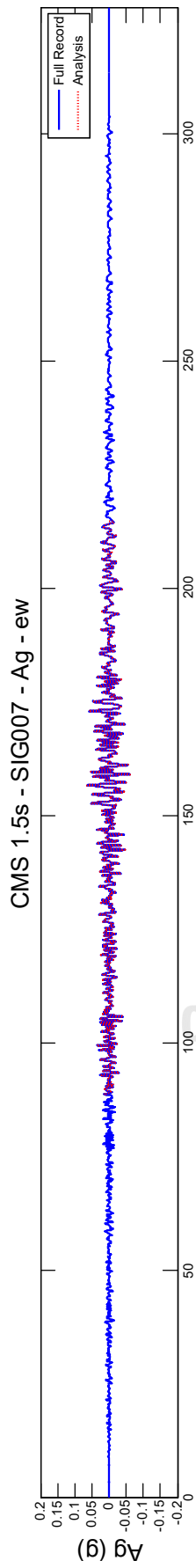


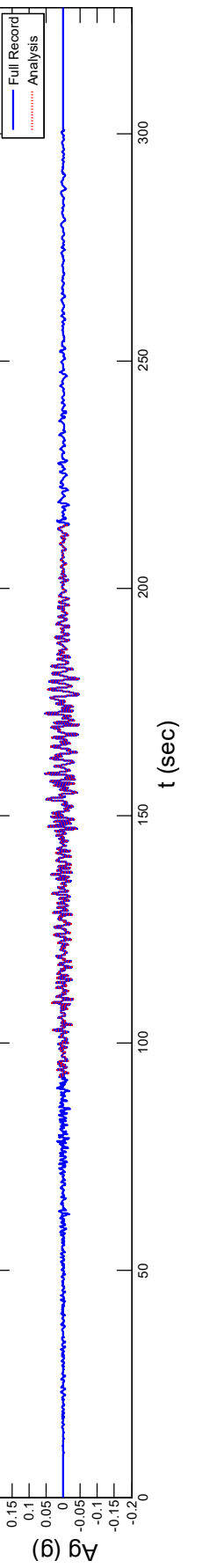
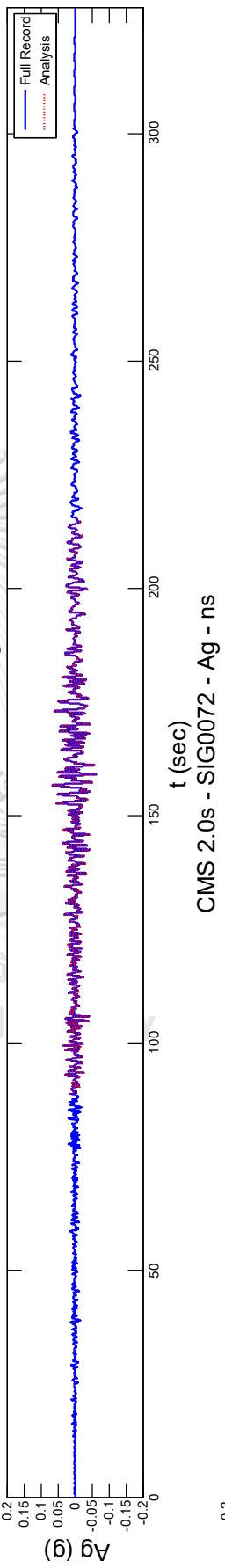
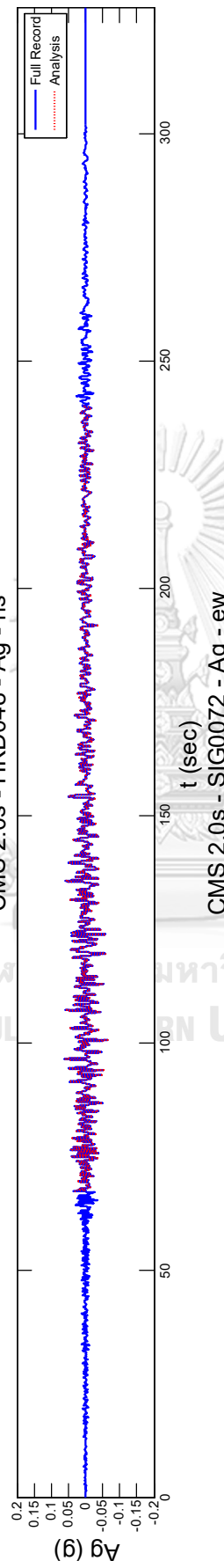
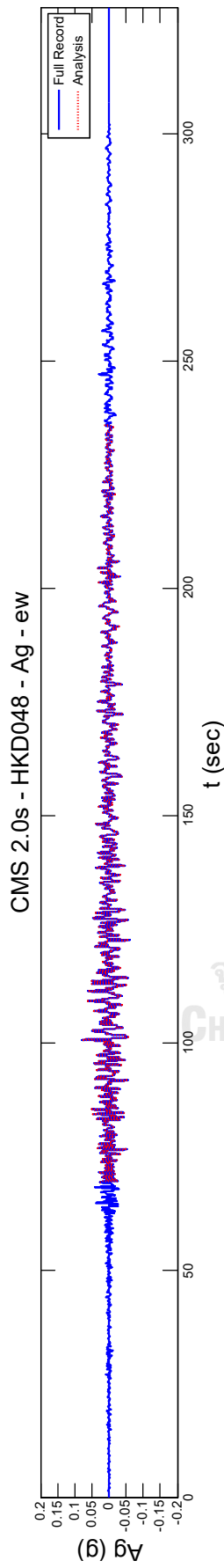


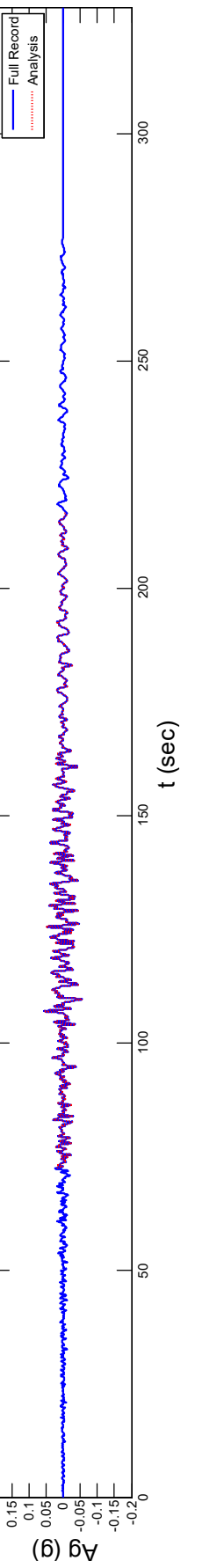
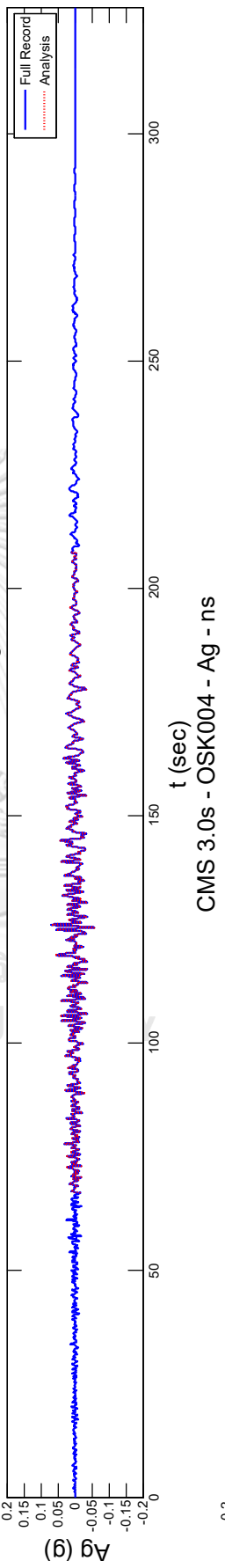
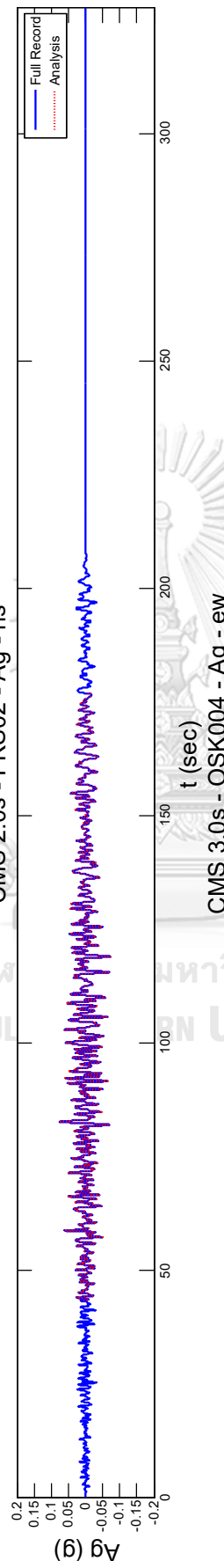
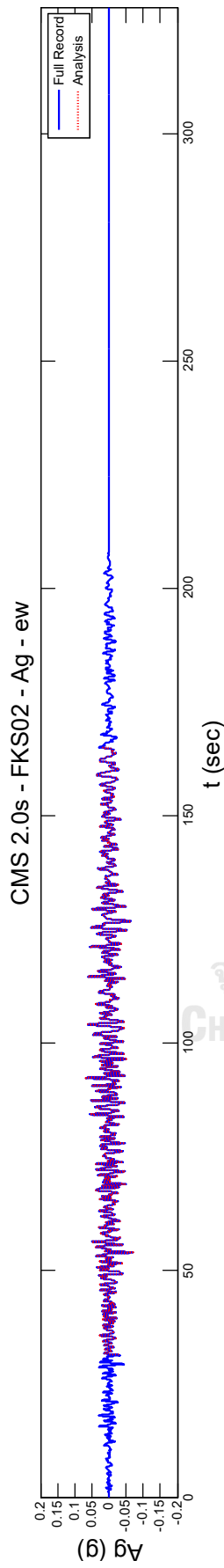


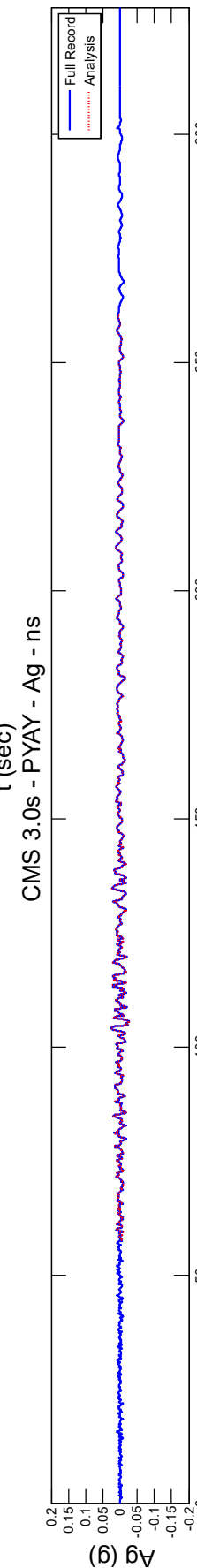
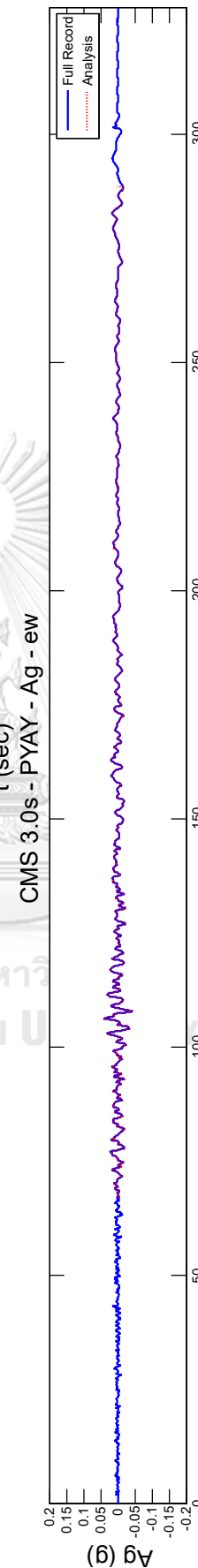
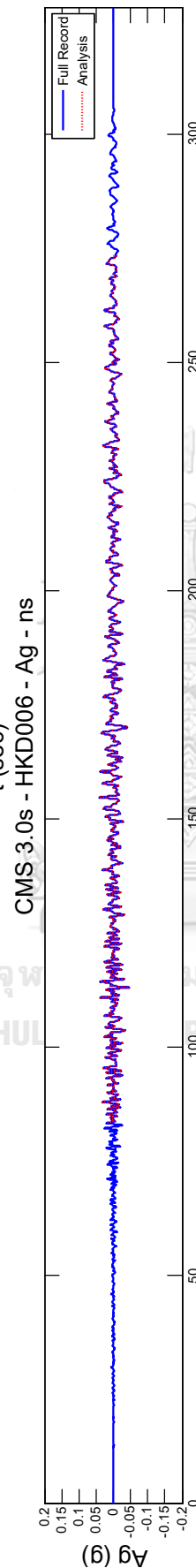
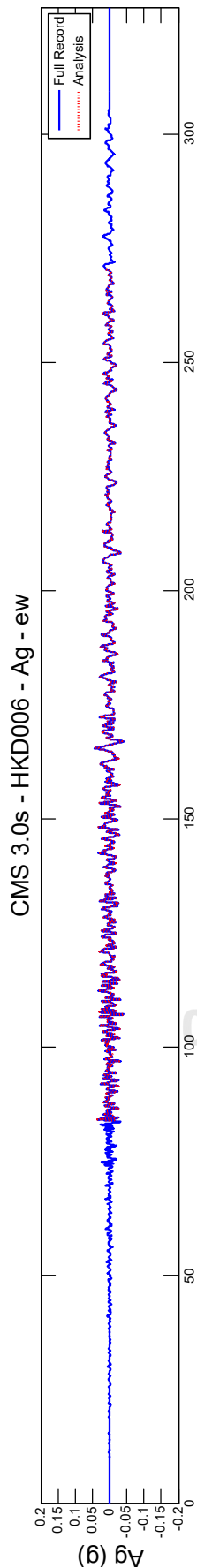


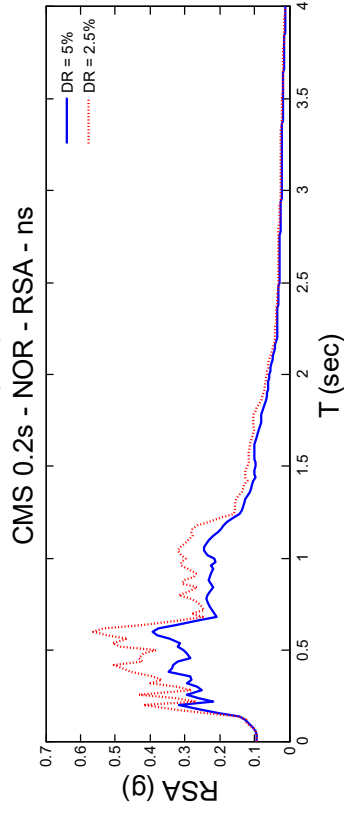
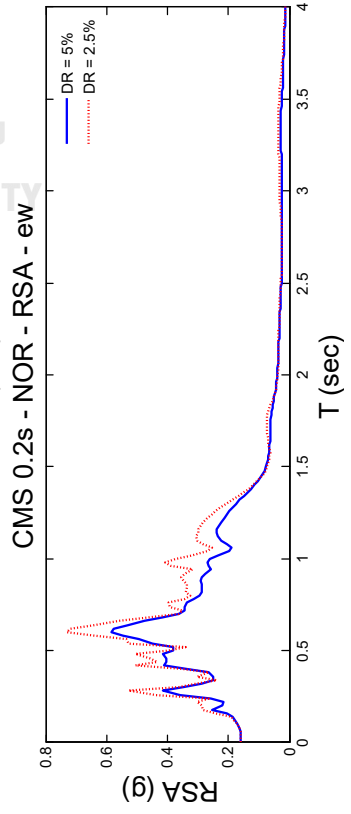
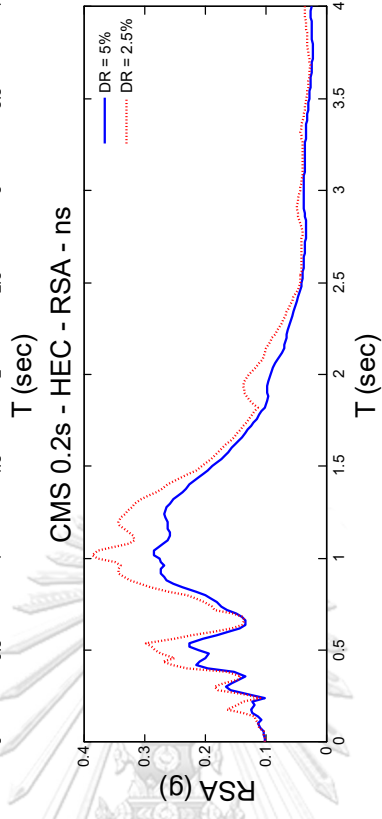
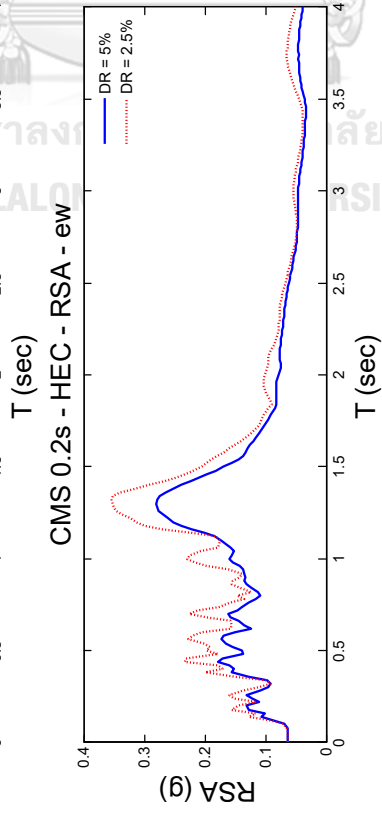
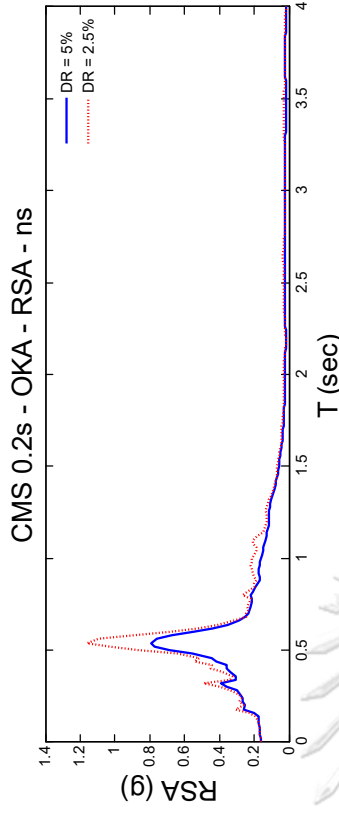
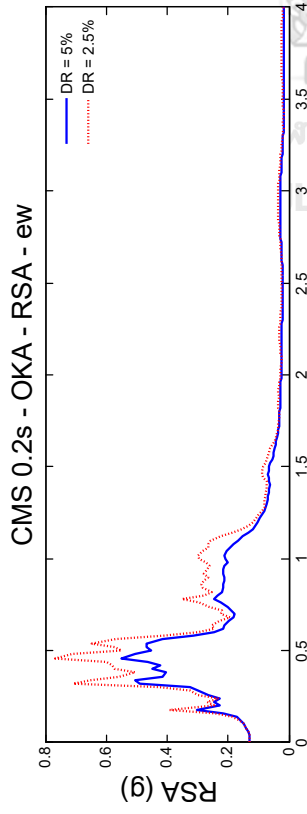


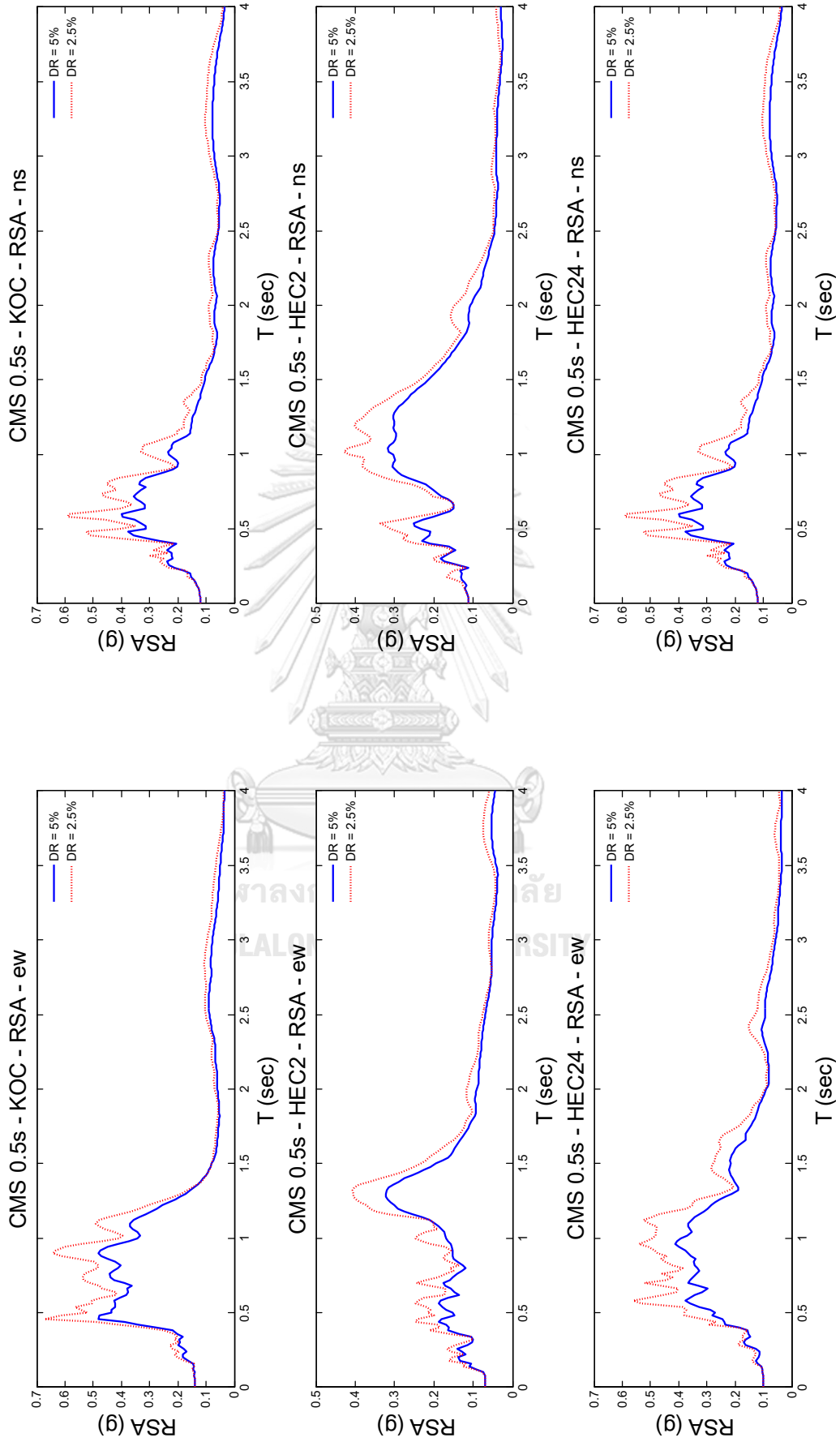


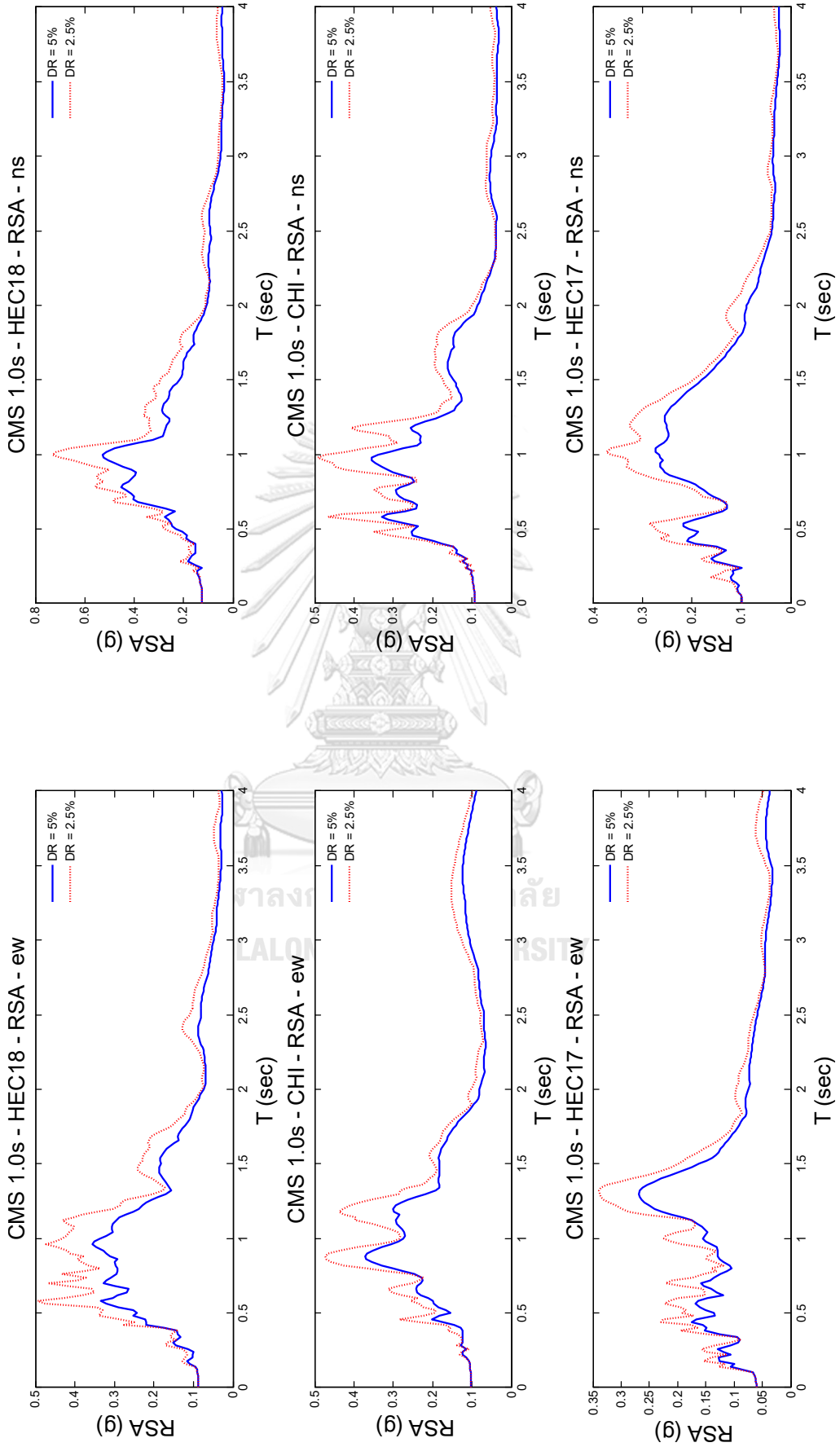


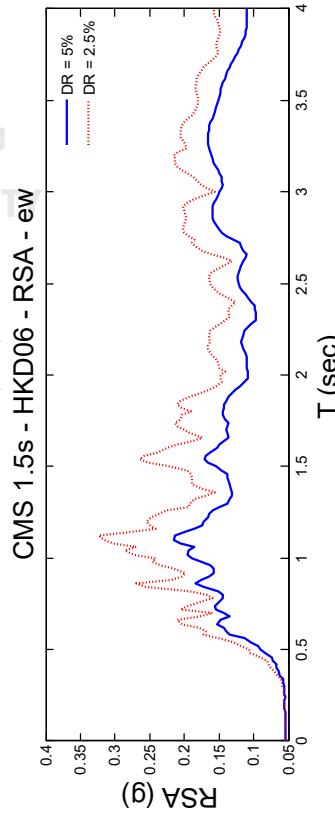
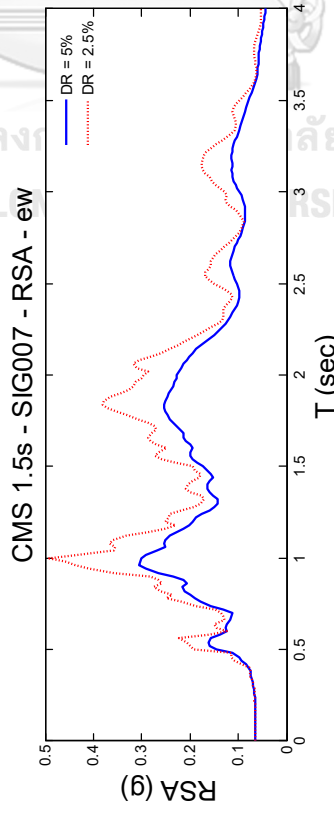
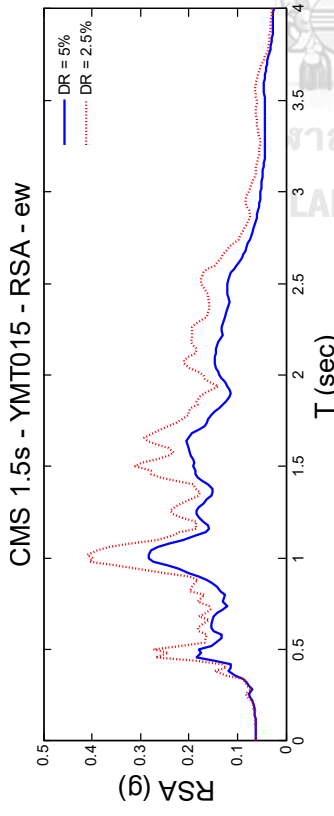
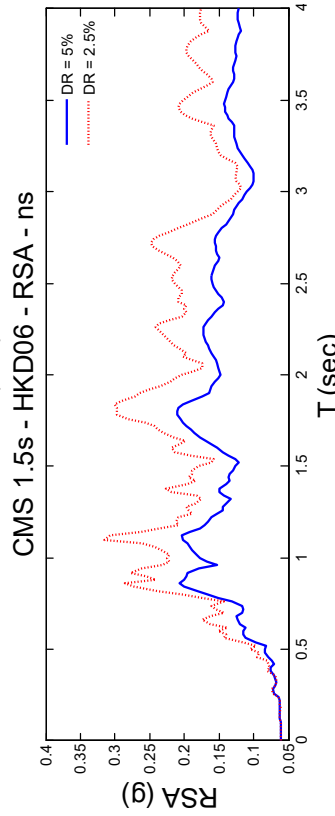
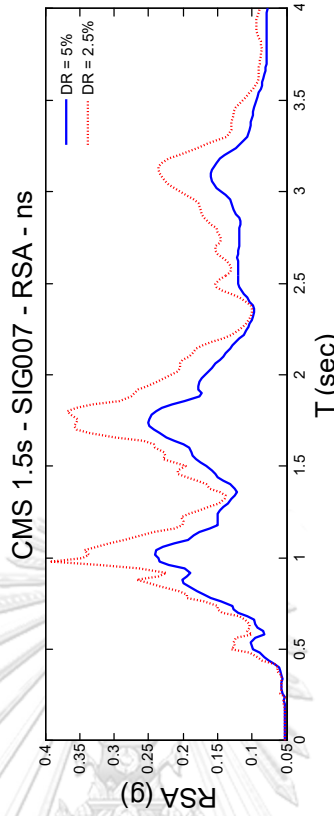
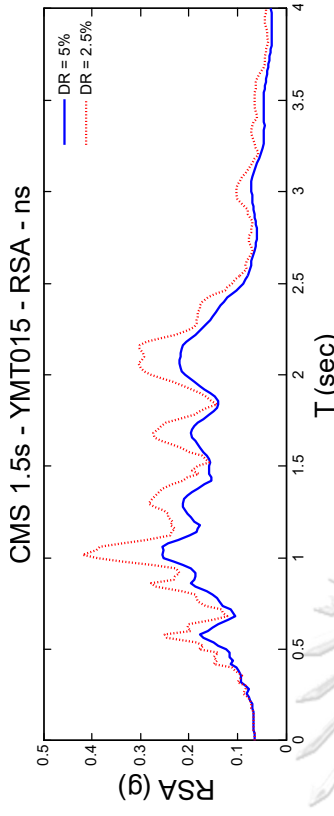


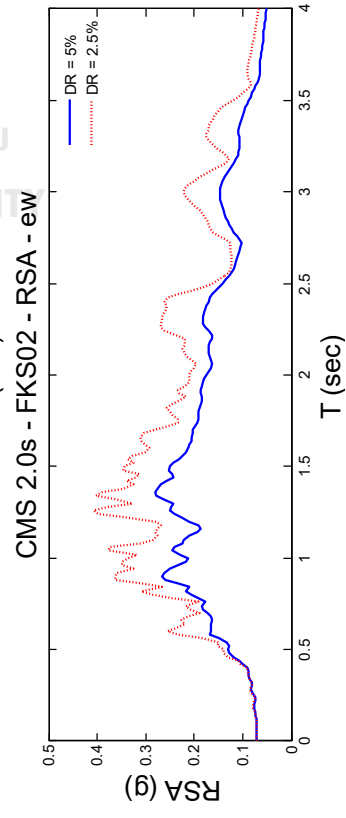
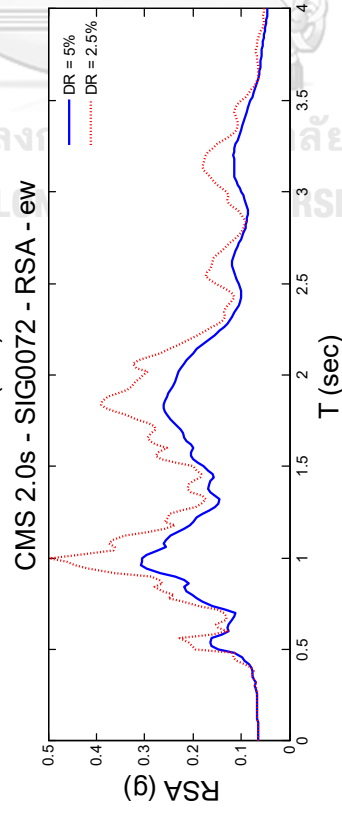
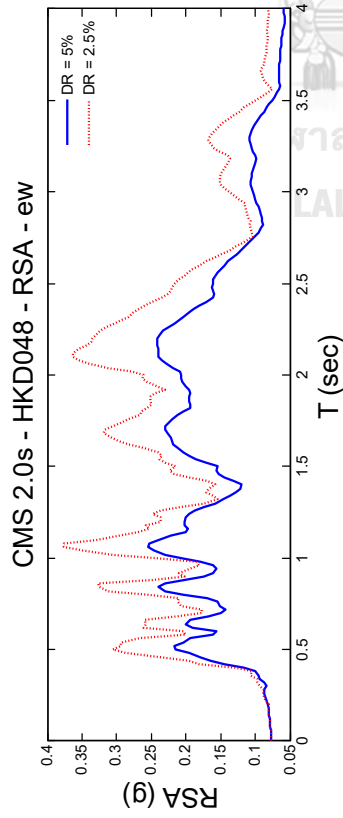
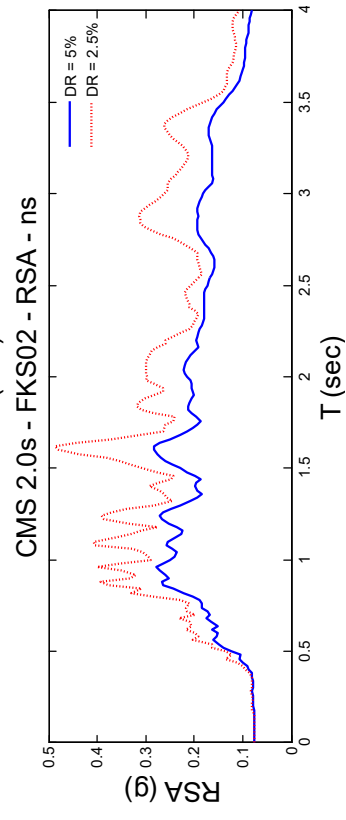
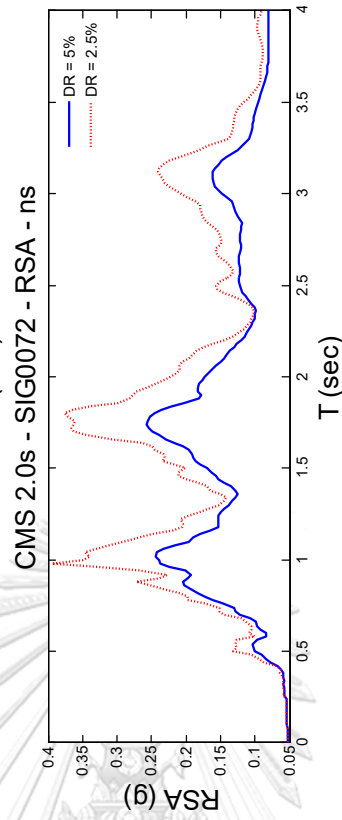
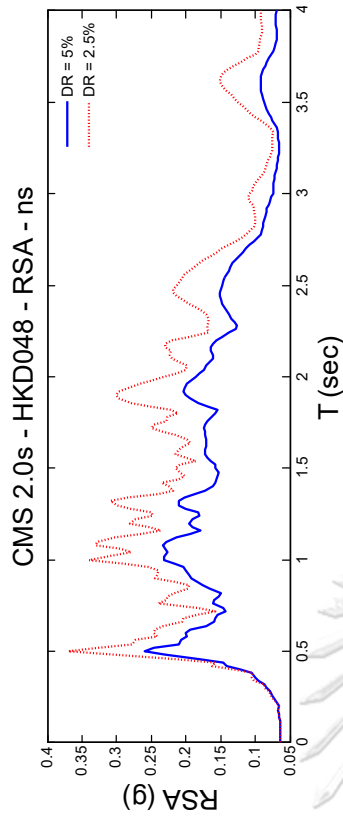


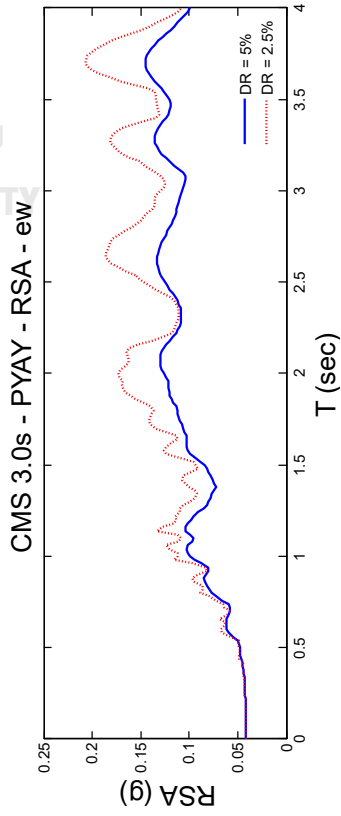
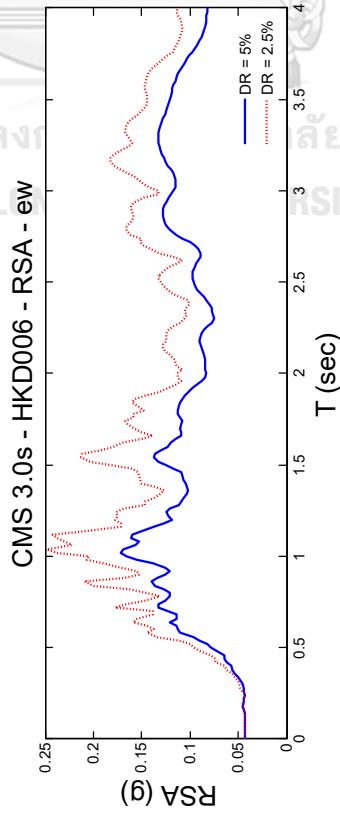
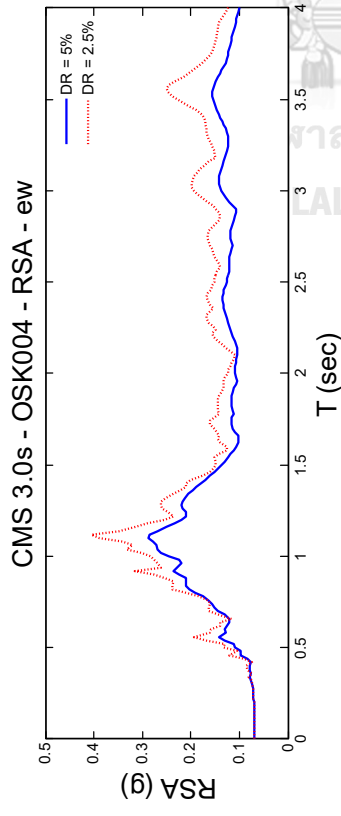
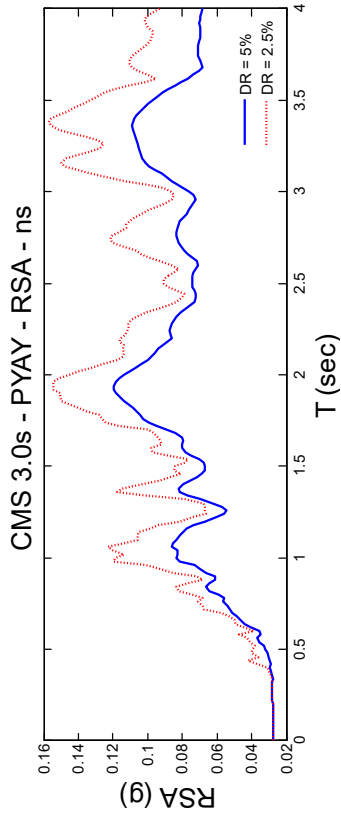
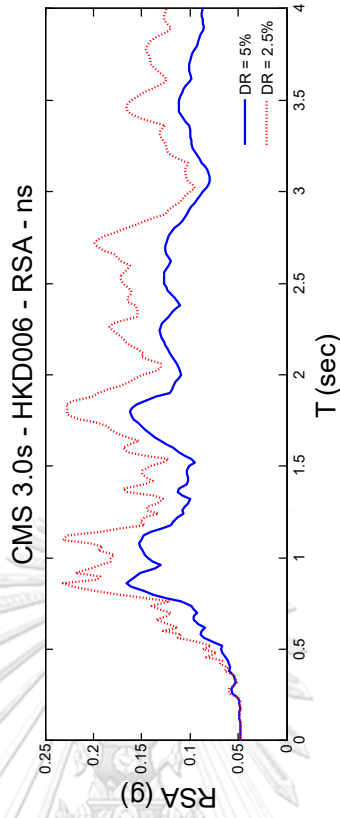
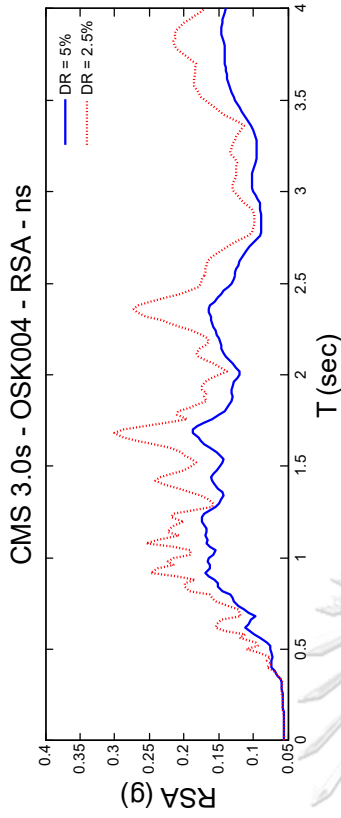












Buildings

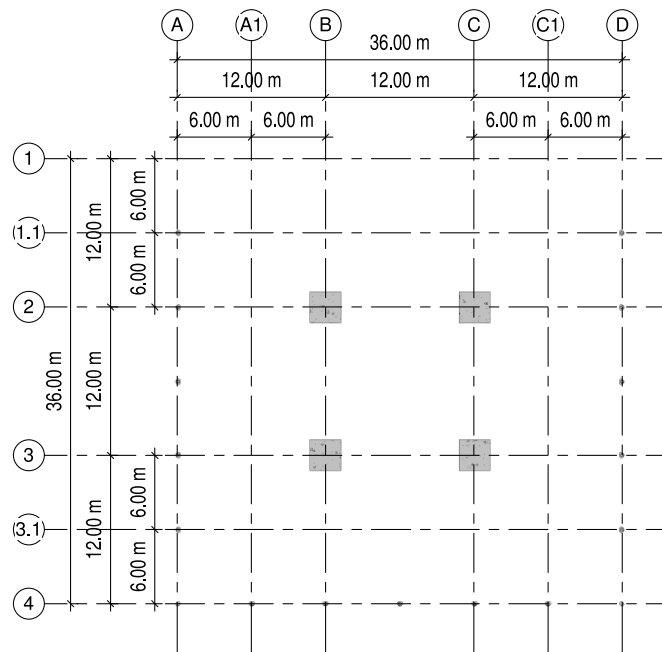
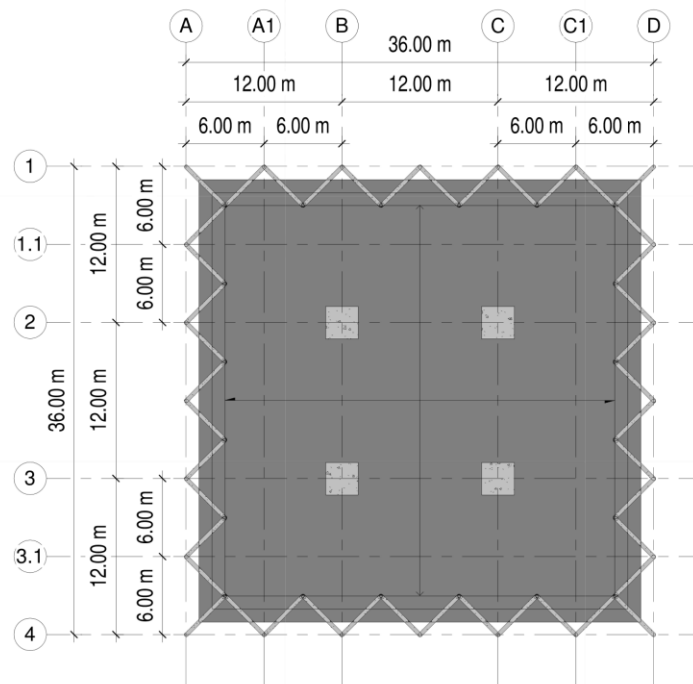


Figure C.1 Story plan for all buildings at ground level.



Level 1
1 : 250

Figure C.2 Story plan for all buildings in-between module.

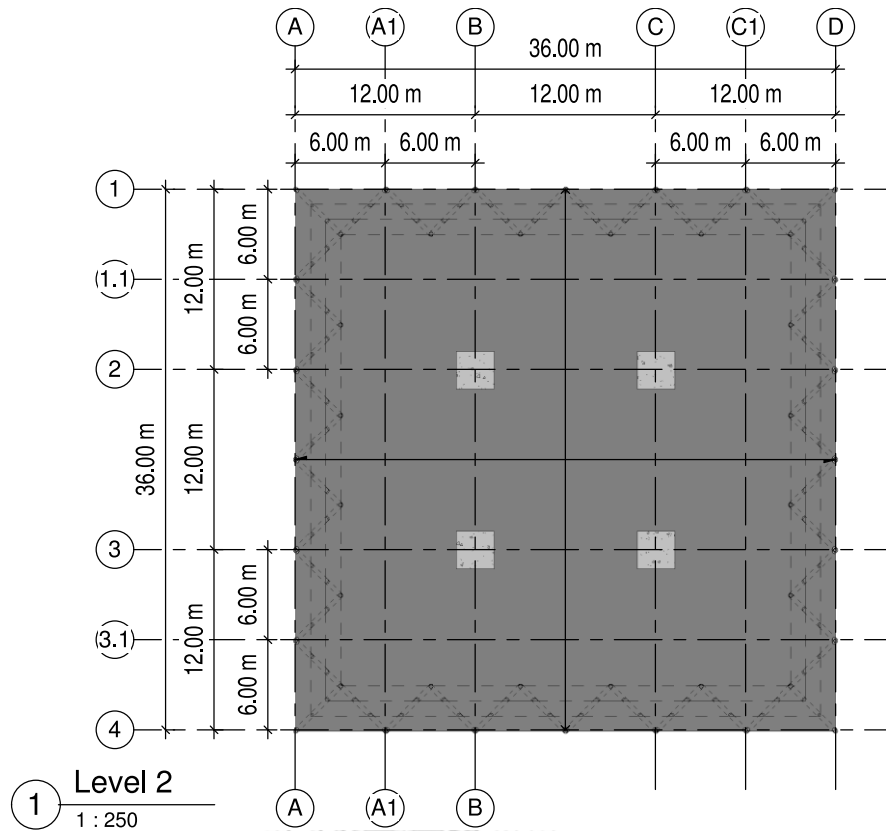


Figure C.3 Story plan for all buildings at mid and end module level.

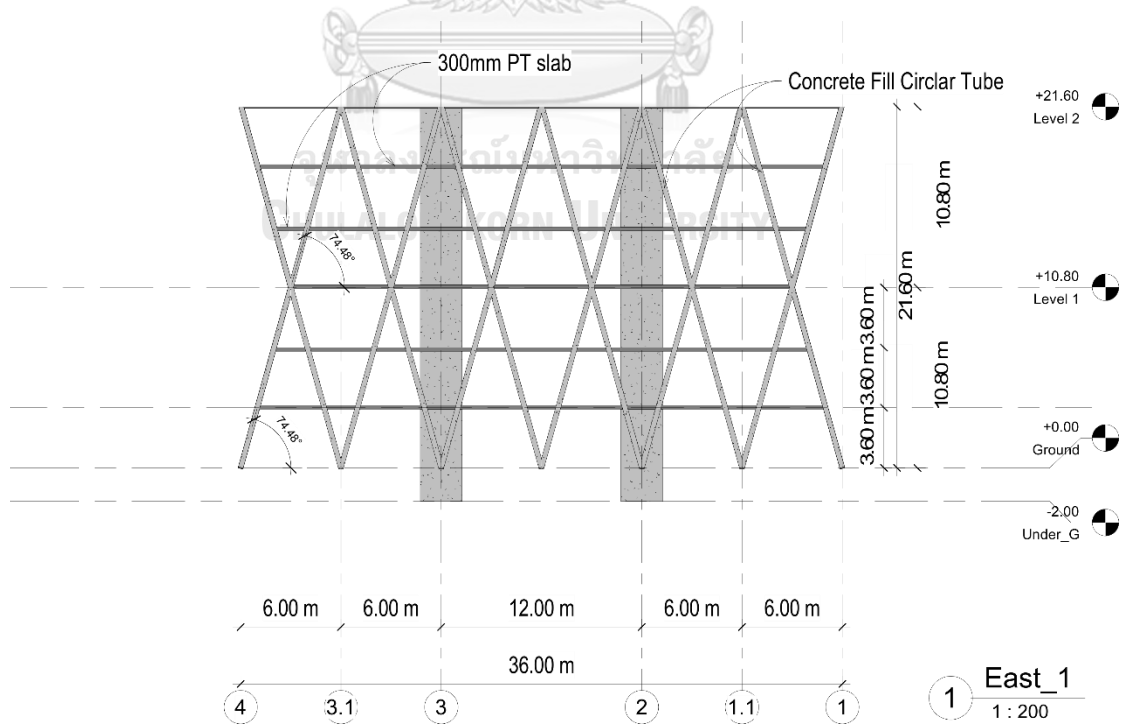


Figure C.4 Sample diagrid module expands to six stories for all buildings.

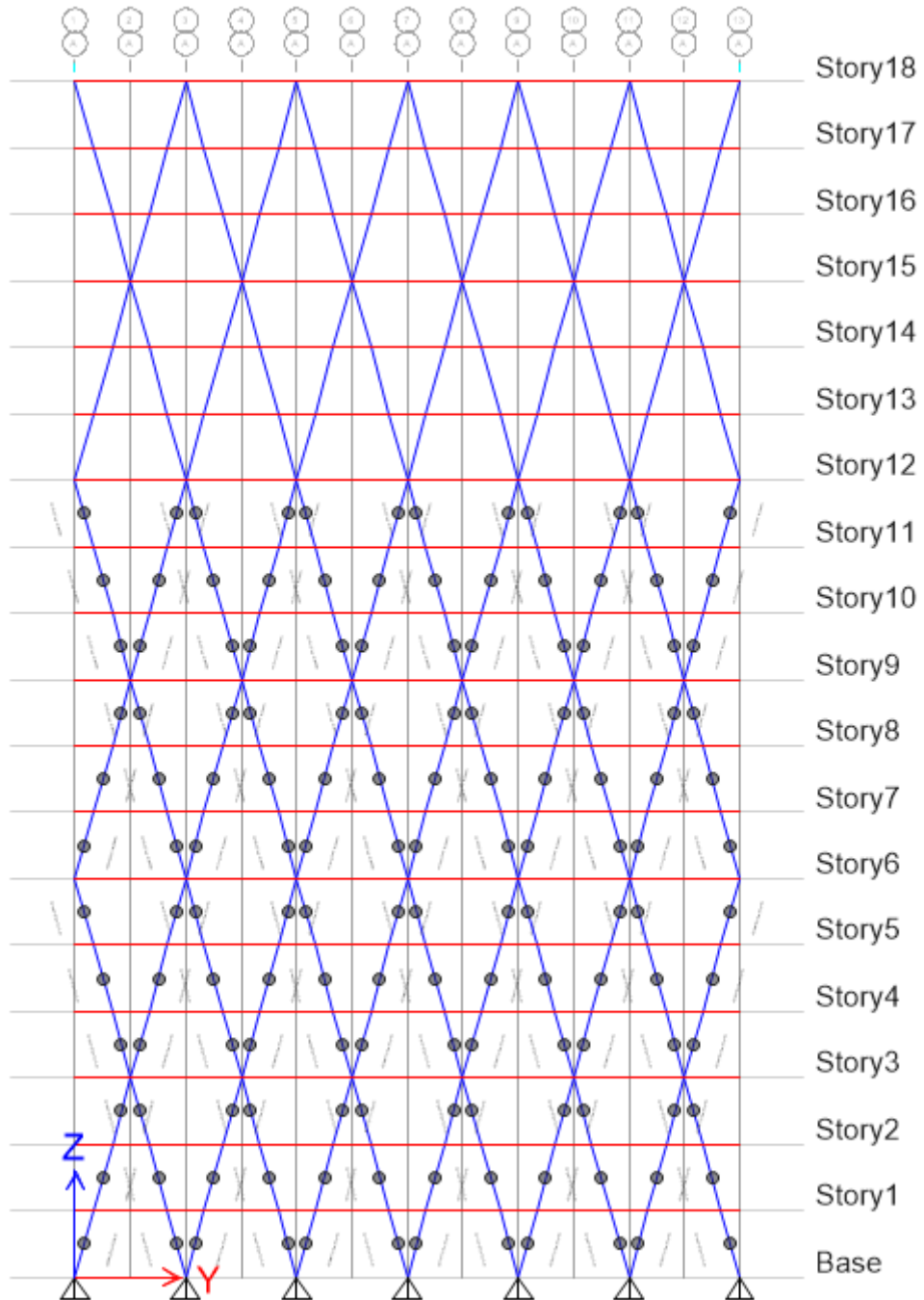


Figure C.5 Elevation view of 18R5 with plastic hinges (CSI, 2015).

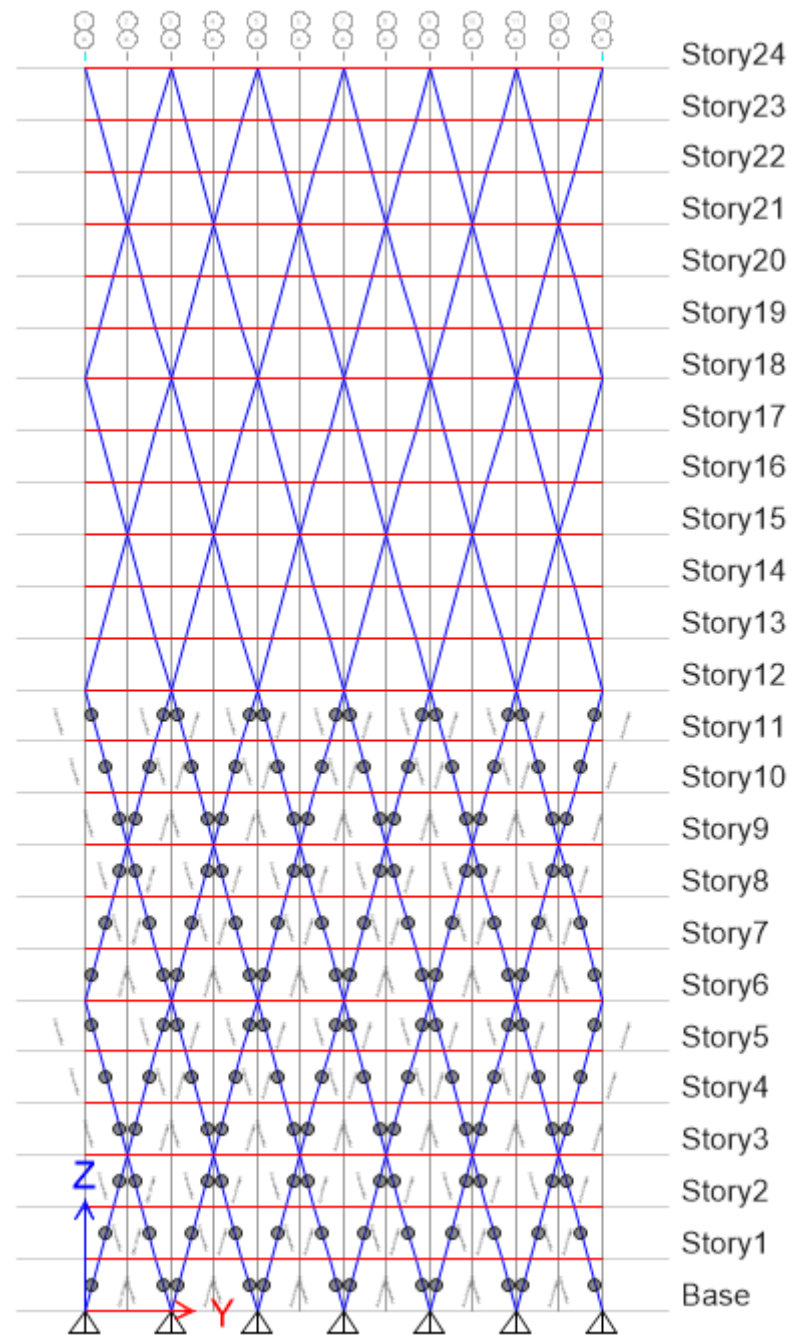


Figure C.6 Elevation view of 24R5 with plastic hinges.

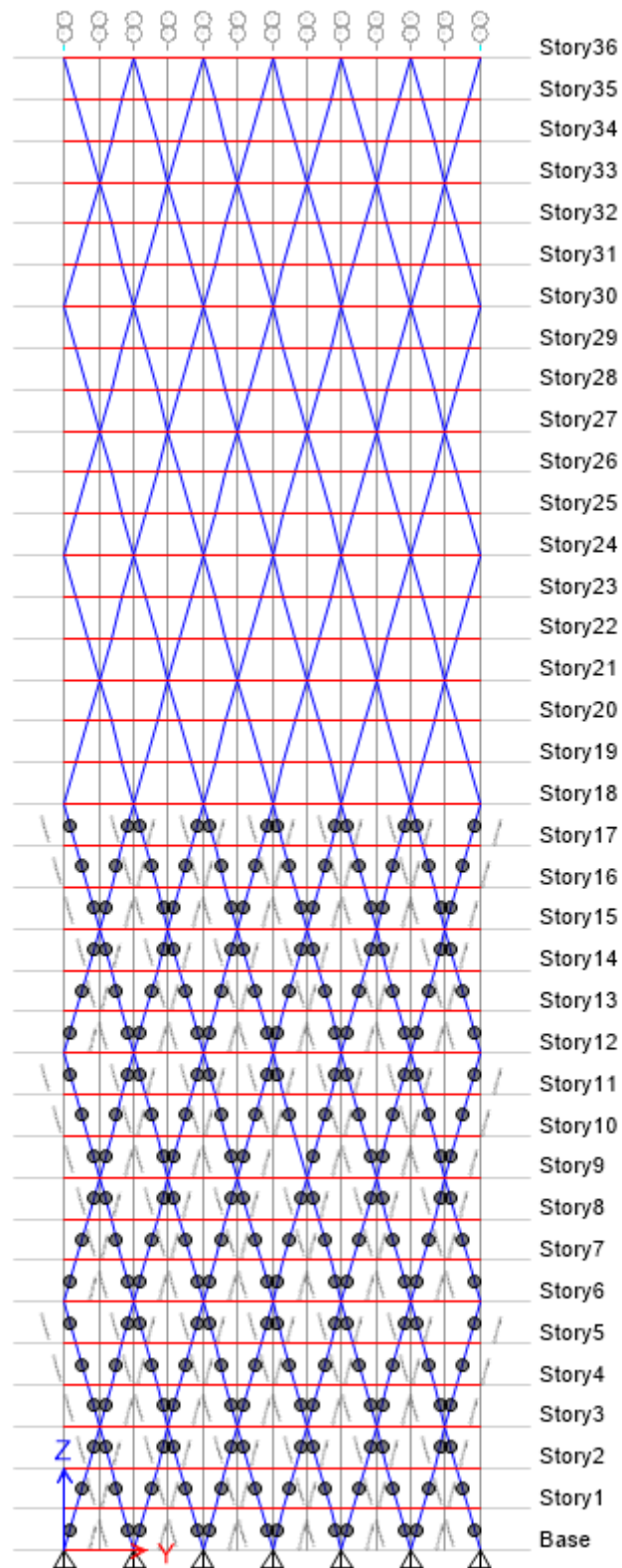


Figure C.7 Elevation view of 36R5 with plastic hinges (CSI, 2015).

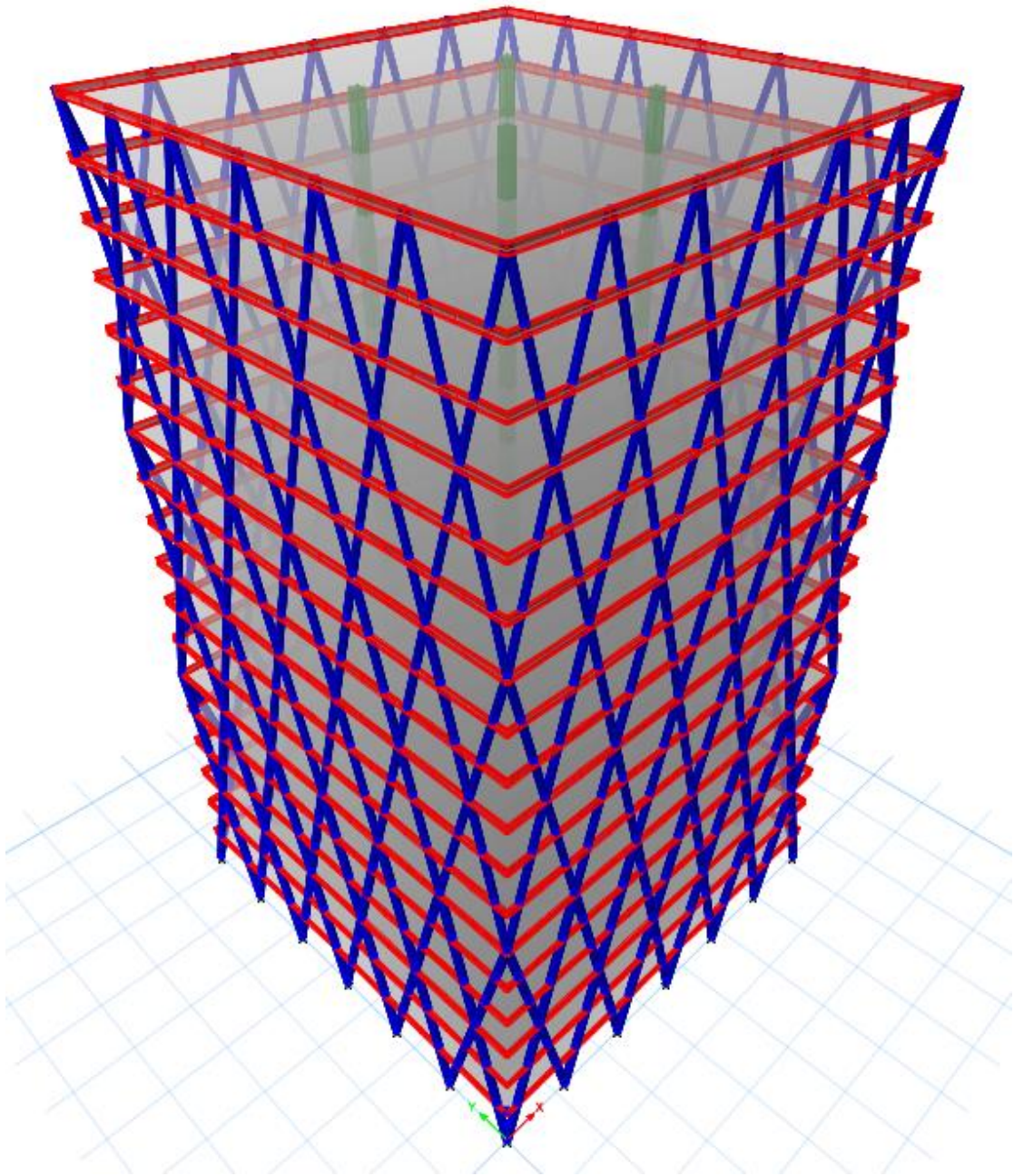


Figure C.8 3D view of 18R5 (CSI, 2015).

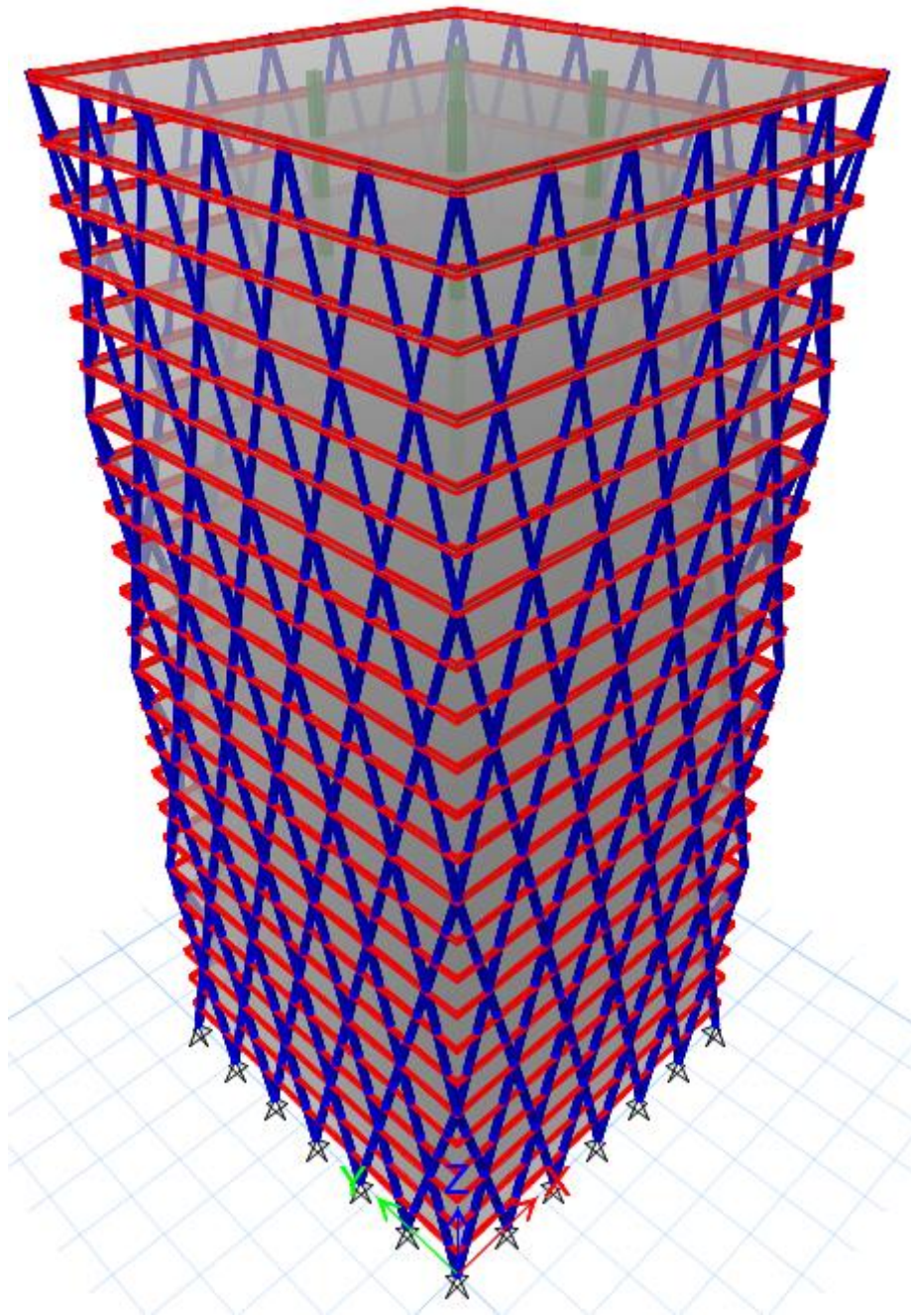


Figure C.9 3D view of 24R5 (CSI, 2015).

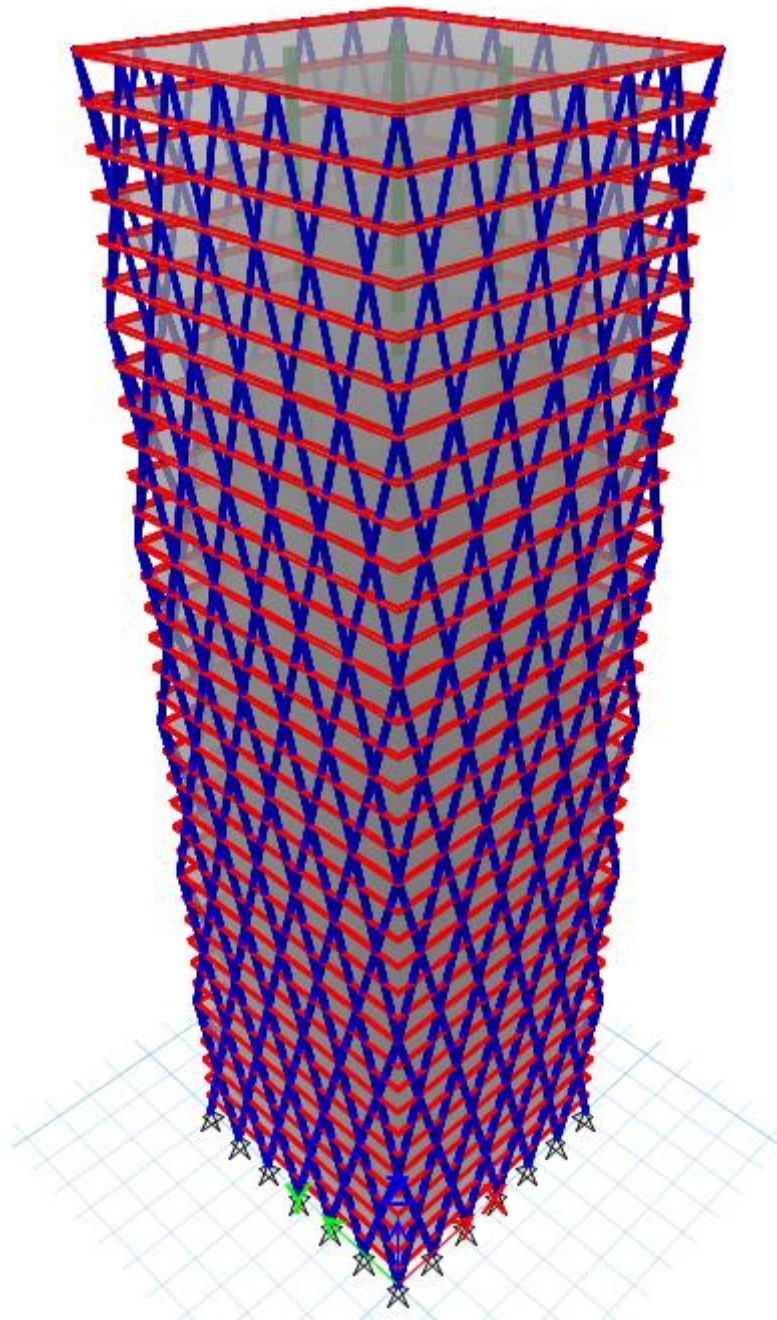


Figure C.10 3D view of 36R5 (CSI, 2015).

Summary

ID	Story	Height	Diagrid Story per module	Diagrid inclination
18R5	18@3.6 m	64.8 m	6	74.5
24R5	24@3.6 m	86.4 m	6	74.5
36R5	36@3.6 m	129.6 m	6	74.5

Design Parameters

ID	R	$T=C_u T_a$ (s)	T_1 (s)	T_2 (s)	C_s (g)	CMS set	S_{MT} (g)
18R5	5	1.67	1.57	0.83	0.030	1.5s,0.5s	0.227
24R5	5	2.06	1.98	1.00	0.033	2.0s,1.0s	0.2465
36R5	5	2.79	3.03	1.37	0.021	3.0s,1.5s	0.155

Base shear for RSA

Assume $C_d = 5$

ID	W (kN)	C_s	K	V (kN)	V_{dyn} (kN)	V_{dyn} - strength design (kN)	Δ_{dyn}	$C_d \Delta_{dyn}$	Limit (ASCE 7-05)
18R5	262077	0.03	1.585	7862	6090	6705	0.000577 (~0.06%)	0.002885 (~0.3%)	2% OK
24R5	358475	0.033	2.0	11830	9312	10109	0.000799 (~0.08%)	0.003995 (~0.4%)	2% OK
36R5	555088	0.021	2.0	11657	8542	9952	0.000775 (~0.08%)	0.003875 (~0.4%)	2% OK

W = Seismic weight of structure

K = Coefficient for equivalent lateral force method

V = Static base shear computed as a product of W and C_s

V_{dyn} = Dynamic base shear computed based on modal periods

V_{dyn} - strength design = Base shear required for strength design of members requiring at least 85% of static base shear.

Δ_{dyn} = Maximum inter-story drift ratio of structure subjected to dynamic base shear

Base Shear Calculation

Example: Base shear calculation of 24R5

$$H = 86.4 \text{ m}$$

$$W = 358,475 \text{ kN}$$

$$R = 5.0$$

$$I = 1.0$$

$$T_a = 0.0488H^{0.75} \text{ (ASCE 7-05) [H in meter]}$$

$$T_a = 0.0488(86.4 \text{ m})^{0.75} = 1.383 \text{ sec}$$

$$\text{Assume } C_u = 1.5$$

$$T = C_u T_a = 1.5 \times 1.383 = 2.06 \text{ sec}$$

$$S_{DT}(T = 2.06\text{s}) = 0.170 + \frac{(0.086 - 0.170)}{(3 - 2)}(2.06 - 2) = 0.166$$

$$C_s = S_{DT} \times \frac{I}{R} = 0.166 \times \frac{1}{5} = 0.0332 \cong 0.033$$

$$V = C_s W = 11,830 \text{ kN (Equivalent Lateral Force: base shear)}$$

$$V_{\text{dynamic-strength}} \geq (85\%)V = 10,109 \text{ kN (Dynamic base shear for strength design)}$$

Gravity load and mass in design and analysis

	Design Phrase (RSA)	Analysis Phrase (Nonlinear)
Gravity load	$1.4(DL+SDL)$ $1.2(DL+SDL)+1.6LL$ (ASCE 7-05)	$1.05(DL+SDL)+0.25LL$ (applied prior to seismic load) (FEMA P695)
Seismic load	$1.2(DL+SDL)+1.0LL+1.0Ex+0.3Ey$ $1.2(DL+SDL)+1.0LL+0.3Ex+1.0Ey$ $0.9(DL+SDL)+1.0Ex+0.3Ey$ $0.9(DL+SDL)+0.3Ex+1.0Ey$ (ASCE 7-05)	$1.0Ex$ (applied in one direction only)
P-Delta load combination (ETABS)	$1.2(DL+SDL)+0.5LL$ (CSI Manual)	$1.05(DL+SDL)+0.25LL$ (use this load combination to be consistent with gravity load)
Seismic weight of structure (W)	$1.0(DL+SDL)$	$1.0(DL+SDL)$

Note: DL = self weight, SDL = superimposed deadload, LL = Liveload

Load Case	Distributed Load ($\text{kN/m}^2 = \text{kPa}$)
Office (typical floor)	$SDL = 3$ $LL = 2.5$ (office floor, ASCE 7-05)
Roof (roof floor)	$LL = 1.5$ (roof floor, ASCE 7-05)

Diagrid

(underlined = nonlinear hinge applied for nonlinear analysis model)

All Steel sections are A53b, $F_y = 245$ MPa (35 ksi)

All concrete specific compressive strength, $f'_c = 42$ MPa (6 ksi)

18R5

Module	Story	Diameter of tube (inch/mm)	Thickness of tube (inch/mm)	D/t
<u>1</u>	1-6	20 / 508	0.5 / 12.7	40
<u>2</u>	7-12	16 / 406.4	0.625 / 15.9	25.6
3	13-18	14 / 355.6	0.625 / 15.9	22.4

24R5

Module	Story	Diameter of tube (inch/mm)	Thickness of tube (inch/mm)	D/t
1	1-6	22 / 558.8	0.625 / 15.9	35.2
<u>2</u>	7-12	20 / 508	0.625 / 15.9	32
3	13-18	18 / 457.2	0.5 / 12.7	36
4	19-24	14 / 355.6	0.625 / 15.9	22.4

36R5

Module	Story	Diameter of tube (inch/mm)	Thickness of tube (inch/mm)	D/t
1	1-6	26 / 660.4	0.625 / 15.9	41.6
<u>2</u>	7-12	24 / 609.6	0.625 / 15.9	38.4
<u>3</u>	13-18	22 / 558.8	0.5 / 12.7	44
4	19-24	20 / 508	0.5 / 12.7	40
5	25-30	18 / 457.2	0.5 / 12.7	36
6	31-36	14 / 355.6	0.5 / 12.7	28

Slab

Slab	Thickness (mm)	f'_c (MPa)	EI eff
A	300	35	0.25

Exterior Beam (A992 $F_y = 50$ ksi, 345 MPa)

Beam	Section	Total Depth (mm)	Web thickness (mm)	Flange Width (mm)	Flange thickness (mm)
A	W21x50	528.3	9.7	165.9	13.6

Reinforced Concrete Column

$$EI_{\text{eff}} = 0.70EI \text{ of gross section}$$

All Rebar size: #18 = 57.3 mm. All Rebar grade is A615Gr60, $F_y = 410$ MPa

All column's concrete specific compressive strength, $f'_c = 60$ MPa (8.7 ksi)

18R5

Module	Story	Height / Width (in)	Height / Width (mm)	# Rebar along 2-dir Face	# Rebar along 3-dir Face
1	1-6	45x45	1143x1143	6	6
2	7-12	35x35	1000x1000	4	4
3	13-18	25x25	635x635	4	4

24R5

Module	Story	Height / Width (in)	Height / Width (mm)	# Rebar along 2-dir Face	# Rebar along 3-dir Face
1	1-6	60x60	1524x1524	6	6
2	7-12	50x50	1270x1270	6	6
3	13-18	35x35	1000x1000	4	4
4	19-24	25x25	635x635	4	4

36R5

Module	Story	Height / Width (in)	Height / Width (mm)	# Rebar along 2-dir Face	# Rebar along 3-dir Face
1	1-6	70x70	1778x1778	10	10
2	7-12	70x70	1778x1778	8	8
3	13-18	60x60	1524x1524	6	6
4	19-24	50x50	1270x1270	6	6
5	25-30	40x40	1016x1016	4	4
6	31-36	25x25	635x635	4	4

Example Calculation of Diagrid Strength

Design of CCFT Section

Yellow = input

Steel Property:

- yield strength of steel $F_y := 35 \text{ ksi} = 241 \text{ MPa}$

- young's modulus of steel $E_s := 29000 \text{ ksi} = 199948 \text{ MPa}$

Concrete Property:

- specific compressive strength of concrete $f'_c := 6 \text{ ksi} = 41.4 \text{ MPa}$

- unit weight of concrete $w_c := 150 \frac{\text{lb}}{\text{ft}^3}$

- young's modulus of concrete $E_c := w_c^{1.5} \cdot \sqrt{f'_c} \left(\frac{\text{ft}^3}{\text{lb}} \right)^{1.5} \cdot \text{ksi}^{0.5} = 4500 \text{ ksi}$

$$E_c = 31026 \text{ MPa}$$

Designed Section:

- diameter of steel tube $D := 22 \text{ in} = 558.8 \text{ mm}$ $r := \frac{D}{2} = 279.4 \text{ mm}$

- thickness of steel tube $t := 0.625 \text{ in} = 15.875 \text{ mm}$

- length of member $L := 147.1 \text{ in} = 3.736 \text{ m}$

Step1: Section Property

- design thickness $t_{\text{design}} := 0.93 \cdot t = 14.764 \text{ mm}$

- D/t ratio $\lambda := \frac{D}{t} = 35.2$

- Highly ductile req. $\lambda_{\text{highly ductile}} := 0.076 \cdot \frac{E_s}{F_y} = 62.971$

if $\lambda < \lambda_{\text{highly ductile}}$, the section is **highly ductile** **YES**

- diameter and radius of concrete section

$$D_c := D - 2 \cdot t_{\text{design}} = 529.3 \text{ mm}$$

$$r_c := \frac{D_c}{2} = 264.6 \text{ mm}$$

- area of concrete section

$$A_c := \pi \cdot (r_c)^2 = 2200 \text{ cm}^2 \quad A_c = 341 \text{ in}^2$$

- moment of inertia of concrete section

$$I_c := \frac{\pi}{4} \cdot r_c^4 = 385201 \text{ cm}^4 \quad I_c = 9254 \text{ in}^4$$

- area of steel section

$$A_s := \pi \cdot (r)^2 - A_c = 252 \text{ cm}^2 \quad A_s = 39.1 \text{ in}^2$$

- moment of inertia of steel section

$$I_s := \frac{\pi}{4} (r)^4 - I_c = 93424 \text{ cm}^4 \quad I_s = 2245 \text{ in}^4$$

- coefficient based on areas of two sections

$$C3 := \begin{cases} \text{if } 0.6 + 2 \cdot \left(\frac{A_s}{A_s + A_c} \right) \leq 0.9 & = 0.806 \quad \text{Less than or equal to } 0.9 \\ \left| \left| \begin{array}{l} 0.6 + 2 \cdot \left(\frac{A_s}{A_s + A_c} \right) \\ \text{else} \\ 0.9 \end{array} \right. \right. & \end{cases}$$

- EI effective of section

$$EI_{eff} := E_s \cdot I_s + C3 \cdot E_c \cdot I_c = 283102 \text{ kN} \cdot \text{m}^2$$

$$EI_{eff} = 98648131 \text{ kip} \cdot \text{in}^2$$

Step2: Compressive Strength $\phi_c := 0.75$

- Euler strength

$$P_e := \pi^2 \cdot \frac{EI_{eff}}{L^2} = 200147 \text{ kN} \quad P_e = 44995 \text{ kip}$$

- coefficient for steel tube

$$C2 := 0.95 \quad (\text{Circular Concrete-filled Steel Tube}) \text{ [AISC-360]}$$

- short column strength

$$P_{no} := F_y \cdot A_s + C2 \cdot f'_c \cdot A_c = 14736 \text{ kN} \quad P_{no} = 3313 \text{ kip}$$

- Nominal Strength

$$P_n := \begin{cases} \text{if } \frac{P_{no}}{P_e} \leq 2.25 & = 14289 \text{ kN} \quad P_n = 3212 \text{ kip} \\ \left| \left| \begin{array}{l} P_n \leftarrow P_{no} \cdot 0.658 \frac{P_{no}}{P_e} \\ \text{else} \\ P_n \leftarrow 0.877 \cdot P_e \end{array} \right. \right. & \end{cases}$$

- Design compressive strength

$$\phi_c P_n := \phi_c \cdot P_n = 10716 \text{ kN} \quad \phi_c P_n = 2409 \text{ kip}$$

Step2: Tensile Strength $\phi_t := 0.9$

$$T_n := F_y \cdot A_s = 6089 \text{ kN} \quad T_n = 1369 \text{ kip}$$

- Design tensile strength

$$\phi_t T_n := \phi_t \cdot T_n = 5480 \text{ kN} \quad \phi_t T_n = 1232 \text{ kip}$$

Design of CCFT Section

Yellow = input

Case of Expected Strength

Steel Property:

- yield strength of steel $F_y := 35 \cdot 1.6 \text{ ksi} = 386 \text{ MPa}$

- young's modulus of steel $E_s := 29000 \text{ ksi} = 199948 \text{ MPa}$

Concrete Property:

- specific compressive strength of concrete $f'_c := 7.63 \text{ ksi} = 52.6 \text{ MPa}$

- unit weight of concrete $w_c := 150 \frac{\text{lb}}{\text{ft}^3}$

- young's modulus of concrete $E_c := w_c^{1.5} \cdot \sqrt{f'_c} \left(\frac{\text{ft}^3}{\text{lb}} \right)^{1.5} \cdot \text{ksi}^{0.5} = 5074.57 \text{ ksi}$

$$E_c = 34988 \text{ MPa}$$

Designed Section:

- diameter of steel tube $D := 22 \text{ in} = 558.8 \text{ mm}$ $r := \frac{D}{2} = 279.4 \text{ mm}$

- thickness of steel tube $t := 0.625 \text{ in} = 15.875 \text{ mm}$

- length of member $L := 147.1 \text{ in} = 3.736 \text{ m}$

Step1: Section Property

- design thickness $t_{\text{design}} := 0.93 \cdot t = 14.764 \text{ mm}$

- D/t ratio $\lambda := \frac{D}{t} = 35.2$

- Highly ductile req. $\lambda_{\text{highly_ductile}} := 0.076 \cdot \frac{E_s}{F_y} = 39.357$

if $\lambda < \lambda_{\text{highly_ductile}}$, the section is **highly ductile** **YES**

- diameter and radius of concrete section

$$D_c := D - 2 \cdot t_{\text{design}} = 529.3 \text{ mm}$$

$$r_c := \frac{D_c}{2} = 264.6 \text{ mm}$$

- area of concrete section

$$A_c := \pi \cdot (r_c)^2 = 2200 \text{ cm}^2$$

$$A_c = 341 \text{ in}^2$$

- moment of inertia of concrete section

$$I_c := \frac{\pi}{4} \cdot r_c^4 = 385201 \text{ cm}^4$$

$$I_c = 9254 \text{ in}^4$$

- area of steel section

$$A_s := \pi \cdot (r)^2 - A_c = 252 \text{ cm}^2 \quad A_s = 39.1 \text{ in}^2$$

- moment of inertia of steel section

$$I_s := \frac{\pi}{4} (r)^4 - I_c = 93424 \text{ cm}^4 \quad I_s = 2245 \text{ in}^4$$

- coefficient based on areas of two sections

$$C3 := \begin{cases} \text{if } 0.6 + 2 \cdot \left(\frac{A_s}{A_s + A_c} \right) \leq 0.9 & = 0.806 \quad \text{Less than or equal to 0.9} \\ \left\| \begin{array}{l} 0.6 + 2 \cdot \left(\frac{A_s}{A_s + A_c} \right) \\ \text{else} \\ 0.9 \end{array} \right\| \end{cases}$$

- EI effective of section

$$EI_{eff} := E_s \cdot I_s + C3 \cdot E_c \cdot I_c = 295398 \text{ kN} \cdot \text{m}^2$$

$$EI_{eff} = 102932735 \text{ kip} \cdot \text{in}^2$$

Step2: Compressive Strength $\phi_c := 0.75$

- Euler strength

$$P_e := \pi^2 \cdot \frac{EI_{eff}}{L^2} = 208840 \text{ kN} \quad P_e = 46949 \text{ kip}$$

- coefficient for steel tube

$$C2 := 0.95 \quad (\text{Circular Concrete-filled Steel Tube}) \text{ [AISC-360]}$$

- short column strength

$$P_{no} := F_y \cdot A_s + C2 \cdot f'_c \cdot A_c = 20738 \text{ kN} \quad P_{no} = 4662 \text{ kip}$$

- Nominal Strength

$$P_n := \begin{cases} \text{if } \frac{P_{no}}{P_e} \leq 2.25 & = 19894 \text{ kN} \quad P_n = 4472 \text{ kip} \\ \left\| \begin{array}{l} P_n \leftarrow P_{no} \cdot 0.658 \cdot \frac{P_{no}}{P_e} \\ \text{else} \\ P_n \leftarrow 0.877 \cdot P_e \end{array} \right\| \end{cases}$$

- Design compressive strength

$$\phi_c P_n := \phi_c \cdot P_n = 14920 \text{ kN} \quad \phi_c P_n = 3354 \text{ kip}$$

Step2: Tensile Strength $\phi_t := 0.9$

$$T_n := F_y \cdot A_s = 9743 \text{ kN} \quad T_n = 2190 \text{ kip}$$

- Design tensile strength

$$\phi_t T_n := \phi_t \cdot T_n = 8768 \text{ kN} \quad \phi_t T_n = 1971 \text{ kip}$$

Strength in ETABS

Assumptions:

- 1) Fully concrete-steel interaction $C2 := 1.0$
- 2) Use a full thickness of steel tube $t_{design} := 1.0 \cdot t$
- 3) Not consider Euler's buckling --> nominal strength equals to short column's strength

$$P_n = P_{no}$$

$$D_c := D - 2 \cdot t_{design} = 527.1 \text{ mm}$$

$$r_c := \frac{D_c}{2} = 263.5 \text{ mm}$$

$$A_c := \pi \cdot (r_c)^2 = 2182 \text{ cm}^2$$

$$A_s := \pi \cdot (r)^2 - A_c = 271 \text{ cm}^2$$

$$P_{no} := F_y \cdot A_s + C2 \cdot f'_c \cdot A_c = 21932 \text{ kN}$$

$$P_n := P_{no} = 21932 \text{ kN}$$

$$T_n := A_s \cdot F_y = 10455 \text{ kN}$$

This is a strength of section during analysis process in ETABS

Modal Period

18R5

Case	Mode	Period (sec)	$\sum U_x$	$\sum U_y$	$\sum U_z$	$\sum R_x$	$\sum R_y$	$\sum R_z$
Ritz	1	1.567	0.7104	0.0494	0	0.0124	0.1788	0
	2	1.567	0.7598	0.7598	0	0.1913	0.1913	0
	3	0.827	0.7598	0.7598	0	0.1913	0.1913	0.8381
	4	0.536	0.9077	0.7872	0	0.2852	0.6979	0.8381
	5	0.536	0.9352	0.9352	0	0.7919	0.7919	0.8381
	6	0.493	0.9352	0.9352	0.5318	0.7919	0.7919	0.8381
	7	0.443	0.9352	0.9352	0.574	0.7919	0.7919	0.8381
	8	0.440	0.9570	0.9354	0.574	0.7921	0.8094	0.8381
	9	0.440	0.9573	0.9573	0.574	0.8096	0.8096	0.8381
	10	0.418	0.9573	0.9573	0.7578	0.8096	0.8096	0.8381
	11	0.386	0.9573	0.9573	0.7654	0.8096	0.8096	0.8381
	12	0.317	0.9573	0.9573	0.8107	0.8096	0.8096	0.8381
	13	0.229	0.9573	0.9573	0.8107	0.8096	0.8096	0.8381
	14	0.109	0.9573	0.9573	0.9532	0.8096	0.8096	0.8381
	15	0.016	0.9573	0.9573	0.9533	0.8096	0.8096	0.8381
Eigen	1	1.567	0.7192	0.0404	0	0.0102	0.1811	0
	2	1.567	0.7597	0.7597	0	0.1913	0.1913	0
	3	0.837	0.7597	0.7597	0	0.1913	0.1913	0.7953
	4	0.573	0.8727	0.781	0	0.2538	0.5230	0.7953
	5	0.573	0.894	0.894	0	0.5855	0.5855	0.7953
	6	0.511	0.894	0.894	0.1905	0.5855	0.5855	0.7953
	7	0.494	0.894	0.894	0.2073	0.5855	0.5855	0.7953
	8	0.489	0.894	0.894	0.2218	0.5855	0.5855	0.7953
	9	0.489	0.894	0.894	0.2219	0.5855	0.5855	0.7953
	10	0.488	0.894	0.894	0.2219	0.5855	0.5855	0.7953
	11	0.488	0.894	0.894	0.2219	0.5855	0.5855	0.7953
	12	0.487	0.894	0.894	0.2219	0.5855	0.5855	0.7953
	13	0.487	0.894	0.894	0.2236	0.5855	0.5855	0.7953
	14	0.486	0.894	0.894	0.2236	0.5855	0.5855	0.7953
	15	0.485	0.894	0.894	0.2287	0.5855	0.5855	0.7953

24R5

Case	Mode	Period (sec)	$\sum U_x$	$\sum U_y$	$\sum U_z$	$\sum R_x$	$\sum R_y$	$\sum R_z$
Ritz	1	1.979	0.6717	0.0652	0	0.0209	0.2151	0
	2	1.979	0.7369	0.7369	0	0.2360	0.2360	0
	3	0.992	0.7369	0.7369	0	0.2360	0.2360	0.8236
	4	0.668	0.8985	0.7618	0	0.3057	0.6892	0.8236
	5	0.668	0.9234	0.9234	0	0.7589	0.7589	0.8236
	6	0.506	0.9234	0.9234	0.5240	0.7589	0.7589	0.8236
	7	0.452	0.9234	0.9234	0.5777	0.7589	0.7589	0.8236
	8	0.450	0.935	0.9235	0.5777	0.7591	0.7703	0.8236
	9	0.450	0.9352	0.9352	0.5777	0.7705	0.7705	0.8236
	10	0.422	0.9352	0.9352	0.7649	0.7705	0.7705	0.8236
	11	0.386	0.9352	0.9352	0.7698	0.7705	0.7705	0.8236
	12	0.328	0.9352	0.9352	0.8164	0.7705	0.7705	0.8236
	13	0.241	0.9352	0.9352	0.8168	0.7705	0.7705	0.8236
	14	0.125	0.9352	0.9352	0.9459	0.7705	0.7705	0.8236
	15	0.015	0.9352	0.9352	0.9459	0.7705	0.7705	0.8236
Eigen	1	1.979	0.6716	0.0652	0	0.0209	0.2152	0
	2	1.979	0.7368	0.7368	0	0.2361	0.2361	0
	3	1.003	0.7368	0.7368	0	0.2361	0.2361	0.7832
	4	0.710	0.8652	0.7527	0	0.2781	0.5747	0.7832
	5	0.710	0.8812	0.8812	0	0.6167	0.6167	0.7832
	6	0.520	0.8812	0.8812	0.2543	0.6167	0.6167	0.7832
	7	0.494	0.8812	0.8812	0.2877	0.6167	0.6167	0.7832
	8	0.490	0.8812	0.8812	0.3191	0.6167	0.6167	0.7832
	9	0.489	0.8812	0.8812	0.3196	0.6167	0.6167	0.7832
	10	0.488	0.8812	0.8812	0.3199	0.6167	0.6167	0.7832
	11	0.487	0.8812	0.8812	0.3199	0.6167	0.6167	0.7832
	12	0.487	0.8812	0.8812	0.3199	0.6167	0.6167	0.7832
	13	0.487	0.8812	0.8812	0.3200	0.6167	0.6167	0.7832
	14	0.487	0.8812	0.8812	0.3202	0.6167	0.6167	0.7832
	15	0.487	0.8812	0.8812	0.3252	0.6167	0.6167	0.7832

36R5

Case	Mode	Period (sec)	$\sum U_x$	$\sum U_y$	$\sum U_z$	$\sum R_x$	$\sum R_y$	$\sum R_z$
Ritz	1	3.032	0.0227	0.6717	0	0.2858	0.0097	0
	2	3.032	0.6945	0.6945	0	0.2955	0.2955	0
	3	1.374	0.6945	0.6945	0	0.2955	0.2955	0.7604
	4	1.029	0.7003	0.8579	0	0.6274	0.3073	0.7604
	5	1.029	0.8638	0.8638	0	0.6392	0.6392	0.7604
	6	0.551	0.8638	0.8638	0.4862	0.6392	0.6392	0.7604
	7	0.517	0.8641	0.9333	0.4862	0.7286	0.6396	0.7604
	8	0.517	0.9336	0.9336	0.4862	0.729	0.729	0.7604
	9	0.498	0.9336	0.9336	0.616	0.729	0.729	0.7604
	10	0.480	0.9336	0.9336	0.616	0.729	0.729	0.9334
	11	0.460	0.9631	0.934	0.616	0.7308	0.8926	0.9334
	12	0.460	0.9634	0.9634	0.616	0.8944	0.8944	0.9334
	13	0.440	0.9634	0.9634	0.8073	0.8944	0.8944	0.9334
	14	0.391	0.9634	0.9634	0.8124	0.8944	0.8944	0.9334
	15	0.383	0.9634	0.9634	0.8133	0.8944	0.8944	0.9334
	16	0.337	0.9634	0.9634	0.8147	0.8944	0.8944	0.9334
	17	0.229	0.9634	0.9634	0.8892	0.8944	0.8944	0.9334
	18	0.198	0.9634	0.9634	0.8917	0.8944	0.8944	0.9334
	19	0.113	0.9634	0.9634	0.9494	0.8944	0.8944	0.9334
	20	0.014	0.9634	0.9634	0.9494	0.8944	0.8944	0.9334
Eigen	1	3.032	0.0227	0.6717	0	0.2858	0.0097	0
	2	3.032	0.6945	0.6945	0	0.2955	0.2955	0
	3	1.374	0.6945	0.6945	0	0.2955	0.2955	0.7602
	4	1.030	0.7385	0.8180	0	0.5463	0.3849	0.7602
	5	1.030	0.8620	0.8620	0	0.6357	0.6357	0.7602
	6	0.594	0.8643	0.9101	0	0.7225	0.6398	0.7602
	7	0.594	0.9124	0.9124	0	0.7267	0.7267	0.7602
	8	0.553	0.9124	0.9124	0.4534	0.7267	0.7267	0.7602
	9	0.524	0.9124	0.9124	0.4534	0.7267	0.7267	0.8774
	10	0.509	0.9124	0.9126	0.4534	0.7477	0.7271	0.8774
	11	0.509	0.9126	0.9126	0.4534	0.7482	0.7482	0.8774
	12	0.507	0.9126	0.9126	0.6000	0.7482	0.7482	0.8774
	13	0.493	0.9126	0.9126	0.6011	0.7482	0.7482	0.8774
	14	0.490	0.9126	0.9126	0.6119	0.7482	0.7482	0.8774
	15	0.489	0.9126	0.9126	0.6131	0.7482	0.7482	0.8774

	16	0.488	0.9126	0.9126	0.6204	0.7482	0.7482	0.8774
	17	0.488	0.9126	0.9126	0.6209	0.7482	0.7482	0.8774
	18	0.487	0.9126	0.9126	0.6209	0.7482	0.7482	0.8774
	19	0.487	0.9126	0.9126	0.6209	0.7482	0.7482	0.8774
	20	0.487	0.9126	0.9126	0.6209	0.7482	0.7482	0.8774



Arias Intensity (Arias, 1970)

Arias Intensity is a measure of the strength of a ground motion. It was proposed by Chilean engineer Arturo Arias in 1970. I_A (Arias Intensity) derives as the integration of the square of whole acceleration record; therefore, I_A includes the characteristics of duration of ground motion, frequency content and amplitude. It represents the total energy per unit weight stored by undamped simple oscillators at the end of motions. The most common case of Arias Intensity is a case of zero damping in single degree of freedom oscillators. Given this condition, Arias Intensity is:

$$I_A = \frac{2\pi}{g} \int_0^{T_d} a(t)^2 dt \quad (\text{m/s})$$

where

g = the acceleration due to gravity (m/s^2)

T_d = the duration of signal above threshold

The study by Chandramohan (Chandramohan et al., 2013) found, “with regard to duration, the 5 to 95% significant duration ($t_5 - t_95$) was identified as the duration metric best suited for use within the performance-based framework, where the collapse capacity is conditioned on ground motion intensity.” In this study, assuming inter-story drift ratio of buildings are increasing as the ground motion intensity increases, a duration of ground motion can be reduced based on Arias Intensity of 5 to 95%.

Baseline Correction (Chiu, 1997)

Since most digital strong-motion data has many baseline errors. Chiu identified the major baseline errors and proposed three steps to correct these errors. The major baseline errors found in digital data consists of constant drift in the acceleration, low-frequency instrument noise, low-frequency background noise, small initial values for the acceleration and velocity, and manipulation errors. The three-step algorithm for baseline correction are:

- 1) The least-squares fitting in acceleration. This step removes the linear trend in the acceleration. This step slightly shifts the baseline, but the baseline errors are significantly reduced. The second order method refers to the second order least squares estimation.
- 2) High-pass filtering in acceleration. This step removes the remaining and high-order random noise. If a proper high-pass filter is selected, the filtering can remove most of the errors in acceleration. The change in acceleration is small, but the baseline errors have been significantly reduced, although the displacement still exhibits a clear linear trend.
- 3) Subtracting of the initial value in the velocity. This step subtracts the initial velocity estimated from the integration of acceleration functions by the Fourier expansion.

Let $\ddot{x}(t)$ represent the time series of acceleration. The Fourier expansions of $\ddot{x}(t)$ is:

$$\ddot{x}(t) = \frac{a_0}{2} + \sum_{n=1}^N [a_n \cos(2\pi f_n t) + b_n \sin(2\pi f_n t)]$$

Where a_n and b_n are coefficients corresponding to the even and odd functions of $\ddot{x}(t)$.

The integration of $\ddot{x}(t)$ from 0 to t gives:

$$\int_0^t \ddot{x}(t) dt = \dot{x}(t) - \dot{x}(0)$$

$$\int_0^t \ddot{x}(t) dt = \frac{a_0 t}{2} + \sum_{n=1}^N \frac{1}{2\pi f_n} [a_n \sin(2\pi f_n t) - b_n \cos(2\pi f_n t)] + \sum_{n=1}^N \frac{b_n}{2\pi f_n}$$

The second summation corresponds to the initial velocity. If this summation does not vanish, the initial velocity will not be zero.



APPENDIX D
RESULTS

จุฬาลงกรณ์มหาวิทยาลัย
CHULALONGKORN UNIVERSITY

Pushover

ID	T (s)	T_1 (s)	W (kN)	V_{\max} (kN)	V_{dyn} - strength design (kN)	Ω	δ_u (cm)	$\delta_{y,eff}$ (cm)	μ_T	SSF
18R5	1.67	1.57	262077	125779	6705	18.8	330.1	49.89	6.617	1.54
24R5	2.06	1.98	358475	151724	10190	14.9	410.5	66.95	6.131	1.52
36R5	2.79	3.03	555088	133510	9952	13.4	752.9	82.31	9.147	1.61

Example calculation of $\delta_{y,eff}$:

$$\delta_{y,eff} = C_0 \frac{V_{\max}}{W} \left[\frac{g}{4\pi^2} \right] (\max(T, T_1))^2$$

$$C_0 = 1.5 \text{ (Assumption)}$$

$$\delta_{y,eff} = 1.5 \frac{151724 \cdot 9.81}{358475 \cdot 4\pi^2} \max(2.06, 1.98)^2 = 0.6695 \text{ m} = 66.95 \text{ cm}$$

$$\mu_T = \frac{\delta_u}{\delta_{y,eff}} = \frac{410.5}{66.95} = 6.131$$

$$SSF = 1.51 + \left(\frac{1.61 - 1.51}{8 - 6} \right) (6.131 - 6) = 1.52$$

NLRHA

Values in underline are values obtained from linear interpolations from adjacent points.

18R5 (T=CuTa=1.67s)

ID	Comp.	SF	Δ_{\max}	Δ_{\min}
CMS 1.5s, 1 [YMT015]	ew	8	0.0284	0.0270
		<u>9</u>	0.0303	0.0317
	ns	<u>6</u>	0.0296	0.0270
		8	0.0357	0.0283
CMS 1.5s, 2 [SIG007]	ew	4	0.0213	0.0242
		6	0.0288	0.0279
		<u>6.5</u>	0.0293	0.0285
	ns	<u>7</u>	0.0294	0.0305
		4	0.0174	0.0174
		6	0.0278	0.0234
CMS 1.5s, 3 [HKD06]	ew	<u>6.48</u>	0.0300	
		8	0.0368	0.0312
		5	0.0254	0.0155
	ns	6	0.0324	0.0238
		5	0.0241	0.0247
		<u>5.66</u>	0.0300	
CMS 0.5s, 1 [KOC]	ew	6	0.0331	0.0296
		8	0.0451	0.0368
		5	0.0126	0.0092
	ns	9	0.0249	0.0254
		<u>9.76</u>		0.0300
		10	0.0263	0.0315
CMS 0.5s, 2 [HEC2]	ew	10	0.0182	0.0276
		<u>10.46</u>		0.0300
	ns	11	0.0198	0.0329
		5	0.0123	0.0142
		10	0.0252	0.0188
		12	0.0289	0.0217
CMS 0.5s, 3 [HEC24]	ew	<u>12.39</u>	0.0300	
		13	0.0316	0.0236
		10	0.0277	0.0271
	ns	<u>10.30</u>		0.0300
		11	0.0285	0.0368
		6	0.0236	0.0212
ns	<u>6.73</u>	0.0300		
	7	0.0324	0.0280	
		10	0.0439	0.0417

* Δ = inter-story drift ratio

IDA results

ID	Comp.	$S_a(g)$ [$\xi = 2.5\%$]	SF	Δ_{\max}	$S_{CT} = SF \times S_a$	$S_{MT}(g)$	CMR
CMS 1.5s, 1 [YMT015]	ew	0.2831	9	0.0303	2.5475	0.227	11.22
	ns	0.2725	6	0.0296	1.6349	0.227	7.20
CMS 1.5s, 2 [SIG007]	ew	0.2839	7	0.0305	1.9876	0.227	8.76
	ns	0.3181	6.48	0.0300	2.0614	0.227	9.08
CMS 1.5s, 3 [HKD06]	ew	0.1824	5.65	0.0300	1.0309	0.227	4.54
	ns	0.2225	5.66	0.0300	1.2583	0.227	5.54
CMS 0.5s, 1 [KOC]	ew	0.0671	9.76	0.0300	0.6551	0.227	2.89
	ns	0.0780	10	0.0296	0.7800	0.227	3.44
CMS 0.5s, 2 [HEC2]	ew	0.1457	10.46	0.0300	1.5239	0.227	6.71
	ns	0.1708	12.39	0.0300	2.1169	0.227	9.33
CMS 0.5s, 3 [HEC24]	ew	0.2504	10.30	0.0300	2.5789	0.227	11.36
	ns	0.2657	6.73	0.0300	1.7872	0.227	7.87
					$\hat{S}_{CT} =$	0.227	6.75
					$SSF =$	1.54	$ACMR =$ 10.40

CFC parameters

ID	$x = S_{CT}$	$\ln x = \ln S_{CT}$	$P(x)$
	0		0
KOC-ew	0.6551	-0.4229	0.083
KOC-ns	0.7800	-0.2485	0.167
HKD06-ew	1.0309	0.0305	0.250
HKD06-ns	1.2583	0.2298	0.333
HEC2-ew	1.5239	0.4213	0.417
YMT015-ns	1.6349	0.4916	0.500
HEC24-ns	1.7872	0.5806	0.583
SIG007-ew	1.9876	0.6869	0.667
SIG007-ns	2.0614	0.7234	0.750
HEC2-ns	2.1169	0.7500	0.833
YMT015-ew	2.5475	0.9351	0.917
HEC24-ew	2.5789	0.9474	1.000

$$\hat{S}_{CT} = 1.533g$$

$$\mu = \ln \hat{S}_{CT} = 0.427$$

$$\sigma = \beta_{RTR} = 0.40$$

24R5 (T=CuTa=2.06s)

ID	Comp.	SF	Δ_{\max}	Δ_{\min}
CMS 2.0s, 1 [FKS02]	ew	3	0.0173	0.0116
		3.5	0.0197	0.0127
		5	0.0248	0.0187
		8	0.0309	0.0237
	ns	5.5	0.0264	0.0252
		6.75		0.0315
CMS 2.0s, 2 [HKD048]	ew	2	0.0101	0.0103
		3	0.0119	0.0110
		6	0.0279	0.0202
		7	0.0301	
	ns	8	0.0323	0.0255
		10	0.0276	0.0292
CMS 2.0s, 3 [SIG0072]	ew	1	0.0057	0.0058
		6	0.0148	0.0188
		10	0.0306	0.0291
	ns	6	0.0230	0.0168
		7	0.0320	0.0207
CMS 1.0s, 1 [HEC18]	ew	11	0.0258	0.0283
		12	0.0261	0.0294
		14	0.0276	0.0342
	ns	8	0.0198	0.0257
		9		0.0321
		10	0.0224	0.0386
CMS 1.0s, 2 [CHI]	ew	15	0.0390	0.0720
		5	0.0103	0.0123
		6	0.0132	0.0192
		6.5	0.0168	0.0234
		7	0.0197	0.0289
	ns	7.1		0.0301
		7.2	0.0218	0.0313
		7.6	0.0191	0.0149
		9	0.0208	0.0175
		12	0.0277	0.0216
CMS 1.0s, 3 [HEC17]	ew	13	0.0294	0.0224
		7	0.0145	0.0152
		12	0.0171	0.0215
		16	0.0214	0.0313
	ns	20	0.0264	0.0410
		14	0.0257	0.0214
		16	0.0272	0.0227
		20	0.0312	0.0273

* Δ = inter-story drift ratio

IDA results

ID	Comp.	$S_a(g)$ [$\xi = 2.5\%$]	SF	Δ_{\max}	$S_{CT} = SF \times S_a$	$S_{MT}(g)$	CMR
CMS 2.0s, 1 [HKD048]	ew	0.3401	7	0.0301	2.3807	0.2465	9.66
	ns	0.1995	11	0.0306	2.1945	0.2465	8.90
CMS 2.0s, 2 [SIG0072]	ew	0.3252	10	0.0306	3.2520	0.2465	13.19
	ns	0.2101	7	0.0320	1.4707	0.2465	5.97
CMS 2.0s, 3 [FKS02]	ew	0.1955	8	0.0309	1.5640	0.2465	6.34
	ns	0.2986	6.75	0.0315	2.0156	0.2465	8.18
CMS 1.0s, 1 [HEC18]	ew	0.078	12	0.0294	0.9360	0.2465	3.80
	ns	0.1092	9	0.0321	0.9828	0.2465	3.99
CMS 1.0s, 2 [CHI]	ew	0.0909	7.1	0.0301	0.6454	0.2465	2.62
	ns	0.0864	13	0.0294	1.1232	0.2465	4.56
CMS 1.0s, 3 [HEC17]	ew	0.0919	16	0.0313	1.4704	0.2465	5.97
	ns	0.1052	20	0.0312	2.1040	0.2465	8.54
				$\hat{S}_{CT} =$	<u>1.528</u>	0.2465	<u>6.20</u>
				$SSF =$	<u>1.52</u>	$ACMR =$	<u>9.42</u>

CFC parameters

ID	$x = S_{CT}$	$\ln x = \ln S_{CT}$	$P(x)$
	0		0
CHI-ew	0.6454	-0.4379	0.083
HEC18-ew	0.9360	-0.0661	0.167
HEC18-ns	0.9828	-0.0174	0.250
CHI-ns	1.1232	0.1162	0.333
HEC17-ew	1.4704	0.3855	0.417
SIG007-ns	1.4707	0.3857	0.500
FKS02-ew	1.5640	0.4472	0.583
FKS02-ns	2.0156	0.7009	0.667
HEC17-ns	2.1040	0.7438	0.750
HKD048-ns	2.1945	0.7860	0.833
HKD048-ew	2.3807	0.8674	0.917
SIG007-ew	3.2520	1.1793	1.000

$$\hat{S}_{CT} = 1.528g$$

$$\mu = \ln \hat{S}_{CT} = 0.424$$

$$\sigma = \beta_{RTR} = 0.40$$

36R5 (T=CuTa=2.79s)

ID	Comp.	SF	Δ_{\max}	Δ_{\min}
CMS 3.0s, 1 [OSK004]	ew	7	0.0210	0.0277
		7.88		0.0300
		9	0.0239	0.0330
	ns	6	0.0275	0.0265
		8	0.0300	0.0341
CMS 3.0s, 2 [HKD006]	ew	8	0.0255	0.0219
		8.92	0.0300	
	ns	10	0.0353	0.0281
		8	0.0220	0.0292
		8.28		0.0300
CMS 3.0s, 1 [PYAY]	ew	8	0.0280	0.0273
		8.5	0.0287	0.0283
		9.19	0.0300	
	ns	10	0.0316	0.0317
		10	0.0268	0.0229
CMS 1.5s, 1 [YMT015]	ew	14	0.0201	0.0258
		16	0.0223	0.0301
		20	0.0299	0.0402
	ns	11	0.0220	0.0243
		12.98		0.0300
CMS 1.5s, 2 [SIG007]	ew	8	0.0183	0.0258
		10	0.0213	0.0301
	ns	8	0.0207	0.0302
		10	0.0256	0.0365
		6	0.0300	0.0235
CMS 1.5s, 3 [HKD06]	ew	8	0.0380	0.0293
		6	0.0209	0.0305

* Δ = inter-story drift ratio

IDA results

ID	Comp.	$S_a(g)$ [$\xi = 2.5\%$]	SF	Δ_{\max}	$S_{CT} = SF \times S_a$	$S_{MT}(g)$	CMR
CMS 3.0s, 1 [OSK004]	ew	0.1594	7.88	0.0300	1.2554	0.155	8.10
	ns	0.1008	6.87	0.0300	0.6917	0.155	4.46
CMS 3.0s, 2 [HKD006]	ew	0.1659	8.92	0.0300	1.4793	0.155	9.54
	ns	0.1720	8.28	0.0300	1.4251	0.155	9.19
CMS 3.0s, 3 [PYAY]	ew	0.1634	9.19	0.0000	1.5022	0.155	9.69
	ns	0.1144	12.00	0.0292	1.3723	0.155	8.85
CMS 1.5s, 1 [YMT015]	ew	0.0882	20.00	0.0299	1.7630	0.155	11.37
	ns	0.0713	12.98	0.0300	0.9247	0.155	5.97
CMS 1.5s, 2 [SIG007]	ew	0.0953	10.00	0.0301	0.9529	0.155	6.15
	ns	0.1506	8.00	0.0302	1.2050	0.155	7.77
CMS 1.5s, 3 [HKD06]	ew	0.2020	6.00	0.0300	1.2121	0.155	7.82
	ns	0.2158	6.00	0.0305	1.2947	0.155	8.35
				$\hat{S}_{CT} =$	1.199	0.155	7.74
				$SSF =$	1.61	$ACMR =$	12.46

CFC parameters

ID	$x = S_{CT}$	$\ln x = \ln S_{CT}$	$P(x)$
	0		0
OSK004-ns	0.6917	-0.3686	0.083
YMT015-ns	0.9247	-0.0783	0.167
SIG007-ew	0.9529	-0.0482	0.250
SIG007-ns	1.2050	0.1865	0.333
HKD06-ew	1.2121	0.1923	0.417
OSK004-ew	1.2554	0.2274	0.500
HKD06-ns	1.2947	0.2583	0.583
PYAY-ns	1.3723	0.3165	0.667
HKD060-ns	1.4251	0.3543	0.750
HKD060-ew	1.4793	0.3916	0.833
PYAT-ew	1.5022	0.4069	0.917
YMT015-ew	1.7630	0.5670	1.000

$$\hat{S}_{CT} = 1.199g$$

$$\mu = \ln \hat{S}_{CT} = 0.182$$

$$\sigma = \beta_{RTR} = 0.40$$

Evaluation of Deflection Amplification Factors

In FEMA P695 procedure, a deflection amplification factor can be computed as:

$$C_d = \frac{R}{B_f}$$

For 2.5% damping ratio, from Table A.10, B_f can be computed by linear interpolation:

$$B_f = \frac{0.8-1.0}{2.0-5.0}(2.5-5.0)+1.0=0.833$$

In this study, a trial R is chosen as 5.0:

$$C_d = \frac{R}{B_f} = \frac{5.0}{0.833} = 6.0$$

This C_d value is found to be higher than R since the system has less damping ratio than a traditional 5%. Nonetheless, in ASCE 7, there is no system that C_d is specified to be higher than R . Therefore, it is more appropriate to not use a value of C_d to be greater than R . The recommended value of C_d is the same value as R .

$$C_d = R = 5.0$$

Source of overstrength in the system

There are many factors causing the strength of sample buildings to be higher than the elastic model designed from specification. These factors result in a higher base shear capacity of the buildings obtained from pushover analysis. There are three portions of overstrength from design base shear to maximum base shear.

(1) The overstrength from a design level to a first yield level.

- This portion represents the overstrength from a design force level to a nominal capacity of section.
- This overstrength comes from:
 - i. The difference in design load combination to analysis load combination. In this study, the sample buildings were designed with gravity load of 1.2DL+1.0LL; however, the gravity load in analysis process was 1.0DL+0.25LL. For a particular member D242 in 24R5, the axial force in brace was reduced from 5410 kN for design load to 4244 kN for analysis load.
 - ii. The material overstrength causes a higher nominal capacity of section from elastic model to inelastic model. For steel, the minimum specific yield strength of steel (F_y) is modified to expected yield strength ($R_y F_y$); as a result, steel's strength increases from 241 to 386 MPa. For concrete, the specific compressive strength of concrete (f_c') is modified to the compressive strength of confined concrete (f_{cc}'); as a result, concrete's strength increases from 41.4 to 52.6 MPa for diameter to thickness (D/t) = 35.2.
 - iii. The nominal capacity from neglecting a factor of safety (ϕ -factor). In compressive circular concrete-filled steel tube (CCFT) member, a ϕ -factor is 0.75. Therefore, the nominal capacity is greater than the design capacity by $1/0.75 = 1.33$.

(2) The overstrength from a first yield level to a maximum force in member level.

- This portion represents the overstrength from a nominal capacity of section to an actual inelastic capacity of a section. The demand that a section can support is usually higher than the capacity computed from steel's specification.
- This overstrength comes from:
 - i. Reduction of compressive strength due to not fully concrete-steel interaction. In AISC-360, the compressive strength of concrete in a circular concrete-filled steel tube can be used only 95%.
 - ii. Reduction of thickness of steel tube in design process. In AISC-360, a design thickness uses as 93% of a nominal thickness of steel tube.
 - iii. Consideration of Euler's buckling. With the consideration of Euler's buckling, this selected short column cannot design with a short column's strength. A designed strength uses a nominal strength which considers a buckling effect.

(3) The overstrength from a maximum force in member level to maximum base shear level.

- This portion represents the overstrength from a redistribution of force. When a demand reaches a capacity of one member in the building, the demand flows into other members that can still support the force.
- This overstrength comes from an overdesigned of sections that still have demand-capacity ratio (DCR) much less than a DCR of a govern member in each module. For example, in module 1 (story 1-6) of 24R5, the section is governed by a design of a first story member with has a higher DCR whereas the section in story 6 has a DCR of 0.66. This causes a capacity higher than the actual required section by a factor of $1/0.66 = 1.5$.

ACRONYMS

- ACMR* = adjusted collapse margin ratio
- ACMR*_{10%} = acceptable value of the adjusted collapse margin ratio (*ACMR*), on average, for the performance group of interest
- ACMR*_{20%} = acceptable value of the adjusted collapse margin ratio (*ACMR*) for an individual archetype of the performance group of interest
- CCFT* = circular concrete-filled steel tube
- CDF* = cumulative distribution function
- CMR* = collapse margin ratio
- CMS* = conditional mean spectra (J. W. Baker, 2011)
- DBE* = design level earthquake as specified in ASCE 7
- IDA* = incremental dynamic analysis (Vamvatsioks & Cornell, 2002)
- MCE* = maximum considered earthquake as specified in ASCE 7
- NLRHA* = nonlinear response history analysis
- PGA* = peak ground acceleration of ground motion record
- PGV* = peak ground velocity of ground motion record
- PGD* = peak ground displacement of ground motion record
- RSA* = response spectrum analysis as specified in ASCE 7
- SDC* = seismic design category as specified in ASCE 7
- SF* = record scale factor required for collapse evaluation of an individual building
- SPFs* = seismic performance factors
- SSF* = spectral shape factor
- UHS* = uniform hazard spectrum

SYMBOLS

B_I	= numerical coefficient as specified in ASCE 7
C_d	= deflection amplification factor as specified in ASCE 7
C_S	= seismic response coefficient for DBE as specified in ASCE 7
C_t	= approximate period coefficient as determined in ASCE 7
C_u	= upper-limit period coefficient as determined in ASCE 7
C_0	= coefficient relating fundamental-mode (SDOF) displacement to roof (MDOF) displacement of an index archetype model as defined in ASCE 7
E	= modulus of elasticity
F_y	= specified minimum yield stress of steel section
f'_c	= specified compressive strength of concrete
g	= constant acceleration due of gravity
H	= height of building to roof
I	= important factor as specified in ASCE 7
R	= response modification coefficient as specified in ASCE 7
S_a	= spectral acceleration
S_{CT}	= collapse level spectral acceleration of specific ground motion at fundamental period of the system (T)
\hat{S}_{CT}	= median spectral acceleration of the collapse level ground motion
S_{DT}	= DBE spectral acceleration at fundamental period of the system (T)
S_{\max}	= maximum spectral acceleration of the fully-yielded system (or V_{\max} normalized by W)
S_{MT}	= MCE spectral acceleration at fundamental period of the system (T)
SD_{CT}	= spectral displacement at the collapse level ground motion
SD_{MT}	= spectral displacement at MCE
T	= fundamental period of the system
T_1	= first modal period of vibration
T_2	= second modal period of vibration

V	= required seismic base shear for design as specified in ASCE 7
V_E	= elastic seismic base shear developed for DBE if the system remains linearly elastic
V_{\max}	= maximum seismic base shear of the fully-yielded system
W	= effective seismic weight of the structure
β_I	= component of effective damping of the structure as specific in ASCE 7
β_{DR}	= design requirement uncertainty
β_{MDL}	= modeling uncertainty
β_{RTR}	= record-to-record uncertainty represents the variability of ground motions
β_{TD}	= test data uncertainty
β_{TOT}	= total collapse uncertainty
δ	= displacement of the yielded system corresponding to DBE
δ_E	= displacement of the system corresponding to DBE if the system remains linearly elastic
$\delta_{y,eff}$	= effective yield roof displacement of the seismic force-resisting system as defined in FEMA P695
δ_u	= roof displacement used to approximate the ultimate capacity of the seismic force-resisting system as defined in FEMA P695
Δ	= inter-story drift ratio in the context of seismic analysis
μ	= <i>arithmetic mean</i> in the context of statistics
μ_T	= period-based ductility
ξ	= damping ratio
σ	= <i>standard deviation</i> in the context of statistics
Ω	= overstrength factor for individual building
Ω_0	= system overstrength factor as specified in ASCE 7

VITA

Mr. Nattanaï Kuangmia was born on the 13th of February 1995 in Bangkok, Thailand. After completing his Associate Degree in Science at Whatcom Community College, United States, he transferred to University of Colorado Boulder, United States. In summer of 2015, he attended Pennsylvania State University. He received a Bachelor of Science with a major in Civil Engineering from University of Colorado Boulder in May 2016. In August 2017, he entered a Master of Engineering program with a major in Civil Engineering with a concentration in Structural Engineering at Chulalongkorn University, Thailand.

